PHOTOCATALYTIC DEGRADATION OF SOME WATER CONTAMINANTS WITH GRAPHITIC CARBON NITRIDE

A

Thesis

Submitted For the Award of the Ph.D. Degree of

PACIFIC ACADEMY OF HIGHER EDUCATION AND RESEARCH UNIVERSITY

by

DEEPIKA PATEL

Under the Supervision of

Dr. MONIKA JANGID **Prof. NEETU SHORGAR**

DEPARTMENT OF CHEMISTRY

FACULTY OF SCIENCE

PACIFIC ACADEMY OF HIGHER EDUCATION AND RESEARCH UNIVERSITY, UDAIPUR

DEPARTMENT OF CHEMISTRY

PAHER UNIVERSITY, UDAIPUR

Dr. MONIKA JANGID
Assistant Professor

CERTIFICATE

Its gives me immense pleasure in certifying that the thesis entitled **"PHOTOCATALYTIC DEGRADATION OF SOME WATER CONTAMINANTS WITH GRAPHITIC CARBON NITRDIDE"** and submitted by **DEEPIKA PATEL** is based on the work research carried out under my guidance. She has completed the following requirements as per Ph.D. regulations of the University;

(i) Course work as per University rules.

(ii) Residential requirements of the University.

(iii) Regularly submitted Half Yearly Progress Report.

(iv) Published/accepted minimum of two research paper in a refereed research journal.

I recommend the submission of thesis.

Date:

(Dr. MONIKA JANDID)
Supervisor

DEPARTMENT OF CHEMISTRY

PAHER UNIVERSITY, UDAIPUR

Prof. NEETU SHORGAR
Professor

CERTIFICATE

Its gives me immense pleasure in certifying that the thesis entitled **"PHOTOCATALYTIC DEGRADATION OF SOME WATER CONTAMINANTS WITH GRAPHITIC CARBON NITRDIDE"** and submitted by **DEEPIKA PATEL** is based on the work research carried out under my guidance. She has completed the following requirements as per Ph.D. regulations of the University;

(i) Course work as per University rules.

(ii) Residential requirements of the University.

(iii) Regularly submitted Half Yearly Progress Report.

(iv) Published/accepted minimum of two research paper in a refereed research journal.

I recommend the submission of thesis.

Date:

(Prof. NEETU SHORGAR)
Co-Supervisor

DECLARATION

I, **DEEPIKA PATEL** D/o **Mr. SURESH PATEL,** resident of Udaipur, Rajasthan, hereby declare that the research work incorporated in the present thesis entitled **"PHOTOCATALYTIC DEGRADATION OF SOME WATER CONTAMINANTS WITH GRAPHITIC CARBON NITRIDE"** is my own work and is original. This work (in-part or in full) has not been submitted to any University for the award of a Degree or a Diploma. I have properly acknowledged the material collected from secondary sources, wherever required. I solely own the responsibility for the originality of the entire content.

Date :
Place:

(DEEPIKA PATEL)

COPYRIGHT

I, **DEEPIKA PATEL,** hereby declare that the Pacific Academy of Higher Education and Research University, Udaipur Rajasthan, shall have the right to preserve, use and disseminate the thesis entitled **"PHOTOCATALYTIC DEGRADATION OF SOME WATER CONTAMINANTS WITH GRAPHITIC CARBON NITRIDE"** in print or electronic format for academic/ research purpose.

Date :
Place:

(DEEPIKA PATEL)

ACKNOWLEDGEMENT

I am grateful to the Supreme Being and the epitome of benevolence, ***"The Almighty God"*** for giving me all the grace that I need to pursue this work.

I am deeply indebted to my Supervisors **Dr. MONIKA JANGID**, Assistant Professor, and **Prof. NEETU SHORGAR,** Professor, Department of Chemistry, PAHER University, Udaipur, who served as my guide throughout the entirety of my research. Her unwavering support, expert guidance, and dedication were pivotal in shaping the direction and outcomes of this study.

I would like to extend my heartfelt appreciation to **Prof. SURESH C. AMETA**, Prof. of Eminence, Department of Chemistry, PAHER University, for his invaluable support and vast knowledge. His critical analysis and insights significantly enriched the quality of this work.

I express my gratitude to **Prof. RAMESHWAR AMETA**, Dean, Faculty of Science, PAHER University for his support and encouragement during this research endeavours.

I am highly thankful to **Prof. HEMANT KOTHARI**, Dean, P.G. Studies, PAHER University, Udaipur for his support, invaluable advice and continuous guidance during my research work.

I am thankful to **Prof. SEEMA KOTHARI, Prof. RAKSHIT AMETA, Dr. PARAS TAK, Dr. PRIYANKA JHALORA, Dr. PURNIMA DASHORA and Dr. LALITA JOSHI** for their constant support and guidance.

Special thanks are due to **Dr. RAVI CHANGWAL, PRIYANKA KUNWAR RAO, Dr. KHUSHBU SHARMA**, and **SARITA CHODHUARY** for their scholarly contributions and unwavering support throughout this research project.

Heartfelt thanks to my parents, **Mr. SURESH PATEL** and **Mrs. CHAMPA DEVI**, for their love, blessings, and unwavering support. I also extend my appreciation to my brother, **ADV. KIRTESH PATEL**, for his encouragement.

I express my deepest appreciation to my husband, **CA LOKESH PATEL**, for his patience and steadfast encouragement throughout my endeavours.

I would also like to acknowledge the non-teaching staff of the Department of Chemistry at PAHER University for their helpful attitude during this study.

Special gratitude to **M/s SHORYA THESIS PRINTING & BINDING**, for his role in shaping the matter, creative design work and bringing out this document meticulously, neatly and timely.

Finally, I extend my thanks to all, who directly or indirectly contributed to this work. My apologies to those, who are inadvertently not acknowledged.

(DEEPIKA PATEL)

PREFACE

Water is a natural resource, which is necessary for life. It is available in various sources like rivers, streams, lakes and oceans. Through the last century, fresh water has been depleted enormously due to the explosion of human population and eco-unfriendly activities. The disposal of human waste in water bodies causes severe threats to the environment which affects all kinds of living organisms. In order to save water bodies, we need to understand the sources of wastewater and its polluting components. Domestic, industrial and agricultural sectors are the three major sectors of wastewater. Domestic wastewater includes water from household activities. Industrial wastewater comes from various sectors of industry like food, chemical, paper & pulp, nuclear & thermal power, laundry, pharmaceuticals, mine, iron & steel, etc. These wastewaters are rich in organic and inorganic contents. But excessive release of such nutrients into the water causes a rise of minerals and nutrients in water bodies leading to the excessive growth of plants and algae, which in turn leads to oxygen depletion in water bodies and, hence, eutrophication. This wastewater can be reused, if treated suitably by removing different pollutants.

Issues pertaining to water contamination becomes of paramount importance due to fundamental role of water in sustaining life. Water constituted a significant portion of the human body (about 70%) and served as a cornerstone of life. The adverse effect of water pollution on human health and environmental integrity deepens the critical nature of water-related concerns. Therefore, an urgent attention is required to find out some solution for pressing need to combat water pollution.

Advanced oxidation processes are genuinely efficient for treating various toxic organic pollutants and complete destruction of contaminants of emerging concern like naturally occurring toxins, pesticides, dyes, and other deleterious contaminants. These organic pollutants interact with hydroxyl radical via addition or hydrogen abstraction pathways, resulting in a carbon-centered radical, which then reacts with molecular oxygen to form a peroxyl radical that undergoes subsequent reactions; thus, generating a host of oxidation products like ketones, aldehydes, or alcohols. Hydroxyl radicals can also form a radical cation by abstracting an electron from electron rich substrates, which can readily hydrolyze in aqueous media giving an oxidized product.

The oxidation products are often less toxic and more susceptible to bioremediation like CO_2, water, etc.

Photocatalysis is a phenomenon, in which an electron-hole pair is generated on exposure of a semiconducting material to light. Photocatalysis can be used to break down a wide variety of organic materials, organic acids, estrogens, pesticides, dyes, crude oil, microbes (including viruses and chlorine resistant organisms), inorganic molecules such as nitrous oxides (NOx) etc.

The present thesis has been divided in four chapters-

Chapter-I deals with introduction of waste water, Advanced oxidation processes, mechanism of photocatalysis and photocatalytic degradation of organic pollutants using different types of photocatalyst.

Chapter-II presents introduction of graphitic carbon nitride, modification of photocatalyst and literature survey related to photocatalytic degradation of organic pollutants using graphitic carbon nitride as photocatalyst.

Chapter -III is divided in six parts as Chapter III A – III F. Each sub-chapter is devoted to the experimental work related to a dye in presence of graphitic carbon nitride. It includes the effect of various parameters such as; pH, dye concentration, amount of photocatalyst, and light intensity on rate of degradation.

Chapter-IV deals with discussion part of the present work.

The order of degradation rate of different dyes was;

Azure A > Methylene blue > Evans blue > Rhodamine B > Alizarin red-S > Rose Bengal.

❐❐❐

CONTENTS

CHAPTER – I

INTRODUCTION

CONTENTS

1.1 INTRODUCTION

Issues pertaining to water contamination becomes of paramount importance due to fundamental role of water in sustaining life. Water constituted a significant portion of the human body (about 70%) and served as a cornerstone of life. The adverse effect of water pollution on human health and environmental integrity deepens the critical nature of water-related concerns. Therefore, an urgent attention is required to find out some solution for pressing need to combat water pollution.

The textile, dyeing, printing industries are largest consumer of fresh water per Kg of treated material. The effluents from these industries contains toxic, carcinogenic, and persistent chemicals such as dyes, formaldehyde, dioxins, heavy metals, etc. Dyes have complex structures and these are degraded naturally at high temperatures in alkaline condition under ultraviolet radiation and with another radical initiator forming toxic by-products, which may be sometimes more toxic to the environment than the parent compound. These dyes are mostly resistant to thermal, chemical, microbial, and photolytic degradation as many of them are recalcitrant in nature. Thus, there is a need of an effective, ecofriendly and economical technique for removing or degrading these dyes from wastewater. Several conventional methods for treating wastewater containing dyes from different industries are used to date, such as photodegradation, adsorption, filtration, coagulation, biological treatments, etc. However, some of these techniques are not much more effective due to the stability of pollutant molecules, and other demerits. Thus, advanced oxidation processes have been reported in oder to degrade such molecules to reduce the load of organic pollutants into wastewater.

1.2 ADVANCED OXIDATION PROCESSES

Advanced oxidation processes are genuinely efficient for treating various toxic organic pollutants and complete destruction of contaminants of emerging concern like naturally occurring toxins, pesticides, dyes, and other deleterious contaminants. These organic pollutants interact with hydroxyl radical via addition or hydrogen abstraction pathways, resulting in a carbon-centered radical, which then reacts with molecular oxygen to form a peroxyl radical that undergoes subsequent reactions; thus, generating a host of oxidation products like ketones, aldehydes, or alcohols. Hydroxyl radicals can

also form a radical cation by abstracting an electron from electron rich substrates, which can readily hydrolyze in aqueous media giving an oxidized product. The oxidation products are often less toxic and more susceptible to bioremediation like CO_2, water, etc.

Advanced oxidation involves these basic steps:

- The first step involves the formation of strong oxidants like $^{\bullet}OH$, $HO_2^{\bullet}$, $O_2^{\bullet-}$, etc.
- In the second step, these oxidants react with organic contaminants presents in the waste water converting them into biodegradable compounds and
- The last step is the oxidation of these biodegradable intermediates leading to complete mineralization in water, carbon dioxide, and inorganic salts.

1.2.1 Types of AOPs

Advanced oxidation processes have mainly these processes.

- UV-Hydrogen Peroxide Processes
- Fenton and Photo-Fenton Processes
- Ferrioxalate-Mediated Processes
- Ozone-Based Processes
- Photocatalysis
- Sonolysis
- Microwave/Hydrogen Peroxide Processes
- Gamma-ray, X-ray and Electron Beam Based Processes
- Supercritical Water Oxidation
- Electrochemical Oxidation Processes
- Catalytic Wet Peroxide Oxidation

1.2.2 Advantages of Advanced Oxidation Processes

- AOP processes can be used to remove or degrade organic pollutants in aqueous medium itself rather than transfer of these pollutants into another phase, such as solid waste.
- The hydroxyl radical reacts with all the non-degradable (recalcitrant) aqueous pollutants, heavy metals, etc., and
- It is commonly used in disinfection.

1.2.3 Limitations of Advanced Oxidation Process

- AOPs involved relatively high capital and maintenance costs.
- A regular addition of some chemical reagents may be required, which may be quite expensive.
- In this procedure, removal of residual peroxide is also to be considered as it can have potential adverse effects on later treatment steps. The residual hydrogen peroxide may be harmful to life.

1.3 PHOTOCATALYSIS

The term photocatalyst is a combination of two words: Photo related to photon and catalyst, which is a substance affecting the reaction rate in its presence. Therefore, photocatalysts may be defined as materials, which can change the rate of a chemical reaction on exposure to light. This phenomenon is known as photocatalysis. The process of photocatalysis includes reactions that take place by utilizing light in presence of a semiconductor. The compound that absorbs light and acts as a catalyst for these chemical reactions is known as a photocatalyst. All such photocatalysts are mostly semiconductors.

The energy difference between the valence band (Highest occupied molecular orbital or HOMO) and the conduction band (Lowest unoccupied molecular orbital or LUMO) is called as the band gap. On the basis of this energy band gap, the materials are classified into three basic categories.

- Metal or Conductor: $E_g < 1.0$ eV
- Semiconductor: $E_g < 1.5$-3.0 eV
- Insulator or Nonconductor: $E_g > 5.0$ eV

These are given diagrammatically in fig. 1.1

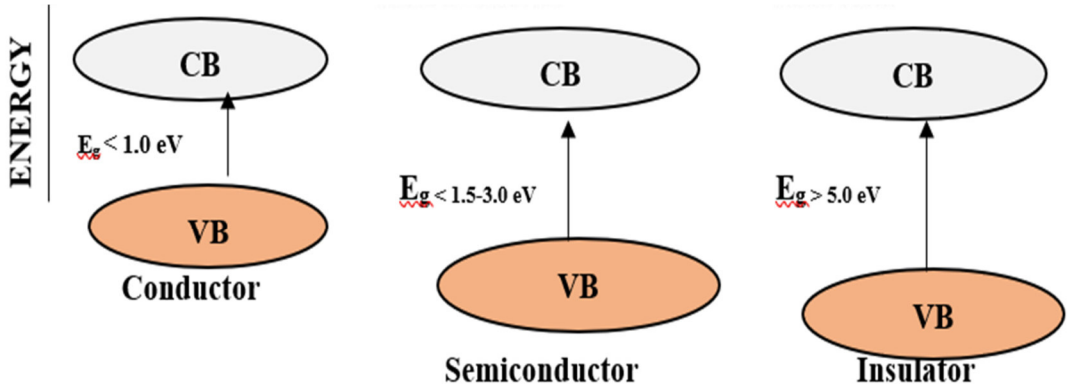

Fig. 1.1 Energy Difference b/w HOMO and LUMO

1.3.1 Types of Photocatalysis

(i) Homogeneous photocatalysis, where substrate and photocatalyst; both exist in the same phases i. e. gas, solid, or liquid, Such photocatalytic reactions are termed as homogeneous photocatalysis. Different dyes and some soluble coordination compounds are used as homogeneous photocatalysts.

(ii) Heterogeneous photocatalysis, in which substrate and photocatalyst exist in different phases. Different semiconducting powders are good examples of heterogeneous photocatalysts. Most of the transition metal chalcogenides are the most common examples of heterogeneous photocatalysts.

1.3.2 Mechanism of photocatalysis

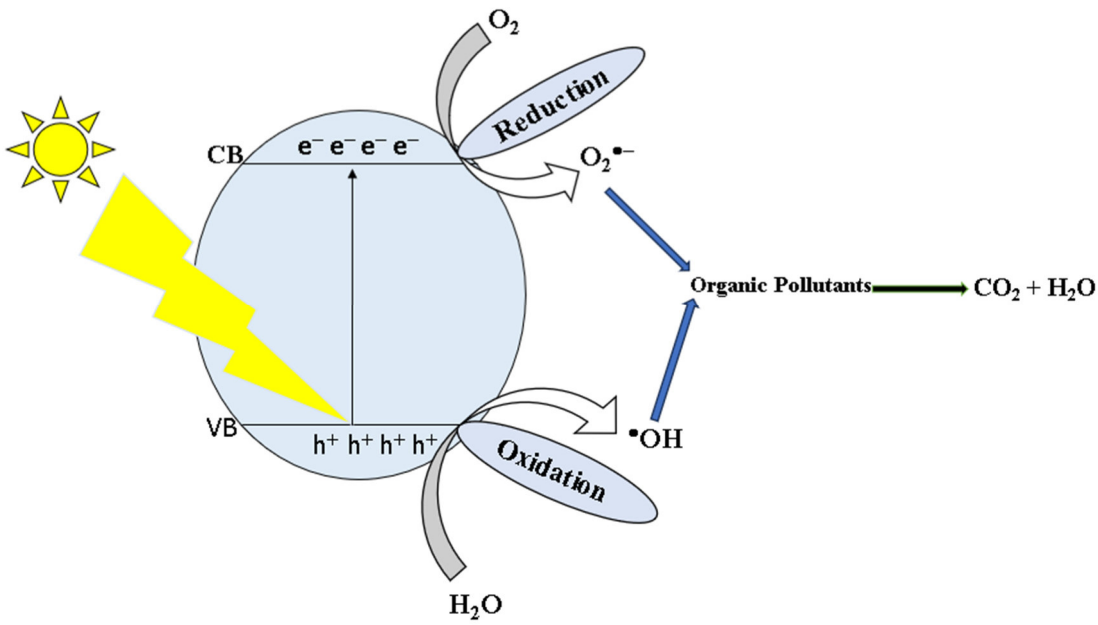

Fig. 1.2 Mechanism of Photocatalysis

Light interacts with the photocatalyst in the process of photocatalysis. When a photocatalyst absorb photon, the e^- present in the valence band is excited to conduction band of the catalyst. As a resultant, electron-hole pair is generated through this photoexcitation. The e^- and hole react with absorbed O_2 and H_2O on the surface of catalyst to from reactive oxidizing species (like $O_2^{\bullet-}$ and $^{\bullet}OH$) that react with the organic pollutants present in water and oxidized it to CO_2 and H_2O through some intermediate steps.

1.3.3 Modification of Photocatalyst

Efficiency of a photocatalyst can be enhanced by:

- Formation of localized state just above the valence band,
- Formation of localized state just below the conduction band,
- Using photocatalyst with low band gap, and
- Color center formation in band gap and surface modification.

Some of the important techniques for modification of photocatalyst are:

- Doping with metal or nonmetal,
- Codoping with various combination of donor and acceptor materials,
- Coupling of photocatalyst, composite formation,
- Sensitization,
- Use of Co-catalyst, and
- Use of heterojunction (Z-scheme and S- scheme).

1.4 PHOTOCATALYTIC DEGRADATION

Bae et al.[1] prepared metal-doped TiO_2 nanoparticles via hydrothermal and sol-gel methods. They used Cr, Co and N-doped TiO_2 for photocatalytic degradation of IPA to CO_2, but it was observed that only Cr-doped TiO_2 could produce H_2 photocatalytically in the presence of methanol-water solution under visible light. It was also revealed that in case of Pt/Co-doped TiO_2, the electron excited to the conduction band has a sufficient reduction potential so as to reduce H^+ ion to hydrogen, but hole present in the valence band has lower oxidation potential than required for degradation of methane to CO_2.

Li et al.[2] prepared tungsten-doped TiO_2/activated carbon catalysts. It was reported that W–TiO_2 layer was coated on the AC surface, which has higher surface area and smaller crystallite size as compared to TiO_2/AC. It was revealed that doping by W is responsible for narrowing the band gap of TiO_2 and as a consequence, its optical response is shifted from the ultraviolet to visible-light region. They evaluated photocatalytic performances of this supported catalyst for degradation of rhodamine B (RhB) under visible-light irradiation. They also investigated effects of tungsten ion content, TiO_2 content, pH, catalyst amount, and initial RhB concentration on degradation of Rh B.

Khairy and Zakaria[3] prepared M-doped TiO_2 nanoparticles (M = Zn, Cu) through sol–gel method. Then they investigated photocatalytic activities of these samples for degradation of methyl orange (MO) and chemical oxygen demand (COD). It was

observed that anatase phase of TiO_2 nanoparticles was formed with crystallite sizes ranging between 9–21 nm. It was observed that doping of ions to TiO_2 lead to an increase in the absorption edge wavelength, and correspondingly, a decrease in the band gap energy of TiO_2 nanoparticles was recorded. It was revealed that Cu doped TiO_2 nanoparticles displayed highest photocatalytic activity as compared to others based on the COD values.

Li et al.[4] synthesized functionalized photocatalyst (Mo- doped WO_3 that is active as well as stable. Here, it was assumed that Mo was homogeneously doped into the crystal lattice of tungsten oxide. It was also revealed that 2D structure of photocatalyst (nanosheet) was beneficial for charge transfer by Mo doping and it changed the band structure of WO_3. As a result, photocatalytic activity of Mo doped WO_3 was improved for degradation of rhodamine B.

Zhang et al.[5] synthesized N-doped mesoporous ZnO nanospheres through solvothermal approach. The photocatalytic activities of as-prepared composites were evaluated for degradation of rhodamine B at room temperature with near-UV light irradiation. It was reported that these nanocomposites exhibited higher photocatalytic activity as compared with pure ZnO nanoparticles. This increase in photocatalytic activity of N-doped ZnO nanoparticles was due to absorption of more photons and reduced electron–hole pair recombination.

Luan et al.[6] prepared Bi_2AlVO_7 and Bi_2InTaO_7 via solid-state reaction. It was reported that band gaps of Bi_2AlVO_7 and Bi_2InTaO_7 were formed to be 2.06 and 2.81 eV, respectively. These catalyst were then used for photocatalytic degradation of methylene blue (MB) dye under visible light irradiation. It was observed that Bi_2AlVO_7 displayed higher photocatalytic activity as compared with Bi_2InTaO_7 for photocatalytic degradation of MB. It was also revealed that complete removal of MB could be achieved in 160 min using Bi_2AlVO_7 as the photocatalyst.

Wahyuni et al.[7] carried out photocatalytic removal of Cu (II), Cd (II), Cr (VI) and Pb (II) with TiO_2 under UV irradiation. The maximum effectiveness of this photocatalytic process was obtained with 50 mg of TiO_2 at pH 5, which can remove 45.56%, 77.72%, 15.23%, and 40.32%, of Cu (II), Cr (VI), Cd (II) and Pb (II), respectively.

Benjwal et al.[8] synthesized reduced graphene oxide (rGO) and metal oxide-based binary (rGO-TiO_2/rGO-Fe_3O_4) and ternary (rGO-Fe_3O_4-TiO_2) nanocomposites in a simple one-step via solvothermal process. It was observed that ferric oxide and titania nanoparticles were firmly anchored over rGO. Then they used as-synthesized nanocomposites for the removal of methylene blue dye under UV as well as visible light irradiations. Ternary (rGO-Fe_3O_4-TiO_2) nanocomposite exhibited the highest dye degradation efficiency (almost 100%) within 5 min as compared to binary nanocomposite.

Das et al.[9] synthesized manganese (III) acetylacetonate complex [Mn (acac)$_3$] over graphitic carbon nitride (GCN), (2-Mn/GCN) via ultrasonication method. This as-prepared 2-Mn/GCN could achieve 99.59% degradation of rhodamine B in 55 min and 97.6% metronidazole (MTZ) was degraded in 40 min, when 0.7% Mn content was there in the catalyst.

Akhundi and Habibi Yangjeh[10] decorated $CuCr_2O_4$ nanoparticles on to g-C_3N_4 nanosheets (g-C_3N_4-NS) through reflux. The photocatalytic performance of g-C_3N_4-NS/$CuCr_2O_4$ nanocomposites was evaluated for degradation of methylene blue, rhodamine B and phenol under visible-light irradiation. When the loading amount of $CuCr_2O_4$ was 10 wt%. The nanocomposite exhibited the highest activity. Activity of the g-C_3N_4-NS/$CuCr_2O_4$ (10%) nanocomposite refluxed for 3 h and calcined at 520 °C for 4 h was almost 11.8 and 4.8 times greater than those of the bulk g-C_3N_4 and g-C_3N_4-NS photocatalysts in degradation of RhB, respectively. In the prepared nanocomposites, nanosheets of g-C_3N_4 act not only as $CuCr_2O_4$ support, but also as co-catalyst. The novel visible-light-active photocatalyst has considerable stability and it can be reused for five times without obvious loss of its photocatalytic activity.

Dahiya et al.[11] synthesized Ag-doped graphitic carbon nitride (AgGCN). The silver nanoparticles, were prepared using leaf extract of the *Ocimum tenuiflorum* (Tulsi) served as a stabilizing as well as capping agent. Different concentrations of the prepared series of nanocomposites Ag-doped GCN (0.5 mM, 1.0 mM, 1.5 mM, and 2.0 mM) were used for photocatalytic degradation of xylenol orange (XO) and rose Bengal (RB) dyes. It was observed that degradation efficiency increased due to the doping of Ag nanoparticles into GCN from 15 to 36% and 54 to 76% in the case of RB and XO,

respectively. It was also revealed that rate constant increased up to 2.5 times when Ag-doped GCN (1.5 mM) nanocomposite was used as compared to GCN.

Parthipan et al.[12] used hydrothermal route to synthesize reduced graphene oxide (PErGO) using *Phyllanthus emblica* fruits extract. The photocatalytic removal of methylene blue (MB) and methyl orange (MO) was investigated in presence of PErGO, and it was observed that about 92 and 91% MO and MB was degraded within 90 min of sunlight exposure, when mixed dye degradation was carried out. The stability and reusability of this catalyst was confirmed and it was revealed that it can be used for five degradation cycles without any significant degradation in its activity.

Gogoi et al.[13] prepared graphene oxide–clay nanocomposite. As-prepared graphene oxide-clay nanocomposite was then used for photodegradation of methylene blue. It was observed that as-prepared nanocomposite was found active against cationic dye, but it was not effective against degradation of other anionic dyes Eosin yellow and methyl orange. It was also evaluated for its reuse and it was found that percentage degradation was 85, 75 and 75 for first, second and third cycles, respectively.

Jin et al.[14] reduced GO to reduced graphene oxide (rGO) by *Eucalyptus* leaf (EL) extract. Results confirmed the oxygen-containing groups in GO were efficiently removed, formation of capping layer on the surface of rGO, and good dispersion of rGO in aqueous solution. The removal of methyl blue (MB) on EL-rGO, activated carbon, graphite powder and commercial graphene was investigated and maximum adsorption capacity of different adsorbents followed the order:

EL-rGO > Commercial graphene > Activated carbon > Graphite powder.

Yuan et al.[15] used potassium ion-doped precursor, potassium sorbate, in melamine configuration during calcination to prepare the potassium-doped g-C_3N_4 (KCN). It was reported that doping of potassium in g- C_3N_4 can modify the band structure so that light absorption and photogenerated carrier separation was enhanced. It was then used for photodegradation of methylene blue (MB).

Kuo et al.[16] modified the surface of Degussa P25 TiO_2 to prepare phosphorus-doped TiO_2 (P-TiO_2). Then they evaluated photocatalytic activity of TiO_2 and P-TiO_2 for

the degradation of bisphenol A (BPA) under UV and sunlight irradiation both. It was reported that band gap of TiO_2 and P-TiO_2 was 3.1 and 3.0 eV, respectively. It was revealed that degradation of BPA by the UV/TiO_2, UV/P-TiO_2, sunlight/TiO_2 and sunlight/P-TiO_2 systems was 59, 65, 84 and 92 % respectively. This degradation obeyed pseudo-first order kinetics. The higher degradation of BPA was attributed to narrowed band gap, reduced recombination of photogenerated electrons and holes and increased number of hydroxyl groups on surfaces.

Pham et al.[17] synthesized graphitic carbon nitride (g-CN), (metal-free photocatalyst) by polymerizing melamine and used it for photodegradation of carbamazepine (CZ) and acetaminophen (AP) in wastewater. It was reported that high removal efficiencies of 89.5% and 98.6% could be obtained for CZ and AP respectively. The rate of photodegradation with synthesized photocatalyst was 0.0321 min^{-1}, which was 2.14 times faster than in case of CZ. It was also revealed that g-CN was active under solar light because it generated highly reactive oxidants such as superoxide ($^{\bullet}O_2^-$) and hydroxyl ($^{\bullet}OH$) radical. The stability of g-CN for treating these pharmaceuticals was also ascertained by using it for three repeated cycles.

Al-Zahrani et al.[18] prepared graphitic carbon nitride (g-C_3N_4) utilized it for photocatalytic degradation of acid red 26 on exposure to UV-A light. It was reported that photocatalytic degradation of acid red 26 involved dealkylation, oxidation, and cleavage of methoxy group The role of reactive species h^+ and $O_2^{\bullet}$ in this degradation process was ascertained byscavengers studies.

Binary metal oxides have also been widely used as photocatalysts for decades because the morphological properties of the individual oxides can be changed by formation of new sites in the interface between the components, or by incorporation of one oxide into the lattice of the other.

Ben et al.[19] synthesized graphitic carbon nitride–bismuth phosphate nanocomposite ($BiPO_4$ g-C_3N_4). It was reported that azo dyes such as reactive red 120 raise great concerns about their increased harmfulness. Photocatalytic degradation is considered to be one of the most efficient techniques for reactive red 120 degradation. The band gap energies of the, $BiPO_4$, g-C_3N_4 and $BiPO_4$ g-C_3N_4 nanocomposite were calculated as 4.20, 2.66, and 2.68 eV, respectively. It was reported that $BiPO_4$ g-C_3N_4

nanocomposite exhibited higher photocatalytic activity towards the degradation of reactive red 120 (RR120) under sunlight. The reaction rate constant of this degradation was found to be seven and four times higher than $BiPO_4$ nanorods and g-C_3N_4 (0.0036 min^{-1}), respectively. It was revealed that catalyst performance was decreased by less than 5% even after five recycles indicated high stability of this nanocomposite.

Dobrosz-Gomez et al.[20] examined photocatalytic degradation of phenol using TiO_2 loaded with some transition metal ions (Co, Cu, Fe and Mo) under both UV; and visible light. It was reported that most efficient one was Mo/TiO_2. It was indicated that Mo made its surface more acidic. It was observed that percentage of degradation of phenol under visible light was relatively lower than under UV radiation. Out of series of prepared catalysts, 2 wt% Mo/TiO_2 was found to be the most efficient one.

Lei et al.[21] prepared highly active CuO-modified TiO_2 photocatalysts via impregnation method. The CuO/TiO_2 was then used for degradation of polybrominated diphenyl ethers. It was reported that photo-reductive degradation of 2,2′,4,4′-tetrabromodiphenyl ether (BDE47) was almost impossible on TiO_2, but it became rapid on CuO/TiO_2 with an short induction time period (20 s). They proposed "switching reduction potential by the valence state of copper" concept in their mechanism.

Xie et al.[22] prepared a series of α-Fe_2O_3/ZnO composites with different α-Fe_2O_3 contents. The photocatalytic activity of as-prepared composites was evaluated in degradation of pentachlorophenol (PCP). It was reported that composites exhibited higher photocatalytic activity under UV–vis light irradiation as compared to ZnO. The pentachlorophenol was almost completely degraded by this composite within 4 h, when molar ratio was kept 1:5.

Sherly et al.[23] prepared nanostructured ZnO and CuO, and coupled oxides, in different molar ratios (1:1, 2:1, and 1:2). It was reported that optical absorption of ZnO was extended into the visible region on loading of CuO. The photocatalytic activities of ZnO, CuO, and ZnO:CuO were evaluated for photodegradation of 2,4-dichlorophenol under visible light irradiation. It was found that coupled metal oxide exhibited higher photocatalytic activity and it was attributed to the extended photo responsive range and charge separation rate in the nanocomposite.

Vignesh et al.[24] sensitized nanoparticles of zinc oxide (ZnO) with silver iodide. It was reported that average crystallite size of nanoparticles was 21.56 and 23.44 nm for ZnO and AgI sensitized ZnO, respectively. The photocatalytic efficiency of AgI-ZnO was observed for decolorization of rosaniline hydrochloride under visible light irradiation. The effect of different operational parameters on degradation was investigated such as pH, catalyst dosage and dye concentration. It was also revealed that maximum decolorization, total organic carbon (TOC) reduction and COD removal were 88, 75 and 68%, respectively under the optimal conditions.

They also synthesized TiO_2–metal vanadate nanocomposites (TiO_2–MV).[25] The photocatalytic activity of as-prepared TiO_2–MV was evaluated for degradation of fast green (FG) under visible light irradiation. It was reported that photocatalytic activity of as-prepared TiO_2–silver vanadate (TiO_2–Ag_3VO_4) was much higher as-compared to all; TiO_2–cadmium vanadate (TiO_2–CdV_2O_6), TiO_2–strontium vanadate (TiO_2–$Sr_3(VO_4)_2$) and TiO_2. The mineralization of fast green was confirmed by chemical oxygen demand (COD) and total organic carbon (TOC) measurements. It was also revealed that TiO_2–Ag_3VO_4 is a reusable photocatalyst.

Karunakara and Senthilvelan[26] observed photocatalyzed oxidation of aniline to azobenzene in presence of ZrO_2 under natural sunlight and UV irradiation (365 nm). It was reported that electron donors such as hydroquinone, triphenylphosphine and diphenylamine enhanced the photocatalysis. It was also revealed that many oxides like TiO_2, V_2O_5, ZnO, Fe_2O_3, CdO, CdS and Al_2O_3 also photocatalyzed the oxidation of aniline to azobenzene with UV light (254 nm) but ZrO_2 was more efficient than all other photocatalysts. The photocatalytic activities of these oxides followed the order:

$$ZrO_2 > ZnO > V_2O_5 > Fe_2O_3 > CdS > Al_2O_3 > CdO > TiO_2.$$

Vinodgopal et al.[27] used nanostructured semiconductor films of SnO2, TiO2, and SnO2/TiO2 and used for photocatalytic degradation of naphthol blue black (NBB). It was reported that degradation rate was significantly higher for SnO2/TiO2 composite films as compared to SnO_2 and TiO_2 films only. This increased degradation rate was attributed to charge separation.

Fabiyi and Skelton[28] used TiO_2 coated buoyant polystyrene beads for photocatalyzed mineralization of methylene blue. These coated beads exhibited high mechanical stability and also significant photocatalytic activity. It was also revealed by thermogravimetric analysis that these beads had no destructive degradation during photocatalytic process. The catalyst activity also remained high for up to 10 successive runs.

Sivalingam et al.[29] prepared anatase phase titania via solution combustion approach with 156 m^2g^{-1} surface area. It was found that average particle size was 8–10 nm. This as-prepared catalyst was then used for photocatalytic degradation of different dyes (Methylene blue, alizarin S, congo red, methyl red and orange G). The effect of various parameter was investigated such as pH, catalyst loading, initial concentrations of the dyes and transition metal doping. It was observed that an adverse effect on the photocatalytic activity. But this inhibition effect was not observed with Pt impregnated TiO_2.

Tan et al.[30] reported that nanosizing of g-C_3N_4 can improve this photocatalytic property. It was also revealed that H_2 evolution performance in the presence of nanosized g-C_3N_4 was 10.8 times higher than that of bulk g-C_3N_4. This improvement was attributed to photoinduced electron-hole separation and photocatalytic efficiency.

Zeng et al.[31] prepared one-dimensional porous architectural g-C_3N_4 nanorods by direct calcination of hydrous melamine nanofibers. It was reported that oxygen atoms were also doped into g-C_3N_4 matrix, which disturbed the symmetry of pristine g-C_3N_4, and as a result, more effective separation of electron/hole pairs could be achieved. It was observed that oxygen-doped g-C_3N_4 nanorods loaded with Pt exhibited excellent visible-light assisted photocatalytic hydrogen evolution (732 $\mu mol\ g^{-1}\ h^{-1}$) in the triethanolamine solution and also overall water splitting (29.6 $\mu mol\ g^{-1}\ h^{-1}$). It was also revealed that removal efficiency of 100% of 2, 4-dinitrophenol degradation could be achieved with for O-doped g-C_3N_4 nanorod within 75 min. They also reported visible-light photocatalytic H_2 evolution (96 $\mu mol\ g^{-1}\ h^{-1}$) along with 2,4-dinitrophenol degradation in presence of Pt g-C_3N_4 nanorods.

Li et al.[32] synthesized g-C_3N_4/TiO_2 hybrid photocatalysts via modified sol–gel technique using different weight ratio of g-C_3N_4. It was observed that heterojunction was formed between g-C_3N_4 and TiO_2 nanoparticles were well dispersed on g-C_3N_4 sheets. Out of as-synthesized hybrid photocatalysts, g-C_3N_4/TiO_2-80% sample displayed highest photocatalytic degradation of methylene blue under visible light irradiation which was around 3.5 times high as compared to pure g-C_3N_4. This increased activity of g-C_3N_4/TiO_2 hybrid photocatalysts was attributed to the effective separation of photogenerated electron–hole pairs and higher absorption capacity. It was also revealed that these photocatalysts exhibited more stability in photocatalytic performance even after five cycles.

Christoforidis et al.[33] prepared hybrid organic/inorganic nanocomposites containg nanosized iron oxide (metastable β-phase) and graphitic carbon nitride (g-C_3N_4). They also evaluated their photocatalytic activity for photodegradation of rhodamine B, methyl orange (MO), and phenol under simulated solar light and visible light irradiation. This improved photoactivity was attributed to improved optical properties, (narrower band-gap), increased visible light absorption efficiency, and efficient separation of the photoinduced charge carriers due to matched band edges in the heterostructure.

Hong et al.[34] synthesized *in situ* sulfur-doped mesoporous g-C_3N_4 (mpgCNS) using thiourea, with SiO_2 nanoparticles as the hard template. It was reported that mpgCNS had a high surface area of 128 $m^2\ g^{-1}$ with mesopores in the range of 10–20 nm. A downshift of 0.25 eV was observed in its conduction band, when carbon is substituted in mpgCNS. It was also revealed that as-prepared mpgCNS was 30 times more active than g-C_3N_4 in evolution of hydrogen from photocatalytic splitting of water.

Bian et al.[35] synthesized S-doped g-C_3N_4 with a hollow microsphere composition (SCNHM) by S doping. This as-prepared SCNHM had high specific surface area (~81 $m^2\ g^{-1}$). It was reported that SCNHM exhibited higher photocatalytic activity for degradation of tetracycline hydrochloride (TC) as compared to CN, SCN and CNHM samples. It was observed that this photocatalyst could eliminate high-concentration of TC (50 mg L^{-1}) in 18 min and removal efficiencies of 100 mg L^{-1} and 200 mg L^{-1} could reach 92 and 60 % in 30 min.

Gao et al.[36] prepared Bi-doped graphitic carbon nitride nanotubes (BCN nanotubes) with a porous structure by polymerizing a mixture of urea, melamine and bismuth nitrate (pentahydrate). It was reported that this as-prepared BCN nanotubes exhibited excellent photocatalytic activity for the degradation of rhodamine (Rh) B, which was 26.8-fold higher than that with PCN under visible light irradiation.

Xie et al.[37] prepared graphite carbon nitride (GCN)/La_2O_3 (CN/La) via a hydrothermal route. The photocatalytic performance of CN/La-x% photocatalysts was observed for degradation of rhodamine B (RhB), methyl orange (MO), methylene blue (MB) under visible light irradiation. It was reported that optimal photodegradation of 66.6, 99.5 and 100% of MO, Rh B and MB could be achieved in 2 h.

Hadadi et al.[38] prepared a composite of g-C_3N_4 with cadmium selenide with four different CdSe mass loadings (1, 2.5, 5, and 10%). It was reported that modified band structure in this nanocomposite not only improved the visible light absorption, but it also retarded the recombination of photo-induced charge carriers. The photocatalytic degradation of methylene blue (MB) and rhodamine B (RhB) was invastigated under visible light. It was observed that highest degradation rate constant was 0.0222 min^{-1} and 0.0178 min^{-1} for MB and RhB, respectively when g-C_3N_4/CdSe nanocomposite was used with 2.5% CdSe mass content.

Chen et al.[39] prepared double Z-type ternary composite long-after glow/graphitic carbon nitride metal–organic framework ($SrAl_2O_4:Eu^{2+}$, Dy^{3+}/g-C_3N_4/NH_2-UiO-66, SGN) via solvothermal method. They used this as a photocatalyst for removal of methylene blue (MB). It was reported that after 30 min of photocatalytic degradation ratio of SGN was found to be 5.86, 4.04 and 10 times more as compared to long-after glow (SAO), g-C_3N_4 and NH_2-UiO-66, respectively. This high photocatalytic activity of the SGN was attributed to double Z-type electron transfer mechanism. It was also revealed that degradation ratio with ternary SGN was about 50 % after 5 h even in the dark. Superoxide anion radical ($^{\cdot}O_2^-$) was identified to be main active species by quenching experiments.

Ahmed et al.[40] prepared La-$CuFe_2O_4$/g-C_3N_4 (LCFO/CN). The photodegradation efficiency of as-prepared LCFO/CN photocatalyst was investigated for removal of rhodamine B (RhB). An excellent photodegradation (97.35 %) was reported by LCFO/CN-2 heterojunction photocatalyst compared to

LCFO/CN-1 (83.14 %), LCFO (67.13 %), and CFO (62.73 %), respectively, The optimal conditions were observed as: (pH = 6.0, [catalyst] = 0.4 gL^{-1}, [RhB] = 30 mg L^{-1}, and T = 25 ± 1 °C). It was also confirmed that the photostability and reusability of the photocatalyst LCFO/CN-2 nanocomposite was good and can it be reused for five successive cycles.

Sousani et al.[41] synthesized $Ni_{0.8}Co_{0.2}/Zn_{0.8}Cd_{0.2}S$ (ZCS)/g-C_3N_4 (CN) ternary nano-photocatalyst through chemical reduction and hydrothermal methods. Photocatalytic degradation of methylene blue (MB) was carried out under LED lamp (100 W, 400–700 nm) irradiation for 3 h. It was observed that high (85%) degradation efficiency of MB could be achieved within 3 h.

Nivetha et al.[42] prepared g-C_3N_4@$BiTiO_2$/NiO heterostructure photocatalyst and used it for degradation of tetracycline (TC) under visible-light radiation. It was reported that g-C_3N_4@$BiTiO_2$/NiO heterostructure photocatalyst exhibited higher light absorption capabilities due to incorporation of g-C_3N_4 in $BiTiO_2$. It was observed that removal efficiency of 91.2% TC could be achieved within 50 min under visible-light radiation. It was also revealed that $O_2^{\bullet-}$ and $^{\bullet}OH$ radicals are the main active oxidizing species in the degradation process as evident from scavenger studies.

Kumawat et al.[43] investigated the photocatalytic activity of iron zinc cuprate for photodegradation of basic fuchsin under visible light. This photocatalyst $FeZn_2Cu_3O_{6.5}$ was synthesized by the ceramic technique. The progress of the degradation was monitored spectrophotometrically at 544 nm. The optimum rate was observed as: Concentration of basic fuchsin = 1.2×10^{-5} M, pH = 6.0, amount of $FeZn_2Cu_3O_{6.5}$ = 0.10 g and light intensity = 50.0 m Wcm^{-2}.

Abbasi-Asl et al.[44] prepared magnetic $Fe_3O_4/Ag_2C_2O_4/Ag_3PO_4$/Ag nanocomposite via co-precipitation method using *calendula officinalis* seed extract as a stabilizer. This as-prepared quaternary photocatalyst was used for degrading herbicide paraquat (PQ) and food dye brilliant blue FCF (BB) under visible light irradiation. It was reported that degradation efficiency of PQ and BB was found to be 92.72 and 88.9%, respectively under optimal conditions.

Akhundi and Habibi-Yangjeh[45] fabricated g-C_3N_4/Fe_3O_4/Ag/Ag_2SO_3 nanocomposites. It was observed that Ag/Ag_2SO_3 nanoparticles were anchored on to surface of g-C_3N_4/Fe_3O_4 nanocomposite, which is reflected in strong absorption in the visible region. The photocatalytic activity of this nanocomposite was evaluated for degradation of rhodamine B as (40%), which was higher as compared with g-C_3N_4 and g-C_3N_4/Fe_3O_4 by factors of 11.7 and 9.3, respectively. The trapping experiments confirmed that superoxide ion radical was the main active species in the photocatalytic degradation process. It was also revealed that this photocatalyst was reusable for five consecutive cycles.

Qarajehdaghi et al.[46] synthesized carboxymethyl cellulose (CMC) based nanocomposite containing CdS, g-C_3N_4, and rGO (CdS/g-C_3N_4/rGO/CMC). They could achieve 81.93 and 68.87%, removal efficiency of Ciprofloxacin (CIP) and TOC, respectively under optimal conditions as: pH 6.1, 8 mg L^{-1} CIP, and 0.6 g L^{-1} catalyst within 35 min.

Gogoi et al.[47] synthesized Ag/Ag_3PO_4–BiOBr–C_3N_4-1and tuned the band gap to 0.56 eV by variation of amount of C_3N_4. The degradation of reactive red (RR 120) was observed in the presence of this composite under visible-light illumination. It was reported that as-prepared composite exhibited 92.6% degradation efficiency of dye with the removal rate as 0.042 min^{-1}, which was about 5.2, 2.7 and 2.5 times more as compared to Ag/Ag_3PO_4, BiOBr and C_3N_4 particles, respectively. The holes, superoxide and hydroxyl radicals were considered responsible for such degradation. It was also revealed that high stability of this photocatalyst was maintained up to four consecutive cycles.

Hasija et al.[48] fabricated carbon quantum data (CQDs) using naturally occurring bamboo leaves as precursors. As-prepared CQDs were then used for construction of Z-scheme P-doped g-C_3N_4/AgI/ZnO/CQDs (PGCN) heterojunction and degradation of 2, 4-dinitrophenol (DNP). It was reported that synergistic effetct of adsorption and photocatalysis was effective for complete mineralization of DNP into H_2O, CO_2 and inorganic ions. It was interesting to note that as-prepared Z-scheme photocatalyst exhibited stability and recyclability for ten consecutive cycles.

Kumar et al.[49] prepared magnetic quaternary BiOCl/g-C_3N_4/Cu_2O/Fe_3O_4 (BGC-F) nano-heterojunction. Its photodegradation activity for degradation of sulfamethoxazole (SME) was evaluated It was reported that about 99.5% of SME (100 μM) could be degraded in 1 h under visible (Xe) lamp and 92.1% in 2 h under natural sunlight. The activity of this quaternary sample was found to be 7.2, 6.8 and 4.2-folds higher than that of C_3N_4/BiOCl/Fe_3O_4, Cu_2O/BiOCl/Fe_3O_4 and Cu_2O/BiOCl/C_3N_4 junctions, respectively. The major oxidizing species were identified as $O_2^{\bullet-}$ and $^{\bullet}OH$ radicals by scavenging experiments. It was also revealed that 41.6% total organic carbon (TOC) removal was there in 3 h under Xe lamp exposure.

Mousavi et al.[50] synthesized g-C_3N_4/Fe_3O_4/Ag_3PO_4/AgCl nanocomposites via ultrasonic- irradiation method. The photocatalytic activity of this composite was evaluated for degradation of fuchsine, rhodamine B, methyl orange, and phenol under visible-light irradiation It was reported that as-prepared g-C_3N_4/Fe_3O_4/Ag_3PO_4/AgCl (30%) nanocomposite exhibited the highest photocatalytic activity. It was observed that activity of this nanocomposite in degradation of rhodamine B was about 22, 6, and 7.5-times higher as compared to g-C_3N_4, g-C_3N_4/Fe_3O_4/Ag_3PO_4 (20%), and g-C_3N_4/Fe_3O_4/AgCl (30%) samples, respectively. It was also revealed that holes were main active oxidizing species based on trapping experiments.

Wang et al.[51] prepared graphitic carbon nitride (g-C_3N_4) and niobium pentoxide nanofibers (Nb_2O_5 NFs) heterojunction. It was confirmed that Nb_2O_5 NFs were tightly attached onto g- C_3N_4 nanosheets in this g- C_3N_4 / Nb_2O_5 heterojunction. It was reported that as-prepared g- C_3N_4 /Nb_2O_5 heterojunction displayed enhanced photocatalytic activity for degradation of phenol and rhodamine B under visible light irradiation as compared to g- C_3N_4 and Nb_2O_5 NFs. The higher catalytic activity was attributed to mainly synergistic effect between g- C_3N_4 sheets and Nb_2O_5 NFs, which promoted the transferring of carriers, but prohibited recombination, of these carriers. It was also revealed that superoxide radical anion and hole were the major active oxidizing as evident from trapping experiments.

Sahu et al.[52] synthesized polymeric oxygen rich exfoliated graphitic carbon nitride (exfoliated GCN, EGCN) It was reported that as-prepared photocatalyst can be used for photocatalytic degradation of bisphenol A (BPA), which could reach to 99%.

Guo et al.[53] synthesized porous thin g-C_3N_4 nanosheets. It was reported that as-prepared photocatalyst can effectively degrade 99.3% of rhodamine B within 15 min under visible light irradiation which was 16.8 times more than bulk g-C_3N_4. It was also confirmed that stronger oxidizability of holes is responsible for its higher photocatalytic activity.

Habib et al.[54] synthesized graphitic nitride (GN) and its derived polyimides using three different dianhydrides. These as-synthesized photocatalyst were tested for degradation of methylene blue (MB) under light irradiation. It was observed that high photocatalytic performance (96% degradation efficiency) could be achieved in 1 h. This better activity was attributed to an improved degree of crystallinity, appropriate porosity, greater charge separation and high quaternary nitrogen content in spite of lower surface area of polyimide, GN-FDA (6.78 $m^2\ g^{-1}$).

Lyu et al.[55] reported preparation of carbon nitride compounds (CN) complexed on the surface of $CuAlO_2$ substrate (CN-Cu (II)-$CuAlO_2$). It was reported that it exhibited very high activity and efficiency for the degradation of bisphenol-A in water through a Fenton-like process. It was observed that removal of bisphenol A was about 25 times higher as compared to $CuAlO_2$. It was observed that Cu (II) generated on the surface of $CuAlO_2$ resulted in significant decrease of surface oxygen vacancies. It was also revealed that in Fenton-like reactions, electron-rich center around Cu was responsible for the efficient reduction of hydrogen peroxide into hydroxyl radicals. This resulted in excellent catalytic performance for degradation of refractory pollutants.

Jin et al.[56] fabricated MoS_2/Ag/g-C_3N_4 (MS/A/CN) Z-scheme composite with a combined strategy by coupling of MoS_2 and Ag deposition on g-C_3N_4 nanosheets. It was reported that this as-prepared MS/A/CN composite can be used for photocatalytic degradation of tetracycline (TC) with peroxomonosulphate (PMS) under visible light irradiation. This MS/A/CN/PMS system displayed excellent degradation of tetracycline (about 98.9%) in 50 min. This may be due to the synergistic effect of photocatalysis and PMS activation.

Li et al.[57] used Fe-doped g-C_3N_4/graphene (rGO) composite catalysts for activation of peroxymonosulfate (PMS) and degradation of trimethoprim (TMP) under visible light irradiation. It was reported that recombination of photogenerated electron-

hole pairs in graphitic carbon nitride may be suppressed by doping it with Fe and incorporation of reduced graphene oxide (rGO). It was reported that degradation of TMP in presence of 0.2% Fe-g-C_3N_4/2 wt% rGO/PMS was 3.8 times higher than with g-C_3N_4/PMS. It was revealed that degradation efficiency was improved from 61.4% at pH = 3 to nearly 100%. It was also reported that eight intermediates were there, which were derived from demethoxylation, hydroxylation, and carbonylation.

Wang et al.[58] prepared a heterogeneous Co-based catalyst by introducing cobalt species to the cavities of *g*-C_3N_4 through Co-N bonds via calcination and impregnation. Then it was applied for activation of PMS for the degradation of organic contaminates under visible light. It was observed that optimum Co loading was 1.0% in weight, which could degrade rhodamine B completely in 25 min with a 70.5% of total organic carbon (TOC) removal.

Although, number of techniques are available for the treatment of waste water, but majority of them have some or other disadvantages. Therefore, search of a green chemical method for such a treatment seems necessary.

Advanced oxidation processes (AOPs) have been advocated as green chemical pathways in achieving this goal. Out of these AOPs, photocatalysis has emerged as a promising candidate for degradation of most of the organic pollutants.

❐❐❐

REFERENCES

1. S.W. Bae, P.H. Borse, S.J. Hong, J.S. Jang, and J.S. Lee, Photophysical properties of nanosized metal-doped TiO_2 photocatalyst working under visible light, J. Korean Phys. Soc., **51**, S22-S26 (2007). doi:10.3938/jkps.51.22.

2. Y. Li, X. Zhou, W. Chen, L. Li, M. Zen, and S. Qin, Photo decolorization of Rhodamine B on tungsten-doped TiO_2/activated carbon under visible-light irradiation, J. Hazard. Mater., **227-228**, 25-33 (2012). doi: org/10.1016/j.jhazmat.2012.04.071.

3. M. Khairy and W. Zakaria, Effect of metal-doping of TiO_2 nanoparticles on their photocatalytic activities toward removal of organic dyes, Egypt. J. Pet., **23**, 419-426 (2014). doi:10.1016/j.ejpe.2014.09.010.

4. N. Li, H. Teng, Li. Zhang, J. Zhou, and M. Liu, Synthesis of Mo-doped WO_3 nanosheets with enhanced visible-light-driven photocatalytic properties, RSC Advances., **5**, 95394-95400 (2015). doi:10.1039/C5RA17098B.

5. D. Zhang, J. Gong, J.J. Ma, G. Han, and Z. Tong, A facile method for synthesis of N-doped ZnO mesoporous nanospheres and enhanced photocatalytic activity, Dalton Trans., **42**, 16556-16561 (2013). doi.org/10.1039/C3DT52039K.

6. J. Luan, W. Zhao, J. Feng, H. Cai, Z. Zheng, B. Pan, X. Wu, Z. Zou, and Y. Li, Structural, photophysical and photocatalytic properties of novel Bi_2AlVO_7, J. Hazard. Mater., **164**(2–3),781–789 (2009). doi.org/10.1016/j.jhazmat.2008.08.088.

7. E. Wahyuni, N. Aprilita, H. Hatimah, A. Wulandari, and M. Mudasir. Wahyuni, Removal of toxic metal ions in water by photocatalytic method, Am. Chem. Sci. J., **5**(2),194–201 (2015). doi:10.9734/acsj/2015/13807.

8. P. Benjwal, M. Kumar, P. Chamoli, and K.K. Kar, Enhanced photocatalytic degradation of methylene blue and adsorption of arsenic (III) by reduced graphene oxide (rGo)–metal oxide (TiO_2/Fe_3O_4) based nanocomposites, RSC Adv., **5**(89), 73249–73260 (2015). doi:10.1039/c5ra13689j.

9. B. Das, M. Devi, S. Deb, and S. Dhar, Boosting photocatalytic property of graphitic carbon nitride with metal complex fabrication for efficient degradation of organic pollutants, Chemosphere., **323**, (2023). doi: 10.1016/j.chemosphere.2023.138230.

10. A. Akhundi and A. Habibi-Yangjeh, Graphitic carbon nitride nanosheets decorated with $CuCr_2O_4$ nanoparticles: Novel photocatalysts with high performances in visible light degradation of water pollutants, J. Colloid Interface Sci., **504**, 697–710 (2017). doi: 10.1016/j.jcis.2017.06.025.

11. S. Dahiya, A. Sharma, and S. Chaudhary, Synthesis of phytoextract-mediated Ag-doped graphitic carbon nitride (Ag GCN) for photocatalytic degradation of dyes, Environ. Sci. Pollut. Res., **30**, 25650–25662 (2023). doi.org/10.1007/s11356-023-25359-0.

12. P. Parthipan, L. Cheng, A. Rajasekar, M. Govarthanan, and A. Subramanian, Biologically reduced graphene oxide as a green and easily available photocatalyst for degradation of organic dyes, Environ. Res., **196**, (2021). doi: 10.1016/j.envres.2021.110983.

13. J. Gogoi, A.D. Choudhury and D. Chowdhury, Graphene oxide clay nanocomposite as an efficient photo-catalyst for degradation of cationic dye, Mater. Chem. Phys., **232**, 438–445 (2019). doi: 10.1016/j.matchemphys.2019.05.010.

14. X. Jin, N. Li, X. Weng, C. Li, and Z. Chen, Green reduction of graphene oxide using eucalyptus leaf extract and its application to remove dye. Chemosphere., **208**, 417–424 (2018). doi: 10.1016/j.chemosphere.2018.05.199.

15. L. Yuan, W. Liu, and W. Zhang, Potassium-doped g-C_3N_4 enables efficient visible-light-driven dye degradation, Environ. Sci. Pollut. Res., **30**(20), 58276–58281 (2023). doi:10.1007/s11356-023-26520-5.

16. C.Y. Kuo, C.H. Wu, J. T. Wu, and Y. R. Chen. Synthesis and characterization of a phosphorus-doped TiO_2 immobilized bed for the photodegradation of bisphenol A under UV and sunlight irradiation, React. Kinet. Mech. Catal., **114** (2), 753-766 (2014). doi.org/10.1007/s11144-014-0783-2.

17. T. H. Pham, N.M. Viet, P.T. Hoai, S. H. Jung, and T. Kim, Graphitic carbon nitride metal-free photocatalyst for the simultaneous removal of emerging pharmaceutical pollutants in wastewater, Environ. Res., **231**, (2023). doi: 10.1016/j.envres.2023.116246.

18. S. A. Al-Zahrani,M. B. Patil, S. N. Mathad, A. Y. Patil, A. Al Otaibi, N. Masood, D. Mansour, A. Khan, V. Gupta, N. S. Topare, A. Somya and M. Ayyar. Photocatalytic azo dye degradation using graphite carbon nitride photocatalyst and UV-A irradiation. Crystals, **13**(4), 577, (2023). doi.org/10.3390/cryst13040577.

19. S. K. Ben, S. Gupta, A. K. Harit, K. K. Raj and V. Chandra. Enhanced photocatalytic degradation of reactive red 120 dye under solar light using $BiPO_4$-g-C_3N_4 nanocomposite photocatalyst, Environ. Sci. Pollut. Res., **29**(56), 84325–84344 (2022). doi:10.1007/s11356-022-21675-z.

20. I. Dobrosz-Gomez, M.A. Gomez-Garcia, S.M. Zamora, E. Pavas, and J. Bojarska, Transition metal loaded TiO_2 for phenol photo-degradation, **18**,1170–1182 (2015). doi:10.1016/j.crci.2015.03.006.

21. M. Lei, N. Wang, L. Zhu, Q. Zhou, and G. Nie. Environmental Photocatalytic reductive degradation of polybrominated diphenyl ethers on CuO/TiO_2 nanocomposites: a mechanism based on the switching of photocatalytic reduction potential being controlled by the valence state of copper. Appl. Catal. B: Environ. **182**,414–423 (2016). doi.org/10.1016/j.apcatb.2015.09.031.

22. J. Xie, Z. Zhou, Y. Lian, Y. Hao, and P. Li, Synthesis of α-Fe_2O_3/ZnO composites for photocatalytic degradation of pentachlorophenol under UV–vis light irradiation, Ceram. Int., **41**, 2622–2625 (2015). doi:10.1016/j.ceramint.2014.10.043.

23. E. D. Sherly, J.J. Vijaya, and L.J. Kennedy, Visible-light-induced photocatalytic performances of ZnO–CuO nanocomposites for degradation of 2,4-dichlorophenol, Chinese J. Catal., **36**, 1263–1272 (2015). doi:10.1016/S1872-2067(15)60886-5.

24. K. Vignesh, A. Suganthi, M. Rajarajan, and S.A. Sara, Photocatalytic activity of AgI sensitized ZnO nanoparticles under visible light irradiation, Powder Technol., **224**, 331–337 (2012). doi:10.1016/j.powtec.2012.03.015.

25. K. Vignesh, R. Hariharan, M. Rajarajan,and A. Suganthi. Visible light assisted photo catalytic activity of TiO_2-metal vanadate (M = Sr, Ag and Cd) nanocomposites, Mater. Sci. Semicond. Proc., **16**,1521–1530 (2013). doi:10.1016/j.mssp.2013.04.025.

26. C. Karunakaran and S. Senthilvelan, Photocatalysis with ZrO_2: Oxidation of aniline, J. Mol. Catal. A Chem., **233**, (2005). doi:10.1016/j.molcata.2005.01.038.

27. K. Vinodgopal, I. Bedja, and P.V. Kamat, Nanostructured semiconductor films for photocatalysis: Photoelectrochemical behavior of SnO_2/TiO_2 composite systems and its role in photocatalytic degradation of a textile azo dye, Chem. Mater., **8**, 2180-2187 (1996a). doi: 10.1021/es00003a037.

28. M.E. Fabiyi and R.L. Skelton, Photocatalytic mineralization of methylene blue using buoyant TiO_2-coated polystyrene beads, J. Photochem. Photobiol. A Chem., **132**, 121-128 (2000). doi.org/10.1016/S1010-6030(99)00250-6.

29. G. Sivalingam, K. Nagaveni, M.S. Hegde, and G. Madras. Photocatalytic degradation of various dyes by combustion synthesized nano anatase TiO_2, Appl. Catal. B Environ., **45**, 23-38 (2003).

30. Y. Tan, Z. Shu, J. Zhou, T. Li, W. Wang, and Z. Zhao, One-step synthesis of nanostructured g-C_3N_4/Tio_2 composite for highly enhanced visible-light photocatalytic H_2 evolution, Appl. Catal. B: Environ., **230**, 260–268 (2018).

31. Y. Zeng, X. Liu, C. Liu, L. Wang, S. Luo, and Y. Pei. Scalable One-step production of porous oxygen-doped g-C_3N_4 nanorods with effective electron separation for excellent visible-light photocatalytic activity, Appl. Catal. B: Environ., **224**, (2018). doi: 10.1016/j.apcatb.2017.10.042.

32. C. Li, Z. Sun, Y. Xue, G. Yao, and S. Zheng, A facile synthesis of g-C_3N_4/TiO_2 hybrid photocatalysts by sol–gel method and its enhanced photodegradation towards methylene blue under visible light, Adv. Powder Tech., **27**(2), 330–337 (2016).

33. K.C. Christoforidis, T. Montini, E. Bontempi, S. Zafeiratos, J. Jaén, and P. Fornasiero, Synthesis and photocatalytic application of visible-light active β -

Fe_2O_3 /g-C_3N_4 hybrid nanocomposites, Appl. Catal. B: Environ.,**187**, 171–180 (2016).

34. J. Hong, X. Xia, Y. Wang, and R. Xu. Mesoporous carbon nitride with in situ sulfur doping for enhanced photocatalytic hydrogen evolution from water under Visible light, J. Mater. Chem., **22**(30), (2012).
35. C. Bian, Y. Wang, Y. Yi, S. Shao, P. Sun, and X. Dong, Enhanced photocatalytic activity of S-doped graphitic carbon nitride hollow microspheres: Synergistic effect, high-concentration antibiotic elimination and antibacterial behavior, J. Colloid Interface Sci., **643**, 256–266 (2023). doi: 10.1016/j.jcis.2023.04.034.
36. Q. Gao, Q. Lei, R. Miao, M. Gao, and H. Liu, Bi-doped graphitic carbon nitride nanotubes boost the photocatalytic degradation of rhodamine B, New J. Chem., **46**(8), 3588–3594 (2022).
37. Y. Xie, J. Wu, C. Sun, Y. Ling, S. Li, and J. Zhao. La_2O_3-modified graphite carbon nitride achieving the enhanced photocatalytic degradation of different organic pollutants under visible light irradiation, Mater. Chem. Phys., **246**, (2020). doi: 10.1016/j.matchemphys.2020.122846.
38. N. A. Hadadi, U. Baig, M. A. Gondal, M. J. and S. Mohamed, Pulsed laser induced synthesis of graphitic carbon nitride-cadmium selenide nanocomposite for photo-catalytic degradation of organic dyes, and electro-catalytic hydrogen evolution reaction, Colloids and Surf. A: Physicochem. Eng. Asp., **658**, (2023). doi: 10.1016/j.colsurfa.2022.130711.
39. M.-L. Chen, S.-S. Li, L. Wen, and Z. Xu, Exploration of double Z-type ternary composite long-afterglow/graphitic carbon nitride metal–organic framework for photocatalytic degradation of methylene blue, J. Colloid and Interface Sci., **629**, 409–421 (2023). doi: 10.1016/j.jcis.2022.08.189.
40. A. Ahmed, R. Alabada, M. Usman, A. A. Alothman, M. K. Tufail, and S. Mohammad, Synthesis of visible-light-responsive lanthanum-doped copper ferrite/graphitic carbon nitride composites for the photocatalytic degradation of toxic organic pollutants, Diam. Relat. Mater., **141**, (2024). doi: 10.1016/j.diamond.2023.110630.

41. F. Sousani, S.K. Sadrnezhaad, P. Abachi, and H. Mahtabpour, $Ni_{0.8}Co_{0.2}/Zn_{0.8}Cd_{0.2}$ S/g-C_3N_4 ternary nano-photocatalyst for improved visible-light-driven photocatalytic H_2 evolution and pollutants degradation, Int. J. Hydrog. Energy, **51**, 281–299 (2024).

42. M. S. Nivetha, N. Abirami, and R. Arulmozhi, A novel g-C_3N_4@biTiO_2/NIO ternary heterostructure photocatalysts for effective degradation of tetracycline under light illumination, Inorg. Chem. Commun., **159**, (2024). doi: 10.1016/j.inoche.2023.111778.

43. P. Kumawat, M. Joshi, R. Ameta, and S. C. Ameta, Photocatalytic degradation of basic fuchsim over quaternary oxide iron zinc cuprate ($FeZn_2Cu_3O_{6.5}$), Adv. Appl. Sci. Res., **6**(7), 209–215 (2015).

44. H. Abbasi-Asl, M.M. Sabzehmeidani, M. Ghaedi, and Z. Moradi, Bifunctional quaternary magnetic composite as efficient heterojunctions photocatalyst for simultaneous photocatalytic visible light degradation of dye and herbicide pollutants from water and bacterial disinfection, J. Environ. Manage., **345**, (2023). doi: 10.1016/j.jenvman.2023.118656.

45. Akhundi, and A. Habibi-Yangjeh, High performance magnetically recoverable G-C_3N_4/Fe_3O_4/Ag/Ag_2SO_3 plasmonic photocatalyst for enhanced photocatalytic degradation of water pollutants, Adv. Powder Technol., **28**(2), 565–574 (2017). doi: 10.1016/j.apt.2016.10.025.

46. M. Qarajehdaghi, A. Mehrizad, P. Gharbani, and G.H. Shahverdizadeh, Quaternary composite of CdS/G-C_3N_4/RGO/CMC as a susceptible visible-light photocatalyst for effective abatement of ciprofloxacin: Optimization and modeling of the process by RSM and ann, Proc. Safety Environ. Prot., **169**, 352–362 (2023). doi: 10.1016/j.psep.2022.11.030.

47. H. P. Gogoi, G. Bisoi, P. Barman, A. Dehingia, S. Das, and A. P. Chowdhury, Highly efficient and recyclable Quaternary Ag/Ag_3PO_4–BiOBr–C_3N_4 composite fabrication for efficient solar-driven photocatalytic performance for anionic pollutant in an aqueous medium and mechanism insights, Optic. Mater., **138**, (2023). doi: 10.1016/j.optmat.2023.113712.

48. V. Hasija, A. Sudhaik, P. Raizada, A. Hosseini-Bandegharaei, and P. Singh, Carbon quantum dots supported AgI /ZnO/phosphorus doped graphitic carbon nitride as Z-scheme photocatalyst for efficient photodegradation of 2, 4-dinitrophenol. J. Environ. Chem. Eng., **7**(4), (2019). doi: 10.1016/j.jece.2019.103272 .

49. A. Kumar, G. Sharma, Mu. Naushad, A.A. Ghfar, and F.J. Stadler, Quaternary magnetic biocl/g-C_3N_4/Cu_2O/Fe_3O_4 nano-junction for visible light and solar powered degradation of sulfamethoxazole from aqueous environment, J. Chem. Eng., **334**, 462–478 (2018). doi: 10.1016/j.cej.2017.10.049.

50. M. Mousavi, A. Habibi-Yangjeh, and M. Abitorabi, Fabrication of novel magnetically separable nanocomposites using graphitic carbon nitride, silver phosphate and silver chloride and their applications in photocatalytic removal of different pollutants using visible-light irradiation, J. Colloid. Inter. Sci., **480,** 218–231 (2016).

51. L. Wang, Y. Li, and P. Han, Electrospinning preparation of g-C_3N_4/Nb_2O_5 nanofibers heterojunction for enhanced photocatalytic degradation of organic pollutants in water, Sci. Rep., **11**, 22950 (2021). doi. org/10.1038/s41598-021-02161-x.

52. R.S. Sahu, Y.-H. Shih, and W.-L. Chen, New insights of metal free 2D graphitic carbon nitride for photocatalytic degradation of bisphenol A, J. Hazard. Mater., **402**, (2021). doi: 10.1016/j.jhazmat.2020.123509.

53. J. Guo, Y. Sun, R. Xiang, H. Xiang, Z. Chen, F. Zhang, and F. Liu, One-step synthesis of porous thin-layered graphitic carbon nitride for enhanced photocatalytic dye degradation, Colloids Surf. A Physicochem. Eng. Asp. Colloid Surface A., **671**, 131600 (2023). doi.org/10.1016/j.colsurfa.2023.131600.

54. S. Habib, M. Serwar, H. M. Siddiqi, U. A. Rana, F. Liaqat, and A. Shabbir, A photocatalytic dye-degradation study on methylene blue by graphitic nitride-based polyimides synthesized via a facile thermal-condensation approach, J. Environ. Chem. Eng., **10**(3), (2022). doi: 10.1016/j.jece.2022.107747.

55. D. Lyu, G. Yu, W. Cao, and C. Hu, Efficient destruction of pollutants in water by a dual-reaction-center fenton-like process over carbon nitride compounds-complexed cu (II)-$CuAlO_2$, Environ. Sci. Technol., **52**, 4294–4304 (2018).

56. C. Jin, J. Kang, Z. Li, M. Wang, Z. Wu, and Y. Xie, Enhanced visible light photocatalytic degradation of tetracycline by MoS_2/Ag/g-C_3N_4 Z-scheme composites with peroxymonosulfate, Appl. Surf. Sci., **514**, (2020). doi:10.1016/j.apsusc.2020.146076.

57. R. Li, J. Huang, M. Cai, Z. Xie, Q. Zhang, Y. Liu, and H. Liu, Activation of peroxymonosulfate by Fe doped g-C_4N_4 /graphene under visible light irradiation for trimethoprim degradation, J. Hazard. Mater., **384,** (2020). doi: 10.1016/j.jhazmat.2019.121435.

58. L. Wang, X. Guo, Y. Chen, S. Ai, and H. Ding, Cobalt-doped g-C_3N_4 as a heterogeneous catalyst for photo-assisted activation of peroxymonosulfate for the degradation of organic contaminants, Appl. Surf. Sci., **467–468**, 954–962 (2019).

❐❐❐

CHAPTER – II

THE PRESENT WORK

CONTENTS

2.1 GRAPHITIC CARBON NITRIDE

The general formula of graphitic carbon nitride (g-CN) is g-C_3N_4. It is a material that contains carbon and nitrogen with little hydrogen as impurity. These are connected through tris- triazine-based pattern. It is very important organic material which is used mostly as semiconductor. It has very high stability even at more than temperature 500 ˚C and it is hard enough. The band gap of graphitic carbon nitride is low [2.7 eV]. The graphitic carbon nitride is pale yellow in colour. The structure of graphitic carbon nitride with the tri-S-triazine is most stable, (Fig. 2.1).

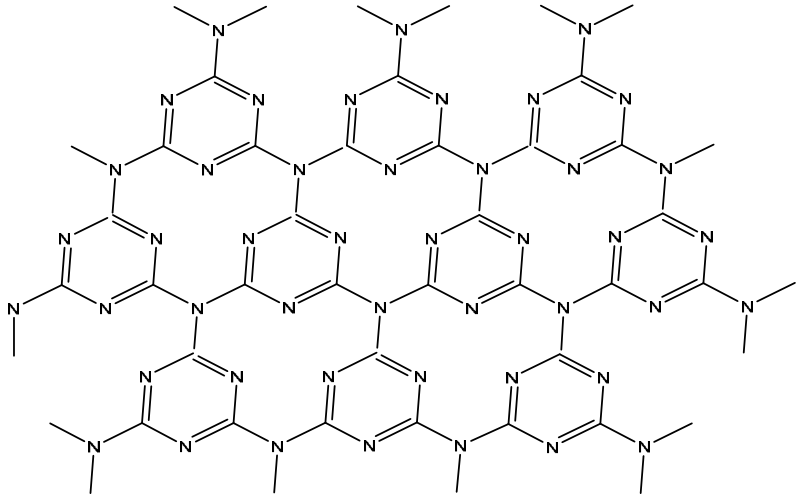

Fig. 2.1: Structure of g-C_3N_4

Graphitic carbon nitride is a metal-free conjugated polymer having two-dimensional (2D) nanosheets like structure. It is electron-rich in properties. It can be made by polymerization of melamine, cyanamide or dicyandiamide.

As it consists of layers, it can be converted into different morphologies (nanosheets, quantum dots, spherical, nanotubes. bulky, tubular and flaky. It is prepared by hydrothermal, solvothermal and thermal polymerization methods.

The graphitic carbon nitride has gained attention all over the globe as it can find applications as sensors for heavy metals, organic contaminants, pharmaceuticals and biomolecules due to its larger surface area and biocompatibility (**Fig. 2.2)**

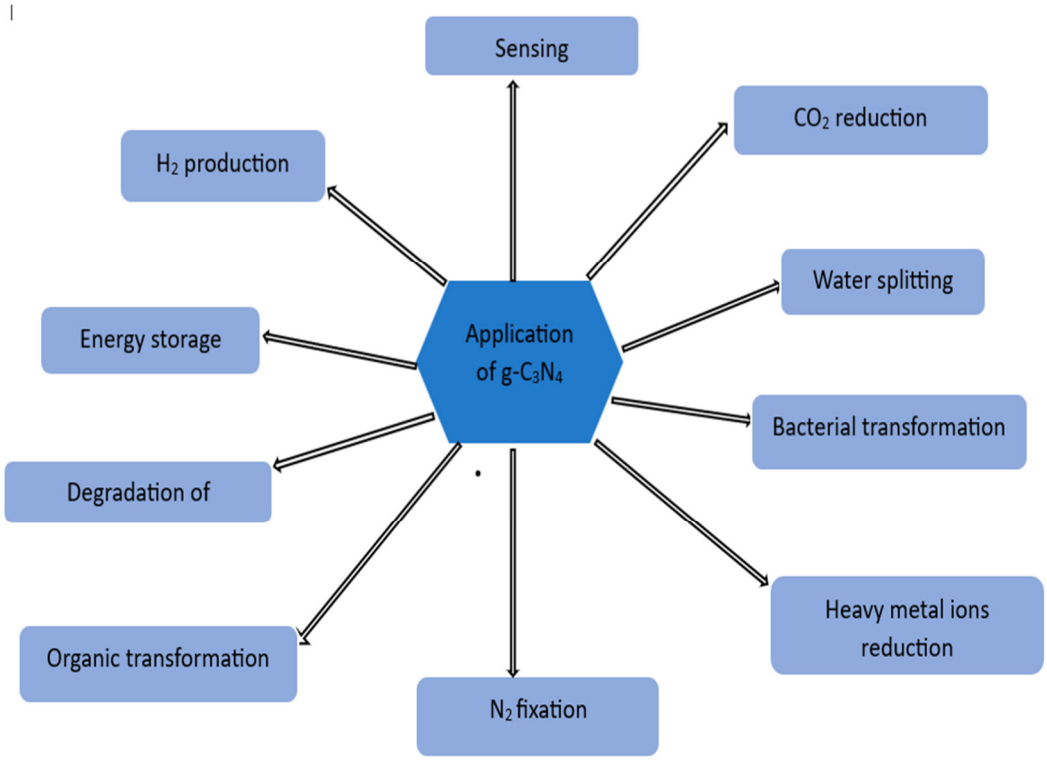

Fig. 2.2: Applications of g-C_3N_4

Graphitic carbon nitride is a metal-free semiconductor, serving as a medium band gap photocatalyst with a commendable response to visible light, extending up to 460 nm. However, pristine g-C_3N_4 is typically hindered by insufficient solar light absorption, low surface area, and rapid recombination of photogenerated electron-hole pairs; thereby, limiting its photocatalytic efficiency. Various types of modifications can be implemented to enhance the photocatalytic performance of g-C_3N_4.

- Coupling with other semiconductors,
- Conjugation with carbon nanomaterials,
- Element doped g-C_3N_4 (X-g-C_3N_4),
    (i) Metal doping, and
    (ii) Non-metal doping
- Core-shell structured g-C_3N_4, and
- Vacancy engineered g-C_3N_4.

2.2 PHOTOCATALYTIC DEGRADATION

2.2.1 Dyes

Ganesan et al.[1] tuned physiochemical properties of g–C_3N_4 by direct thermal exfoliation (TE–g–C_3N_4) Later, they used it for photocatalytic degradation of rhodamine B (RhB), methylene blue (MB), and methyl orange (MO). It was reported that degradation efficiencies for RhB, MB and MO were $95 \pm 0.4\%$, $92 \pm 0.18\%$ and $93 \pm 0.31\%$, respectively in an hour under UV light irradiation. It was also revealed that TE–g–C_3N_4 had higher surface area (48.20 m^2g^{-1}) as compared to bulk g–C_3N_4 (5.03 m^2g^{-1} It was also confirmed that superoxide radicals played an important role in the photodegradation of dye, as compared to a hydroxyl radical ($^{\bullet}OH$) and the photo-induced holes (h^+), This as-prepared TE–g–C_3N_4 also displayed excellent stability for up to five cycles with only a slight decrease in its activity from 92 to 86.2%.

Sewnet et al.[2] synthesized graphitic carbon nitride using mixtures of thiourea and urea at temperatures of calcination ranging from 500 to 650 °C for 3 h in air. It was reported that 94.83% rhodamine B (RhB) could be removed using g-C_3N_4 calcined at 600 °C within 3 h under visible LED light irradiation.

Nguyen et al.[3] synthesized water-dispersible graphitic carbon nitride using some nitrogen-rich organic precursors such as thiourea, urea, melamine and dicyandiamide via thermal treatment. The photocatalytic degradation of methylene blue (MB) was observed in presence of as-prepared g-C_3N_4**.** It has high surface area, increased band gap, and reduction in the recombination rate of photogenerated electron-hole pairs.

de Lima et al.[4] synthesized mesoporous graphitic carbon nitride using surfactant Tween-40. It was used as a visible-light active photocatalyst in degrading rhodamine B. It was reported that 93.0% rhodamine B could be degraded by as-prepared catalyst after 1 h under visible-light irradiation, while mesoporous graphitic carbon nitride and bulk graphitic carbon nitride with Pluronic F127 could degrade only 86.0 and 30.5% of rhodamine B, respectively.

Nunna et al.[5] fabricated mesostructured graphitic carbon nitride (MCN) composites from Ag-doped melamine at room temperature. It was reported that Ag nanoparticles were distributed uniformly on the surface of MCN sheets, The photocatalyst degradation of crystal, and violet, methylene blue was observed, which

was more than 96% in presence of MCN/Ag-MCN composite. Sidewise, photocatalytic hydrogen evolution (5.24 mmol. $g^{-1}.h^{-1}$) was also observed.

Utomo et al.[6] modulated particle size and morphology of ZnO by variation of pH (8.0, 9.0, 10.0, and 11.0). It was observed that at higher pH (10.0), smaller particle size and cone-like strcture was there on the edge of ZnO particle. Highest MB degradation (97.7%) could be achieved with this as-prepared composite in 150 min.

Zhao et al.[7] used 0.75 wt % 2,3-pyridinedicarboxylic anhydride (PDA) as dopant to modifiy graphitic carbon nitride with ultrarace doping (3MCN-PDA3). It was reported that photodegradation efficiency of rhodamine B (RhB) over as-prepared composite reached 92.4% in 1 h under visible light and almost complete removal (99.2%) was observed in 200 min.

Bandoh et al.[8] synthesized cobalt and graphitic carbon nitride (g-C_3N_4) co-doped ZnO through co-precipitation and used for eosin yellow degradation under visible light. It was reported that a marginal rise in absorbance was observed in the visible region due to decrease in band gap from 3.10 to 2.52 eV. It was observed that ZnO has an average crystallite size of 42 nm. The optimal photocatalytic performance was observed with 0.8 % Co-doped ZnO-g-C_3N_4, which could degrade 96 % of eosin yellow in 3 h.

Amritha and Badhulika.[9] prepared vanadium oxide and graphitic carbon nitride nanocomposite and used for degradation of methylene blue (MB) and rhodamine B (RhB). The band gap of as-prepared nanocomposite was determined as 1.89 eV. It was reported that as-synthesized nanocomposite exhibited an excellent degradation with 100 and 90% degradation of RhB and MB, respectively, within 1 h under daylight. It was also confirmed that hydroxyl and oxygen anion ($O_2^{-\bullet}$) radicals were primary oxidizing species in the degradation.

Lyu et al.[10] prepared three dimensions (3D) flower-shaped g-C_3N_4/MoS_2 composite by immobilizing molybdenum disulfide on carbon nitride. The photocatalytic performance of this composite was observed under simulated sunlight. This as-prepared composite could remove about 98 % of MB within 1 h and retained its activity to 96.4 % after 5 cycles. The apparent rate constant of this degradation was 0.0523 min^{-1}, which was 13.9, 11.5, and 8.2 times higher as compared to MoS_2, g-C_3N_4 and C_3N_4 with structural defects.

Naz et al.[11] prepared Cu and Fe doped nanocomposites $NiCo_2O_4$/g-C_3N_4 with different dopant concentrations via precipitation and ultrasonication routes. It was reported that $NiCo_2O_4$ nanoparticles have spherical shape (ranging between 18 to 32 nm). They also evaluated photocatalytic activity of doped $Ni_{0.75}Cu_{0.25}Co_{1.5}Fe_{0.25}O_4$/g-$C_3N_4$ ($NCCF_3$/g-CN) for removal of Congo red (CR) and rhodamine B (RhB) under visible light irradiation. It was observed that $NCCF_3$/g-CN nanocomposite could remove 89 % of the dye as compared to undoped nanocomposite (50 %). It was attributed to efficient separation of charge carriers by migration of photo-induced electrons from g-C_3N_4 surface to $NiCo_2O_4$.

Salehi et al.[12] prepared ternary heterogeneous Mg–Al LDH g-C_3N_4 XAg_3PO_4Y (X = wt % of g-C_3N_4 with respect to Mg–Al layered double hydroxide (LDH) and Y = wt % of Ag_3PO_4 loaded on Mg–Al LDH g-C_3N_4 30) nanocomposite and used for degradation of methylene blue (MB). The photocatalytic removal of MB under 150 W mercury lamp increased significantly in the presence of the composite of Mg–Al LDH and g-C_3N_4 as compared to Mg–Al LDH alone. It was observed that highest photodegradation activity (99%) could be obtained using this as-prepared composite. It was also revealed that effective agents in the photodegradation of MB were holes and hydroxyl radicals as evident from scavenger tests.

Qiaofang et al.[13] prepared vermiculite g/C_3N_4/TiO_2 composites from TiO_2,melamine and vermiculite. It was reported that the best sample was obtained with calcination at 200 °C for 3 h. It was observed that 99.33 % degradation of methylene blue (MB) could be achieved. This composite still has good degradation efficiency even after using it four times.

Huang et al.[14] prepared Ag_3PO_4-g-C_3N_4 photocatalyst. It was reported that as-obtained Ag_3PO_4-g-C_3N_4 heterojunction exhibited excellent photodegradation performance for removal of methyl orange (MO) and rhodamine B (RhB). It was also revealed that its performance remained more than 90% after even six cycles.

Bhakar et al.[15] synthesized Z-scheme heterojunction-based ZnO-$MnWO_4$g-C_3N_4 ternary nanocomposite via coprecipitation and ultrasonication. It was observed that 94.5% methylene blue (MB 10 ppm) could be degraded under visible light irradiation using 10 mg of catalyst within 50 min. Out of all samples, ZnO-$MnWO_4$g-

C_3N_4 (1CN:1ZM) (1:1) exhibited excellent degradation (94.50%) towards MB as compared to two other ratios (1:2 and 2:1). It was found that degradation rate was 2.57 times more than the pure g-C_3N_4.

An et al.[16] synthesized zinc oxide-decorated graphitic carbon nitride composite (ZnO/gC_3N_4 or ZCN). It was found that ZnO has a spherical shape with an average diameter of 30–80 nm and it is distributed uniformaly on the CN sheets. They also used ZCN for photodegradation of methylene blue (MB), which could degrade 99.16% dye after 3 h of visible irradiation. The optimal conditions obtained were: pH 9, 50 mg of catalyst, and 10 mg L^{-1} of dye concentration. Its degradation ability for malachite green (MG) and methyl orange (MO) was about 96.42 and 57.57 %, respectively. The reusability of this composite was also ascertained as only 10 % decrease was there after five cycles.

Lan et al.[17] prepared oxygen-phosphorus-codoped graphitic carbon nitride (O, P-GCN) via thermal decomposition of oxalic acid, urea, and ammonium phosphate. This as-prepared O, P-GCN photocatalyst was used for degradation of rhodamine B (RhB). It was reported that 1 wt% oxygen and phosphorus in GCN improved its photocatalytic performance, significantly and degradation efficiency of RhB could reach up to 97.25%. It was found that various kinds of reactive species were generated such as hydroxyl radicals, superoxide radicals, and holes. There played a major role in the photocatalytic degradation of RhB.

Kumaravel et al.[18] modified graphitic carbon nitride g-C_3N_4 (GCN), with tungsten oxide WO_3/g-C_3N_4 (WGCN) as well as tungsten oxide and silver nanoparticles WO_3/Ag/g-C_3N_4 (WAgGCN) also. They used this WAgGCN composite for photocatalytic decolorization of crystal violet (95%), and methylene blue (98%). It has high chemical stability and excellent recyclability also. A decrease in total organic carbon (TOC) and chemical oxygen demand (COD) also confirmed that dyes were mineralized.

Vuggili et al.[19] synthesized nitrogen-doped g-C_3N_4/CoS (CSNG) nanocomposites by polycondensation-hydrothermal method with deferent concentrations of nitrogen-doped g-C_3N_4 (NG). It was reported that industrial real samples (RS.I and RS. II,) could be degraded by 60 and 41% in 20 and 70 min, respectively. It was also observed that a mixture of RS I with methylene blue (MB) was degraded 79 and 98% in 20 min, while

its mixture with RS II degraded 72% and 99% in 40 min. It was revealed that superoxide anion radical played an important role in the photodegradation of MB. It also exhibited excellent photostability with a loss of just 0.7% in five consecutive cycles.

Zhou et al.[20] synthesized NiS-loaded on S-doped carbon nitride photocatalysts. The activities of these photocatalysts were evaluated in photodegradation of RhB under visible-light irradiation. It was reported that the photocatalyst (SCN/NiS-1) with 0.89 wt% sulfur doping and 1 wt% NiS loading showed excellent photocatalytic activity of removing 98.5% RhB in 15 min.

Onwudiwe et al.[21] prepared graphitic carbon nitride and copper-doped bismuth sulphide heterostructure (g-C_3N_4/Cu–Bi_2S_3) by solvothermal method. Photocatalytic activity was investigated for degradation of methyl orange. It was reported that about 95% degradation of methyl orange was achived on using this heterostructure photocatalyst. It was also revealed that superoxide radicals and holes played major roles in this photocatalytic degradation.

Kumaravel et al.[22] fabricated x% Ag/g-C_3N_4 (x% AgGCN) composite with different weight percentages (x = 1, 3, 5, and 7 wt.%). It was reported that 99% photodegradation rate of methyl orange could be achieved under solar light irradiation with 5% AgGCN composite photocatalyst. It was observed that degradation with 5% AgGCN was 14.83 times more than with GCN catalyst alone. This photocatalyst could retain good efficiency up to five successive cycles. It was also indicated that $O_2^{\bullet-}$ radicals played a crucial role in degradation of MO.

Amritha and Badhulika.[23] fabricated $NaTiO_3$/g-C_3N_4 heterojunction photocatalyst and used it for removal of methylene blue (MB) and crystal violet (CV) dyes and their binary mixture under sunlight irradiation. It was reported that $NaTiO_3$ nanoparticles were aggregated on g-C_3N_4 sheet-like surface. The band gap of as-prepared sample was found to be 2.3 eV. It was observed that complete degradation of MB, and CV was observed within 25 min, while binary mixture took 20 min for complete degradation. It was also indicated that the radical species h^+ and $^{\cdot}OH$ played the major role in the photocatalytic degradation of these dyes. It was also revealed that it has good stability up to five cycles.

Chopan and Chishti[24] fabricated polypyrrole (PPy) and graphitic carbon nitride (g-C_3N_4) nanoparticles on ZnO surface as g-C_3N_4/PPy/ZnO (GPZ). The

photocatalytic activity of as-prepared photocatalyst was evaluated for degradation of RhB where it could degrade 99.0% of RhB in 1h at pH 7.

2.2.2 Pharmaceutical drugs

Falletta et al.[25] synthesized graphitic carbon nitride as powder and alginate floating beads, using two different precursors (urea and melamine). These were than used for their activity in photodegradation of diclofenac under solar light irradiation. It was reported that almost 99 and 90% degradation for diclofenac and isoproturon could be achieved. The floating photocatalysts displayed good stability during recycling experiments and it can be used up to five cycle.

Liu et al.[26] prepared layered phosphorus-doped carbon nitride ($HPCN_{0.5}$) by hydrothermal route and used for photocatalytic degradation of dinotefuran. On addition of phosphorous acid, $HPCN_{0.5}$ (tube-like structure) was obtained, where planar sheets were stacked inside these tubes. It was reported that the degradation efficiency of dinotefuran was six times higher as compared to bulk g-C_3N_4. It was observed that photodegradation proceed through demethylation and hydroxylation steps.

Pham et al.[27] synthesized and used graphitic carbon nitride in alkaline conditions for photodegradation of carbamazepine (CZ) and acetaminophen (AP) in wastewater. This was reported that it exhibited high removal efficiencies of 98.6 and 89.5% for AP and CZ, respectively. Increasing the catalyst dose facilitated the removal of antibiotic contaminants with an optimum catalyst dose of 0.1 g, achieving a photodegradation efficiency of 90.2% and 82.7% for AP and CZ, respectively. It was also revealed that as synthesized photocatalyst could remove over 98% of AP within 2 h, which was 2.14 times faster than removal of CZ. The participation of highly reactive oxidants such as hydroxyl and superoxide radical were confirmed. A good stability of g-CN was there in treating pharmaceuticals as it can be reused for three repeated cycles.

Tao et al.[28] synthesized carbon-defective carbon nitride (with pore structure) via thermal polymerization at 600°C (CCN-600) and used it for photodegradation of mepivacaine, lidocaine, and ropivacaine. It was reported that degradation followed pseudo-first-order kinetics with 5.05×10^{-2} min^{-1} rate constant, which was about 2.5 times higher as compared to g-C_3N_4. It was reported that superoxide radical played a major role in this degradation.

Villanueva et al.[29] prepared coupled g-C_3N_4 /TiO_2 and used it for degradation of ciprofloxacin, tetracycline, and ibuprofen under simulated solar irradiation. They used SBA-15 silica as hard template. The photocatalytic activity was examined through the degradation of tetracycline, ciprofloxacin, and ibuprofen. It was observed that dispersion of TiO_2 nanoparticles could be obtained on using a mesoporous g-C_3N_4 sample. It was also revealed that samples with 1 wt.% g-C_3N_4 displayed highest photocatalytic performance in the degradation of ciprofloxacin, tetracycline, and ibuprofen.

Govindasamy et al.[30] constructed eggshell derived hydroxyapatite nanoparticles entrenched on two-dimensional g-C_3N_4 nanosheets. They evaluated photocatalytic performance of this as-prepared HAp/gC_3N_4 photocatalyst for degradation of doxycycline under UV–visible light exposure. It was reported that as-prepared photocatalyst exhibited excellent photocatalytic activity for degradation of doxycycline drug (83.08%) as compared to g-C_3N_4 and bare HAp nanosheets. It was indicated that this photocatalyst can be recycled for four times and reused without any significant loss in degradation performance.

Razavi-Esfali et al.[31] used SiO_2 clusters as template to fabricate mesoporous graphitic carbon nitride nano-clusters (NC MCN). It was reported that NC MCN exhibited high photocatalytic activity for degrading tetracycline under visible light irradiation and complete degradation of 15 mL solution of tetracycline (15 ppm) could be achieved in half an hour as compared to the bulk catalyst in more than 3 h. Furthermore, This NC MCN also exhibited high stability as it can be reused for eight consecutive cycles.

Minh Tri et al.[32] synthesized Ag-doped graphitic carbon nitride (Ag-GCN) and used it as a photocatalyst for degradation of hospital wastewater containing tetracycline (TC) under solar light. It was revealed that the highest photocatalytic degradation efficiency of TC (96.8%) was obtained in 2 h under solar light irradiation, when content of Ag doping was kept 3 mmol. The removal efficiency of TC was only 25.6 and 31.8% under dark conditions, respectively in presence of g-C_3N_4 and Ag-doped g-C_3N_4 (AgCN). It was also reported that AgGCN exhibited extremely high stability after six cycles without any significant loss in its efficiency.

Pham et al.[33] fabricated cobalt doped GCN (Co/GCN) and used it for the photodegradation of paracetamol (PC) in the wastewater. It was reported that as-

prepared Co/GCN exhibited a removal efficiency of 82.6% under sunlight in 1 h even at high PC initial concentration, which was 1.7 times higher than undoped GCN. The Co/GCN was capable of decomposing PC completely (100%) at low initial concentration of ≤ 1 mg L^{-1}.

Xu et al.[34] synthesized CeO_2/N-doped g-C_3N_4 (CeNCN) composite photocatalysts. It was observed that CeNCN exhibited excellent photodegradation of tetracycline (80.09%) within an hour, which is 7.86 and 2.29 times more than graphitic carbon nitride and N-doped GCN, respectively. It was reported that degradation efficiency of tetracycline is more than 75%, even after five cycles, which indicated its good stability.

Sun et al.[35] synthesized graphitic carbon nitride nanosheet modified with dodecyl benzene sulfonate (DBS). Its photocatalytic performance for removal of moxifloxacin (MOX) was evaluated. It was reported that this catalyst could remove high concentration of MOX, (100 mg L^{-1}) in half an hour of irradiation. They also observed the effect of different parameters on this degradation such as: pH, concentration of MOX and dosage of photocatalyst It was also claimed that DBS/CNNS hybrid is a potential visible light driven photocatalyst for elimination of high-concentrations of antibiotics in wastewater.

Zhang et al.[36] introduced a group on terminal amino group of g-C_3N_4 (G-CN) via in acetic acid under 80 °C to afford HAC-CN. It was reported that photocatalytic degradation efficiency of some antibiotics; sulfamethoxazole (SMZ), tetracycline hydrochloride (TC), and ciprofloxacin (CPFX)) over HAC-CN was significantly improved, which are 1.50, 1.50, and 1.99 times than that with G-CN. It was revealed that especially $O_2^{\bullet-}$ was dominant oxidized species in their degradations.

Rajiv et al.[37] loaded haematite on graphitic carbon nitride via hydrothermal approach and its photocatalytic activity was evaluated for degradation of ciprofloxacin (CIP). It was reported that g-C_3N_4/Fe_2O_3/UV exhibited higher degradation efficiencies than UV and g-C_3N_4/Fe_2O_3. They could achieve maximum removal of CIP (100%) and TOC (93.86%) at pH 7 in 1 h. It was also revealed that h^+ and $^{\bullet}OH$ played major role in the degradation of CIP. An excellent stability and recyclability of this composite was confirmed by five degradation cycles.

Bian et al.[38] reported S-doped g-C_3N_4 with hollow microsphere composition (SCNHM). It was reported that SCNHM had high specific surface area (~81 $m^2 g^{-1}$). The S dopant improved electronic structure so that band gap was narrowed down and promoted charge separation/transfer capability. The as-prepared SCNHM improved photocatalytic activity for degradation of tetracycline hydrochloride (TC) due to synergistic effect as compared to CN, SCN and CNHM samples. It was reported that it could eliminate high-concentration TC (50 mg L^{-1}) in 18 min, while removal efficiencies of 100 mg L^{-1} and 200 mg L^{-1} could reach 92 and 60 %, in half an hour.

Chin et al.[39] prepared GCN with different precursor (GCN-urea, GCN-thiourea and GCN-melamine). They also investigated abilities of these as-prepared photocatalyst to degrade oxytetracycline (OTC). It was reported that GCN-urea has high surface area 73.62 $m^2 g^{-1}$, as compared to 5.82 and 3.99 m^2 g^{-1} GCN-thiourea and GCN-melamine respectively. The GCN-urea has the highest band gap as 2.7 eV, and GCN-melamine and GCN-thiourea have lower band gaps as 2.3 and 2.2 eV, respectively. The highest OTC degradation was achieved by GCN-urea at ~60%, which was almost 2.5 times higher than the other two

Wang et al.[40] reported the synthesis of oxygen and terminal methyl moiety co-modified g-C_3N_4 (CNNx). It was reported that synthesized CNNx (CNN25) could achieve high photocatalytic activity for photocatalytic degradation of 74, 99, 92 and 65% sulfathiazole, tetracycline, doxycycline, and ofloxacin, respectively within 30 min under visible light.

Shen et al.[41] prepared metal-free carbon/g-C_3N_4 (CNC) photocatalyst with persulfate (PDS), (CNC-PDS) and used it for photocatalytic degradation of paracetamol (PCM) under simulated sunlight. It was reported that excellent photocatalytic activity was exhibited and PCM was completely degraded in 40 min under simulated sunlight, which was about 9.5 times more as compared to g-C_3N_4 and PDS coupled systems. It was also indicated that $O_2^{\cdot-}$, h^+ and $^1O_2$ were the main active species for degradation of PCM over CNC-PDS system under simulated sunlight, and their contribution was in order the $O_2^{\bullet-} > {}^1O_2 > h^+$.

2.3 OTHERS

Zheng et al.[42] synthesized N-deficiently porous graphitic carbon nitride, particularly UMCN, which was prepared using a mass ratio of 1: 5 for melamine to urea. It was reported that high specific surface area was (183.7 m^2g^{-1}). It was observed that UMCN exhibited higher photocatalytic activity for degradation of rhodamine B (RhB) with removal rate 99.3% within half an hour under visible light. It was also revealed that excellent recyclability is there and degradation rate of RhB still remained 95.6% even in the 7th run.

Song et al.[43] prepared graphitic carbon nitride by one-step polycondensation of urea. It was observed that it has surface area of 114 $m^2\ g^{-1}$, which permitted adsorption of the rhodamine B (RhB) dye and also its photocatalytic degradation upon light irradiation in 20 min.

Poiyamozhi and Thivya.[44] synthesized a composite of g-C_3N_4 and $NiSe_2$ via ultrasonication-assisted hydrothermal method. The band gap of this hybrid composite was found to decrease from 2.72 to 2.30 eV. The photocatalytic degradation of reactive blue 5 (RB 5) and reactive violet 5 (RV 5) was observed over $NiSe_2$/g-C_3N_4 composites. The highest degradation rates for RB 5 (86%) and RV 5 (89.4%) could be obtained with 30 % g-C_3N_4 incorporated into $NiSe_2$.

Khan et al.[45] immobilized $Ag_3PW_{12}O_{40}$ on graphitic carbon nitride (2D sheet) through grinding and prepared separately $C_3N_4Ag_3PW_{12}$ heterojunction. It was reported that C_3N_4-Ag_3PW_{12}-30% composite photocatalyst displayed efficient photocatalytic activity and removed 99 and 99.4% methylene blue and rhodamine B in 75 and 60 min respectively, whereas 26.3 and 37.7 % of methylen blue and 43.54 and 53.38 % of rhodamin B was removed by Ag_3PW_{12} and C_3–N_4 respectively.

2.3.1 Pesticides

Ejeta and Imae[46] synthesized oxygen-doped graphitic carbon nitride (Og-CN). It was then used for photocatalytic degradation of 2,4-dichlorophenoxyacetic acid (2,4-D) under UV and visible light irradiation. It was observed that degradation efficiency of Og-CN was better as compared to g-CN, and UV light was more effective than visible light. The Og-CN has good stability as there was only 4% decrease in its activity after three

photocatalytic cycles. A high total organic carbon removal (88 %) was observed in 2 h, which confirmed mineralization of 2, 4-D.

Vigneshwaran et al.[47] used graphitic carbon nitride (g-C_3N_4) incorporated into chitosan for photocatalytic degradation of an organic pesticide, chlorpyrifos (O, O-diethylO-3,5,6-trichloro-2-pyridyl phosphorothioate (CPFS)). It was reported that degradation of this insecticide showed good efficiency of about 85% on using CS/g-C_3N_4.

Liu et al.[48] used graphitic carbon nitride as a photocatalyst for photodegradation of imidacloprid which has become a research hotspot, due to its high toxicity to bees and other nontarget organisms. Photodegradation is a common method for removing imidacloprid in an aquatic environment. The g-C_3N_4 was used photodegradation of imidacloprid under visible-light illumination, which resulted in about 90% removal in 5 h. They also identified 4,5-dihydro-N-nitro-1-(3-pyridinylmethyl)-1H-imidazol-2-amine and 1-((6-chloropyridin-3-yl) methylhydroxy) imidazolidin-2-ylidenenitramide) as main photoproducts as evident from LC-MS analysis.

Zong et al.[49] synthesized modified carbon nitride (TEA-CN-30) via photochemical reduction using triethanolamine. Then it was used for photocatalytic degradation of atrazine. It was reported that about 90% atrazine degradation could be achieved in an hour. The possible degradation pathways were suggested as hydroxylation, dealkylation, and dichlorination.

2.3.2 Polycyclic Aromatic Hydrocarbon

Halim et al.[50] prepared composite of graphitic carbon nitride from different combinations of precursors through thermal polycondensation at 600°C. They used these for photocatalytic degradation of polycyclic aromatic hydrocarbons (pyrene). It was reported that best performance of composite g-C_3N_4 photocatalyst was obtained, when it was prepared from a wet mixture of guanidine carbonate and dicyandiamide precursors (mass ratio of 1:1), which could degrade 43.9 % pyrene under visible light irradiation in 4 h. It was observed that as-prepared photocatalyst was stable and can be reused up to five cycles. The holes and hydroxyl radicals were identified as the primary and secondary dominant reactive species based on scavenging studies.

Azmoon et al.[51] synthesized graphitic carbon nitride with nanorod structure (Nr-GCN). They prepared polystyrene (PS) fibrous mat and used it as a support for stabilizing nanoparticles. The performance of as-synthesized nanoparticles and photocatalytic fibers (PS/Nr-GCN) was evaluated in treatment of oilfield-produced water under visible light irradiation. It was reported that 96.6 and 98.4% removal of chemical oxygen demand (COD) could be achieved by Nr-GCN and PS/Nr-GCN, respectively at pH 4 in 150 min.

Bharathi et al.[52] synthesized g-C_3N_4–Ni nanocomposites and used for photocatalytic degradation of benzopyrene the most potent polycyclic aromatic hydrocarbons (PAH). It was reported that these nanocomposites are nanospheres with an average particle size of 22 nm. It was observed that degradation of benzopyrene increased with increasing pH till 3 h (incubation period) but afterward its percentage declined. It was also revealed that UV light enhanced degradation of benzopyrene more than sunlight.

2.3.4 Phenols

Jilani et al.[53] prepared sulfonated polyaniline, (s-PANI) graphitic carbon nitride (*g*-C_3N_4) and its nanocomposites with graphene. Different weight ratios of GN were used (1, 3, and 5%) with weight of *g*-C_3N_4. They used as-prepared nanocomposites for degrading phenol moieties. It was revealed that enhanced photocatalytic degradation of phenol was there with GN-based sulfonated s-PANI@*g*-C_3N_4/$GN_{(1–5\%)}$. An increase in photocatalytic activity was attributed to the involvement of the sp^2 carbon atoms, the interaction of the O C carbon atoms, and the high migration efficiency of charge carriers.

Rana et al.[54] synthesized metal-free graphitic carbon nitride and used for photocatalytic degradation of phenol using visible light-emitting diodes (LEDs). It was reported that exfoliated g-C_3N_4 completely degraded phenol in 90 min, while only 25% phenol could be degraded with bulk g-C_3N_4 in 3 h, because the exfoliated g-C_3N_4 has more availability of active sites, which promoted the degradation of phenol.

Kavitha and Kumar[55] prepared polymeric g-C_3N_4 (GCN) and used it as photocatalytic material for degradation of phenolic compounds (reduction of 4-nitrophenol (4-NP) to respective 4-aminophenol (4-AP)) in aqueous medium.

Photocatalysis has a potential to degrade majority of organic contaminants present in polluted water. But mostly, the photocatalysts used so far contain some metals. There is an urgent demand to search for some metal free semiconductor as a photocatalyst. In this direction, graphitic carbon nitride can be considered a suitable candidate for treatment of waste water as it is metal free as well as has a desired band gap in the range of semiconductor (Eg = 2.7 eV). Therefore, it was planned to carry out some systematic investigations for the degradation of some commonly used dyes such as; Azure A, Evans blue, Rose Bengal, Methylene blue, Rhodamine B, and Alizarin red-S in presence of graphitic carbon nitride and light.

❐❐❐

REFERENCES

1. S. Ganesan, T. Kokulnathan, S. Sumathi, and A. Palaniappan, Efficient photocatalytic degradation of textile dye pollutants using thermally exfoliated graphitic carbon nitride (TE–g–C_3N_4), Sci. Rep., **14**, 2284 (2024). doi.org/10.1038/s41598-024-52688-y.

2. A. Sewnet, E. Alemayehu, M. Abebe, D. Mani, S. Thomas, N. Kalarikkal, and B. Lennartz, Single-step synthesis of graphitic carbon nitride nanomaterials by directly calcining the mixture of urea and thiourea: Application for rhodamine B (RHB) dye degradation, Nanomaterials., **13**(4), (2023). doi;10.3390/nano13040762.

3. T. K. Nguyen, T. T. Pham, H. Nguyen-Phu, and E. W. Shin, The effect of graphitic carbon nitride precursors on the photocatalytic dye degradation of water-dispersible graphitic carbon nitride photocatalysts, Appl. Surf. Sci., **537**, (2021). doi: 10.1016/j.apsusc.2020.148027.

4. B.R.M. de Lima, N.M.P. do Nascimento, and J.R Zamian, Higher dye degradation using a visible-light photocatalyst made of mesoporous graphitic carbon nitride prepared with the tween-40 surfactant, Environ. Chem. Lett., **18**, 1413–1422 (2020). doi.org/10.1007/s10311-020-01008-7.

5. G. P. Nunna, P. Rosaiah, S. Sangaraju, G. Ramalingam, A. Jwuiyad, S. Adem, and T. J. Ko, Mesostructured graphitic carbon nitride composites with silver nanoparticle decoration as the best visible-light-driven photocatalysts for dye degradation and H_2 production, Colloids Surf. A Physicochem. Eng. Asp. Colloid surface a, **680**, (2024). doi.org/10.1016/j.colsurfa.2023.132615.

6. W. P. Utomo, P. A. I. Afifah, A. I. Rozafia, A. A. Mahardika, E. Santoso, R. Liu, and D. Hartanto, Modulation of particle size and morphology of zinc oxide in graphitic carbon nitride/zinc oxide composites for enhanced photocatalytic degradation of methylene blue, Surf. Inter., **46**, (2024). doi.org/10.1016/j.surfin.2024.104017.

7. Y. Zhao, M. Sun, F. Zhou, and G. Xu, Ultrarace aromatic anhydride dopant as intermediate island to promote charge transfer of graphitic carbon nitride for enhancing the photocatalytic degradation of rhodamine B, Langmuir, **40** (3), 1858-1868 (2024). doi: 10.1021/acs.langmuir.3c03198.

8. C. K. Bandoh, B. Y. Danu, E. S. Agorku, F. K. Ampong, and R. K. Nkum, The effect of cobalt-doped ZnO-g-C_3N_4 heterostructures on photocatalytic degradation of eosin yellow dye in water under simulated solar light, Results Mater., **21**, (2024). doi.org/10.1016/j.rinma.2023.100515.

9. V. K. Amritha and S. Badhulika, Efficient sunlight-assisted degradation of organic dyes using V_2O_3/g-C_3N_4 nanocomposite catalyst, Opt. Mater., **147**, (2024). doi.org/10.1016/j.optmat.2023.114633.

10. H. Lyu, W. Zhu, K. Chen, J. Gao, and Z. Xie, 3D flower-shaped g-C_3N_4/MoS_2 composite with structure defect for synergistic degradation of dyes, J. Water Process Eng., **57**, (2024). doi.org/10.1016/j.jwpe.2023.104656.

11. A. Naz, I. Bibi, F. Majid, A. Dahshan, Kashif Jilani, Babar Taj, Aamir Ghafoor, Zarish Nazeer, F. M. Alzahrani, and M. Iqbal, Cu and Fe doped $NiCo_2O_4$/g-C_3N_4 nanocomposite ferroelectric, magnetic, dielectric and optical properties: Visible light-driven photocatalytic degradation of RhB and CR dyes, Diam. Relat. Mater., **141**, (2024). doi.org/10.1016/j.diamond.2023.110592.

12. G. Salehi, M. Bagherzadeh, R. Abazari, M. Hajilo and D. Taherinia, Visible light-driven photocatalytic degradation of methylene blue dye using a highly efficient Mg–AL ldhg-$c_3n_4ag_3po_4$ nanocomposite, ACS Omega., **9** (4), 4581-4593 (2024). doi: 10.1021/acsomega.3c07326.

13. F. Qiaofang, T. Fangyu, and W. Ying, Preparation of vermiculite/g-C_3N_4/TiO_2 composites and their degradation of dye wastewater, Polyhedron., **247**, (2024). doi.org/10.1016/j.poly.2023.116713.

14. G. Huang, D. Zeng, P. Ke and Y. Chen, Preparation and characterization of Ag_3PO_4 g-C_3N_4 photocatalysts for dye wastewater treatment under visible-light irradiation, Inorg. Chem. Commun., **160**, (2024). doi.org/10.1016/j.inoche.2023.111889.

15. K. Bhakar, N. A. Rajpurohit, M. E. Sillanpää and D. Kumar, Design and synthesis of Z-scheme heterojunction-based ZnO-$MnWO_4$ g-C_3N_4 ternary nanocomposite for efficient methylene blue degradation, Inorg. Chem. Commun., **160**, (2024). doi.org/10.1016/j.inoche.2023.111884.

16. H. An, L. M. Huong, N. M. Dat, N. D. Hai, C. Q. Cong, N. T. H. Nam, D. N. M. Thi, H. B. Nghi, N. T. T. Huyen, D. T. Y. Oanh, M.T. Phong and N. H. Hieu, Photocatalytic degradation of organic dyes using zinc oxide-decorated graphitic carbon nitride composite under visible light, Diam. Relat. Mater.,**131**, (2023). doi.org/10.1016/j.diamond.2022.109583.

17. Z.-Y. Lan, D, Vasu, Y.-C. Liu, Y.-F. You, T.-W. Chiu and P. C. Chen, Oxygen-phosphorus-cooped graphitic carbon nitride nanosheets with better photocatalytic ability towards the degradation of rhodamine-B dyes, New J. Chem., **47**, 13117-13126 (2023). doi.org/10.1039/D3NJ02083E.

18. S. Kumaravel, M. Durai, R. Sepúlveda, E. Chicardi, S. Kumaravel, M.-J. Kim, K. Balu, I. Hasan, K. Srinivasan, and Y.-H. Ahn, Fabrication of $Ag/WO_3/g\text{-}C_3N_4$ composites for the photocatalytic degradation of harmful dyes, Opt. Mater.,**144**, (2023). doi.org/10.1016/j.optmat.2023.114322.

19. S. B. Vuggili, U. K. Gaur, T. Tyagi and M. Sharma, 2D/2D nitrogen-doped graphitic carbon nitride/cobalt sulfide nanostructures for fast photodegradation of methylene blue dye and real industrial sewage effluents, Environ. Sci.: Adv., **2**, 795-814 (2023). doi.org/10.1039/D2VA00208F.

20. G. Zhou, Z. Zhou, Y. Xia, W. Yin, J. Hou, X. Zhu, J. Yi, S. Wang, X. Ning and X. Wang, Synchronous synthesis of S-doped carbon nitride/nickel sulfide photocatalysts for efficient dye degradation and hydrogen evolution, Appl. Surf. Sci., **608**, (2023). doi.org/10.1016/j.apsusc.2022.154974.

21. D. C. Onwudiwe, V. M. Nkwe, O. C. Olatunde and H. Ferjani, Graphitic carbon nitride functionalized with Cu-doped Bi_2S_3 as a heterostructure photocatalyst for the visible light degradation of methyl orange, Ceram. Int., **49**(11), 19451-19462 (2023). doi.org/10.1016/j.ceramint.2023.03.077.

22. S. Kumaravel, C. Chandrasatheesh, G. Palanisamy, J. Lee, I. Hasan, S. Kumaravel, B. Avula, U. D. Pongiya and K. Balu, Highly efficient solar-light-active Ag-decorated $g\text{-}C_3N_4$ composite photocatalysts for the degradation of methyl orange Dye. Micromachines., **14**, (2023). doi.org/10.3390/mi14071454.

23. V. K. Amritha and S. Badhulika, A visible light-driven $NaTiO_3$/g-C_3N_4 heterojunction photocatalyst for ultra-fast organic dye degradation, New J. Chem.**, 47**, 17897-17907 (2023). doi.org/10.1039/D3NJ02907G.

24. N. A. Chopan and H.-T.-N. Chishti, Polypyrrole-decorated ZnO/g-C_3N_4 S-scheme photocatalyst for rhodamine B dye degradation: Mechanism and antibacterial activity, Mater. Today, Chem., **32**, (2023). doi.org/10.1016/j.mtchem.2023.101643.

25. E. Falletta, M. Longhi, A, D. Michele, D. C. Boffito, and C. L. Bianchi, Floatable graphitic carbon nitride/alginate beads for the photodegradation of organic pollutants under solar light irradiation, J. Clean. Production., **371**,(2022). doi.org/10.1016/j.jclepro.2022.133641.

26. X. Liu, Y. Zhou, Y. Ma, S. Fang, F. Kong, and X. Pang, Photocatalytic degradation of dinotefuran by layered phosphorus-doped carbon nitride and its mechanism, J. Photochem. Photobiol. A: Chem., **414**, (2021). doi.org/10.1016/j.jphotochem.2021.113287.

27. T. H. Pham, N. M. Viet, P. T. T. Hoai, S. H. Jung, and T. Y. Kim, Graphitic carbon nitride metal-free photocatalyst for the simultaneous removal of emerging pharmaceutical pollutants in wastewater, Environ. Res., **231**, (2023). doi.org/10.1016/j. envres.2023.116246.

28. L. Tao, H. Zhang, G. Li, C. Liao , and G. Jiang, Photocatalytic degradation of pharmaceuticals by pore-structured graphitic carbon nitride with carbon vacancy in water: Identification of intermediate degradants and effects of active species, Sci. Total Environ., **824**, (2022). doi.org/10.1016/j.scitotenv.2022.153845.

29. J. C. Villanueva, A. Vázquez, and S. Obregón, Photocatalytic degradation of pharmaceuticals through bulk and mesoporous g-C_3N_4/TiO_2 systems, J. Photocatal., **2**(2), 105-113 (2021). doi.org/10.2174/2665976X02666210122160124.

30. P. Govindasamy, B. Kandasamy, and P. Thangavelu, Biowaste derived hydroxyapatite embedded on two-dimensional g-C_3N_4 nanosheets for degradation of hazardous dye and pharmacological drug via Z-scheme charge transfer, Sci Rep., **12**, (2022). doi.org/10.1038/s41598-022-15799-y.

31. Razavi-Esfali, T. Mahvelati-Shamsabadi, H. Fattahimoghaddam, and B. Lee, Highly efficient photocatalytic degradation of organic pollutants by mesoporous graphitic carbon nitride bonded with cyano groups, J. Chem. Eng., **419**, (2021). doi.org/10.1016/j.cej.2021.129503.

32. N. L. Minh Tri, J. Kim, B. L. Giang, T. M. Al Tahtamouni, P. T. Huong, and C. Lee, Ag-doped graphitic carbon nitride photocatalyst with remarkably enhanced photocatalytic activity towards antibiotic in hospital wastewater under solar light J. Indust. Eng. Chem., **80**, 597-605 (2019). doi.org/10.1016/j.jiec.2019.08.037.

33. T. H. Pham, J.-W. Park, and T. Y. Kim, Enhanced photodegradation of paracetamol from water by cobalt doped graphitic carbon nitride, Solar Energy, **215**, 151-156 (2021). doi.org/10.1016/j.solener.2020.12.034.

34. F. Xu, N. An, C. Lai, M. Zhang, B. Li, L. Qin, and H. Yan, Nitrogen-doping coupled with cerium oxide loading co-modified graphitic carbon nitride for highly enhanced photocatalytic degradation of tetracycline under visible light, Chemosphere, **293**, (2022). doi.org/10.1016/j.chemosphere.2022.133648.

35. P. Sun, Y. Liu, F. Mo, M. Wu, Y. Xiao, W. Wang, and X. Dong, Efficient photocatalytic degradation of high-concentration moxifloxacin over dodecyl benzene sulfonate modified graphitic carbon nitride: Enhanced photogenerated charge separation and pollutant enrichment, J. Clean. Prod., **393,** (2023). doi.org/10.1016/j.jclepro.2023.136320.

36. S. Zhang, J. Chen, C Fang, Y. Zhang, Z. Xu, and Z. Yan, enhanced photocatalytic removal of antibiotics over graphitic carbon nitride induced by acetic acid post-treatment, Colloid. Surf. A: Physicochem. Eng. Aspec., **664,** (2023). doi.org/10.1016/j.colsurfa.2023.131165.

37. P. Rajiv, N. Mengelizadeh, G. McKay, and D. Balarak, Photocatalytic degradation of ciprofloxacin with Fe_2O_3 nanoparticles loaded on graphitic carbon nitride: mineralisation, degradation mechanism and toxicity assessment, Int. J. Environ. Analyt. Chem., **103**(10), 2193-2207 (2023). doi: 10.1080/03067319.2021.1890059.

38. C. Bian, Y. Wang, Y. Yi, S. Shao, P. Sun, Y. Xiao, W. Wang, and X. Dong, Enhanced photocatalytic activity of S-doped graphitic carbon nitride hollow

microspheres: Synergistic effect, high-concentration antibiotic elimination and antibacterial behavior, J. Colloid. Inter. Sci., **643**, 256-266 (2023). doi.org/10.1016/j.jcis.2023.04.034.

39. J. Y. Chin, A. L. Ahmad, and S. C. Low, Graphitic carbon nitride photocatalyst for the degradation of oxytetracycline hydrochloride in water, Mater. Chem. Phys., **301**, (2023). doi.org/10.1016/j.matchemphys.2023.127626.

40. Y. Wang, A. Liu, J. Song, Y. Zheng, H. Xian, Z. Liu, and T. Jiang, Methyl-terminated graphite carbon nitride with regulatable local charge redistribution for ultra-high photocatalytic hydrogen production and antibiotic degradation, Chemosphere, **340,** (2023). doi.org/10.1016/j.chemosphere.2023.139736.

41. M. Shen, X. Zhang, S. Zhao, Y. Cai, and S. Wang, A novel photocatalytic system coupling metal-free carbon/g-C_3N_4 catalyst with persulfate for highly efficient degradation of organic pollutants, Chemosphere, **314**, (2023). doi.org/10.1016/j. chemosphere.2022.137728.

42. H. Zheng, Y. Chen, X. Sun, X. Zheng, X. Zhang, and X. Guan, Enhanced photocatalytic performance and mechanism of N-deficiently porous g-C_3N_4 in organic pollutant degradation, Mater. Res. Bull., **169**, (2024).doi.org/10.1016/j.materresbull. 2023.112510.

43. X. Song, Q. Yang, M. Yin, D, Tang, and L, Zhou **,** Highly efficient pollutant removal of graphitic carbon nitride by the synergistic effect of adsorption and photocatalytic degradation, RSC Adv**.**, **8**, 7260-7268 (2018). doi.org/10.1039/C7RA11467B.

44. M. V. V. Poiyamozhi, and J. Thivya, Design and fabrication of graphitic carbon nitride incorporated nickel selenide hybrid composite for effective degradation of organic pollutants under UV and natural sunlight irradiations, Diam. Relat. Mater. **142**, (2024), doi.org/10.1016/j.diamond.2023.110726.

45. A. Khan, W. Li, X.Ma, M. Dong, L. Geng, Y. Li, Y. Fan, S. Khan, and G. Yasin, Novel and facile strategy for immobilization of Ag_3PW_{12} crystals on graphitic carbon nitride (g-C_3N_4) sheets, a superior photocatalyst for decomposition of organic waste, J. Solid State Chem., **329,** (2024). doi.org/10.1016/j.jssc.2023.124405.

46. S. Y. Ejeta, and T. Imae, Photodegradation of pollutant pesticide by oxidized graphitic carbon nitride catalysts, J. Photochem. Photobiol. A: Chem., **404**, (2021). doi.org/10.1016/j.jphotochem.2020.112955.

47. S. Vigneshwaran, J. Preethi, and S. Meenakshi, Removal of chlorpyrifos, an insecticide using metal free heterogeneous graphitic carbon nitride (g-C_3N_4) incorporated chitosan as catalyst: Photocatalytic and adsorption studies, Int. J. Biol. Macromol., **132**, 289-299 (2019). doi: 10.1016/j.ijbiomac.2019.03.071.

48. X. Liu, X. Wu , Z. Long , C. Zhang , Y. Ma , Xi. Hao , H. Zhang, and C. Pan, Photodegradation of imidacloprid in aqueous solution by the metal-free catalyst graphitic carbon nitride using an energy-saving lamp, J. Agric. Food Chem., **63**(19), doi: 10.1021/acs.jafc.5b01105.

49. H. Zong, X. Liu, X. Tan, X. Wang, J. Qiu, F. Kong, J. Zhang, and S. Fang, Facile synthesis of modified carbon nitride with enhanced activity for photocatalytic degradation of Atrazine, J. Environ. Chem. Eng.,**9**(5), (2021). doi: 10.1016/j.jece.2021.105807.

50. S. N. S. A. Halim, N. A. M. Nazri, and N. A. M Nordin, Comparative effects of graphitic carbon nitride precursors on the photocatalytic degradation of pyrene, Mater. Sci. Forum*.,* **1076**. 181-191 (2022). doi:10.4028/p-y056c4.

51. P. Azmoon, M. Farhadian, A. Pendashteh, and A. H. Navarchian, Synergistic effect of adsorption and photocatalytic degradation of oilfield-produced water by electrospun photocatalytic fibers of polystyrene/nanorod-graphitic carbon nitride, J. Environ. Sci., **141**, 287-303 (2024). doi.org/10.1016/j.jes.2023.05.041.

52. D. Bharathi, J. Lee, M. F. Albeshr, A. F. Alrefaei, T. T. Le, and T. Mathimani, Enhanced photocatalytic degradation of polycyclic aromatic hydrocarbon by graphitic carbonitride-nickel (g–C_3N_4–Ni) nanocomposite, Chemosphere, **345**, (2023). doi.org/10.1016/j.chemosphere.2023.140464.

53. A. Jilani, G. U. Rehman, M. O. Ansari, M. H. Othman, S. Z. Hussain, and M. R. Dustgeer, Sulfonated polyaniline-encapsulated graphene graphitic carbon nitride nanocomposites for significantly enhanced photocatalytic degradation of phenol: A mechanistic study, New J. Chem., **44**(45), 19570-19580 (2020). doi: 10.1039/d0nj03684f.

54. A. G. Rana, M. Tasbihi, M. Schwarze, and M. Minceva, Efficient advanced oxidation process (AOP) for photocatalytic contaminant degradation using exfoliated metal-free graphitic carbon nitride and visible light-emitting diodes, Catalysts, **11**(6), (2021). doi.org/10.3390/catal11060662.

55. R. Kavitha and S. G. Kumar, Polymeric graphitic-carbon nitride and its composites for the photocatalytic removal of phenolic compounds, Nanoscale graphitic carbon nitride, 141-168 (2022). doi: 10.1016/b978-0-12-823034-3.00009-1.

❐❐❐

CHAPTER – IIIA

AZURE A- GRAPHITIC CARBON NITRIDE SYSTEM

CONTENTS

3.1 AZURE A

Azure A is light blue to dark blue dye. It is used for a monitoring test of mucopolysaccharides.

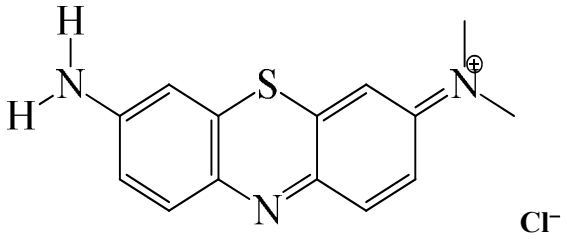

Fig. 3.1: Structure of Azure A

IUPAC Name	:	N',N'-Dimethylphenothiazin-5-ium-3,7-diamine chloride
Molecular Formula	:	$C_{14}H_{14}ClN_3S$
Molecular Mass	:	291.80 g mol^{-1}
λ max	:	620 nm
Solubility	:	Water

3.2 EXPERIMENTAL

- Absorbance of dye solution was measured by UV-Visible spectrophotometer, (Systronics model 106)
- The pH was determined using a pH meter (Systronics model 335), and
- The light intensity was recorded by a Solarimeter Suryamapi (CEL Model SM 201).

A 1.0×10^{-4} M solution of azure-A (HIMEDIA) was prepared by dissolving 0.0292 g of azure-A in 100.0 mL of distilled water. This solution was used served as a stock solution. The absorbance (A) of azure-A dye solution was measured using a spectrophotometer (Systronics model 106) at a wavelength of λ max = 620 nm. The dye solution was divided into four portions.

- The first beaker containing dye solution was kept in dark,
- The second beaker containing dye solution was exposed to 200 W tungsten lamp,
- The third beaker containing dye solution and 0.08 g of graphitic carbon nitride was kept in dark, and
- The fourth beaker containing dye solution and 0.08 g photocatalyst graphitic carbon nitride was exposed to 200 W tungsten lamp.

It was observed that the absorbance of the first beaker remained almost same even after 3-4 h. while the second beaker had a slight decrease in initial value of its absorbance. The initial absorbance of the third beaker also showed a slight decrease. The absorbance of the fourth beaker had a significant reduction. These observations indicate that the reaction between azure-A and photocatalyst is a photocatalytic reaction only.

The 0.08 g of g-C_3N_4 was added to 1.00×10^{-4} M dye solution and pH was maintained at 7.0, Then it was exposed to a 200 W tungsten lamp at 70.0 m W cm^{-2}. The absorbance of azure A was found to decrease with increasing exposure time. A linear relationship was observed on plotting 1 + log A against time. The rate constant (k) of the reaction was calculated using the expression k = 2.303 × slope. The results are reported in Table 3.1: and represented in Fig. 3.2:

Table 3.1: A typical run

pH = 7.0 g-C_3N_4 = 0.08 g

[Azure-A] = 1.00×10^{-4} M Light intensity = 70.0 mW cm^{-2}

Time (min)	Absorbance (A)	1 + log A
0.00	0.476	0.6776
10.0	0.442	0.6454
20.0	0.342	0.5340
30.0	0.282	0.4502
40.0	0.258	0.4116
50.0	0.227	0.3560
60.0	0.203	0.3074
70.0	0.168	0.2253
80.0	0.148	0.1702
90.0	0.132	0.1205

Rate constant (k) = 2.54×10^{-4} s^{-1}

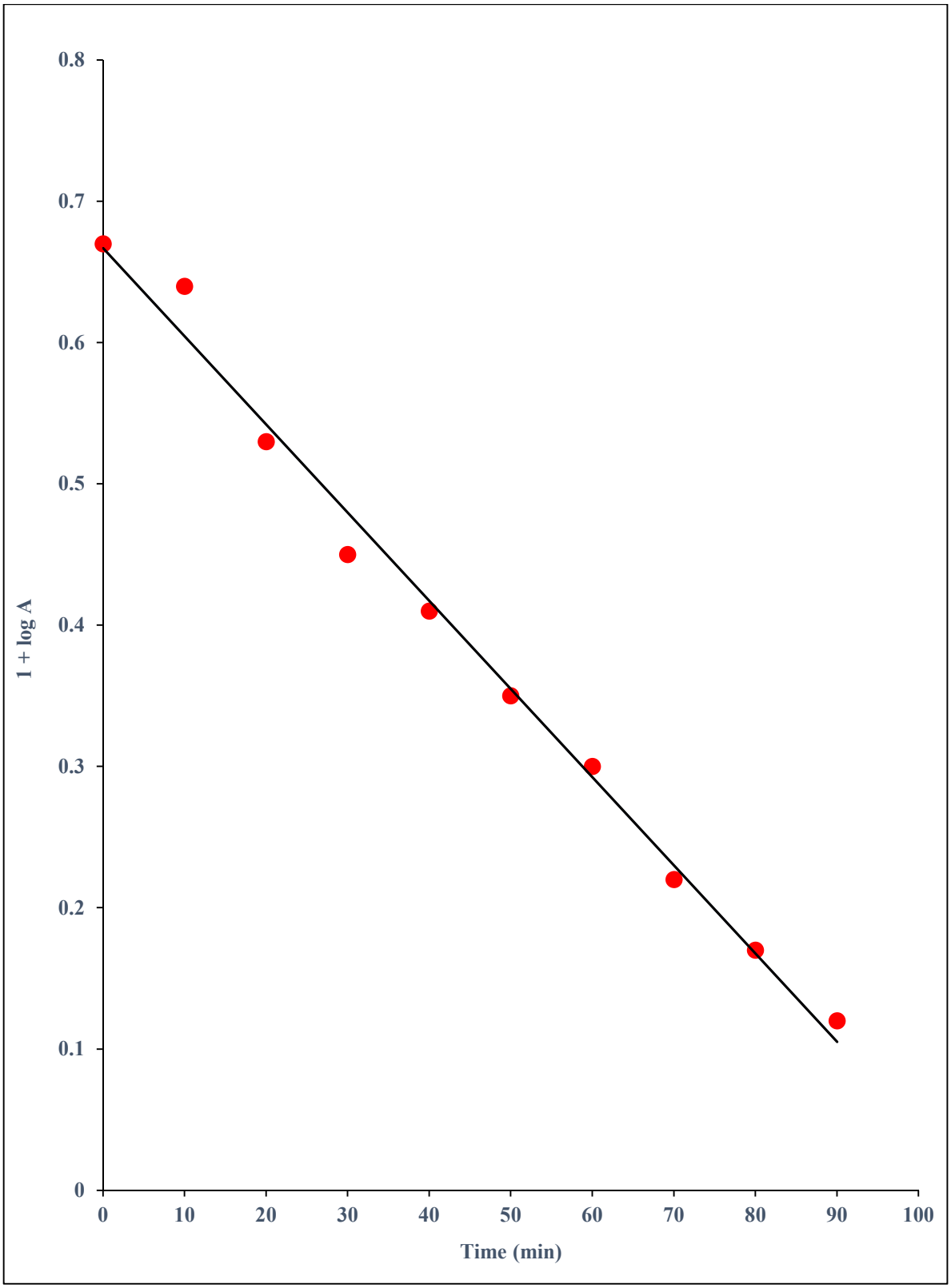

Fig. 3.2: A typical run

3.2.1 Effect of pH

The effect of pH on photocatalytic degradation was observed in the range of 5.0 to 9.0. The results are shown in Table 3.2: and Fig. 3.3:

Table 3.2: Effect of pH

[Azure A] = 1.00×10^{-4} M g-C_3N_4 = 0.08 g

Light Intensity = 70.0 mW cm^{-2}

pH	**Rate constant (k) × 10^4 (s^{-1})**
5.0	0.266
5.5	0.308
6.0	1.34
6.5	1.65
7.0	**2.54**
7.5	1.69
8.0	1.38
8.5	1.12
9.0	0.70

The rate of degradation of azure-A increases with increasing pH of solution up to 7.0, but above this value of pH, the rate of photodegradation of azure-A started decreasing.

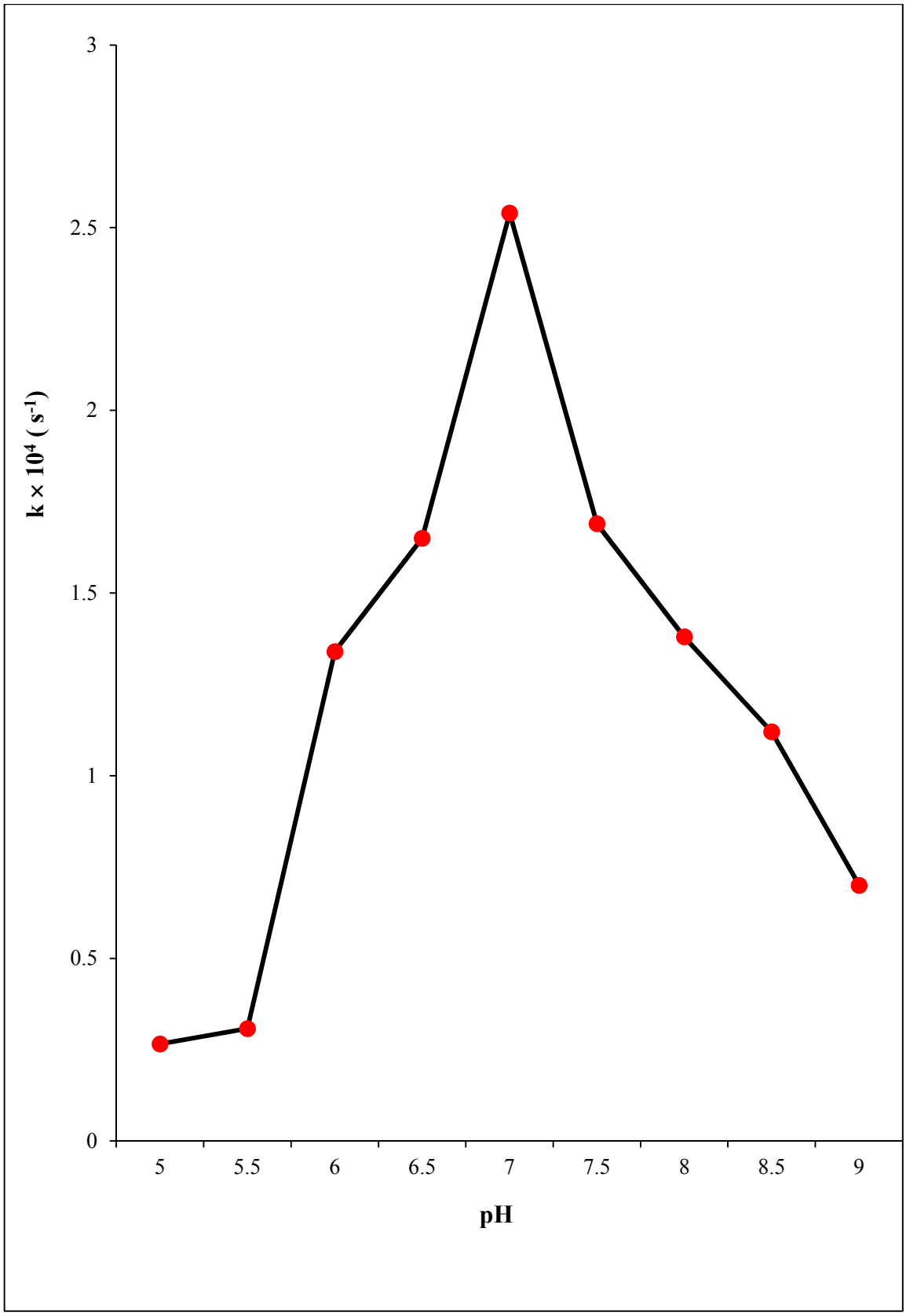

Fig. 3.3: Effect of pH

3.2.2 Effect of Dye Concentration

The effect of dye concentration on the rate of reaction was also observed using different concentrations of azure A solution in the range of 6.0×10^5 M to 2.6×10^4M. The results are tabulated in Table 3.3: and presented Fig. 3.4:

Table 3.3: Effect of dye concentration

pH = 7.0 Light intensity = 70.0 mW cm^{-2}

g-C_3N_4 = 0.08 g

[Azure A] × 10^4 M	**Rate constant (k)× 10^4 (s^{-1})**
0.6	2.24
0.8	2.43
1.0	**2.54**
1.2	1.78
1.4	1.39
1.6	1.27
1.8	1.25
2.2	1.09
2.4	0.95
2.6	0.94

It was noticed that the rate of photocatalytic degradation increases with dye concentration up to 1.00×10^4 M. but it started declining on increasing the dye concentration further.

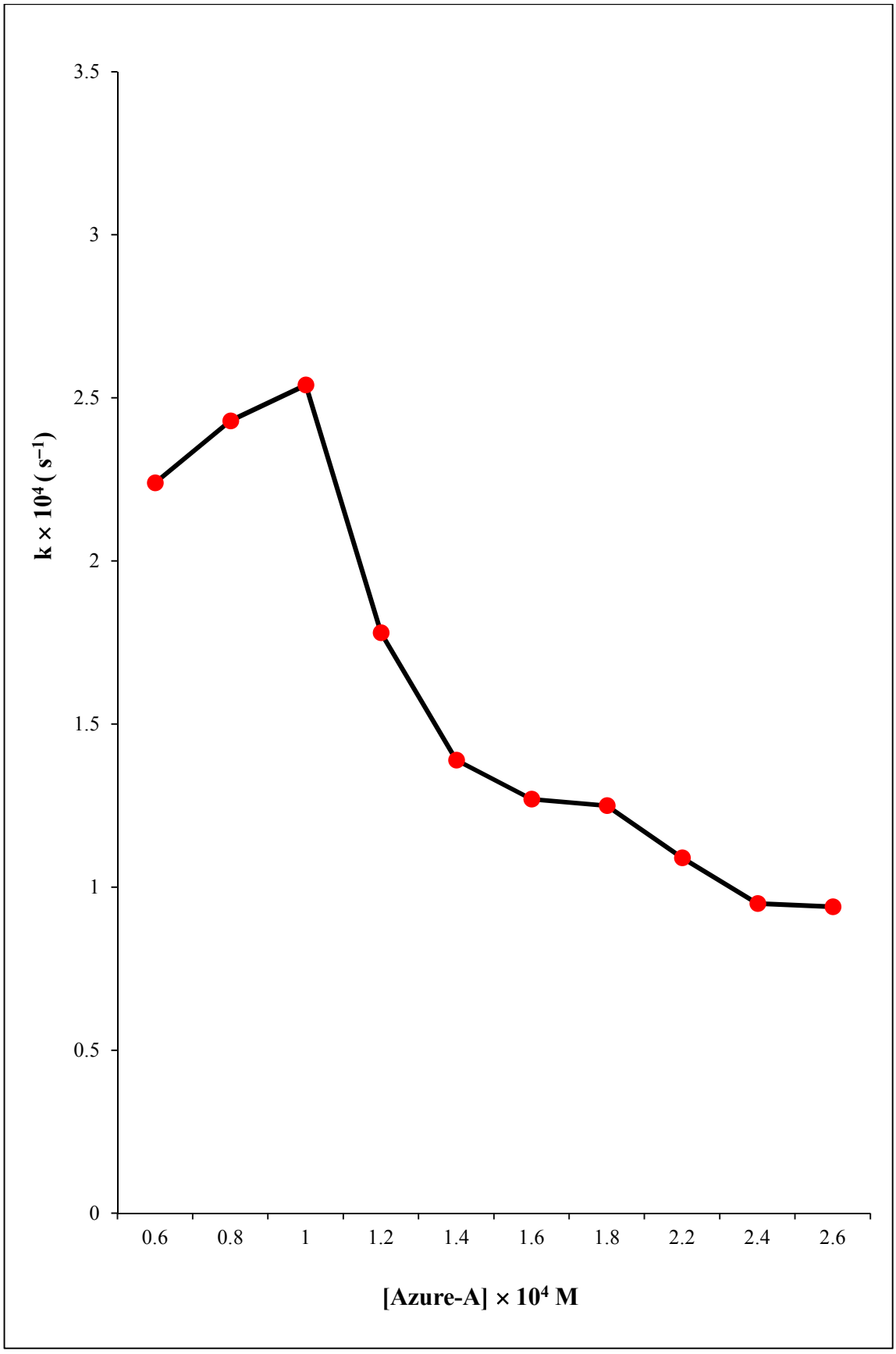

Fig. 3.4: Effect of dye concentration

3.2.3 Effect of Amount of Photocatalyst

The effect of amount of photocatalyst on the rate of photocatalytic degradation of azure-A was also observed between 0.02 to 0.14 g. The results are shown in Table 3.4: and Fig. 3.5:

Table 3.4: Effect of amount of photocatalyst

[Azure-A] = 1.00×10^4 M pH = 7.0

Light intensity = 70.0 mW cm^{-2}

g-C_3N_4 (g)	**Rate constant (k) × 10^4 (s^{-1})**
0.02	1.26
0.04	1.85
0.06	2.19
0.08	**2.54**
0.10	2.25
0.12	1.94
0.14	1.42

It was observed that reaction rate increases on increasing quantity of photocatalyst till 0.08 g, beyond which the rate of degradation exhibited a declining behaviour.

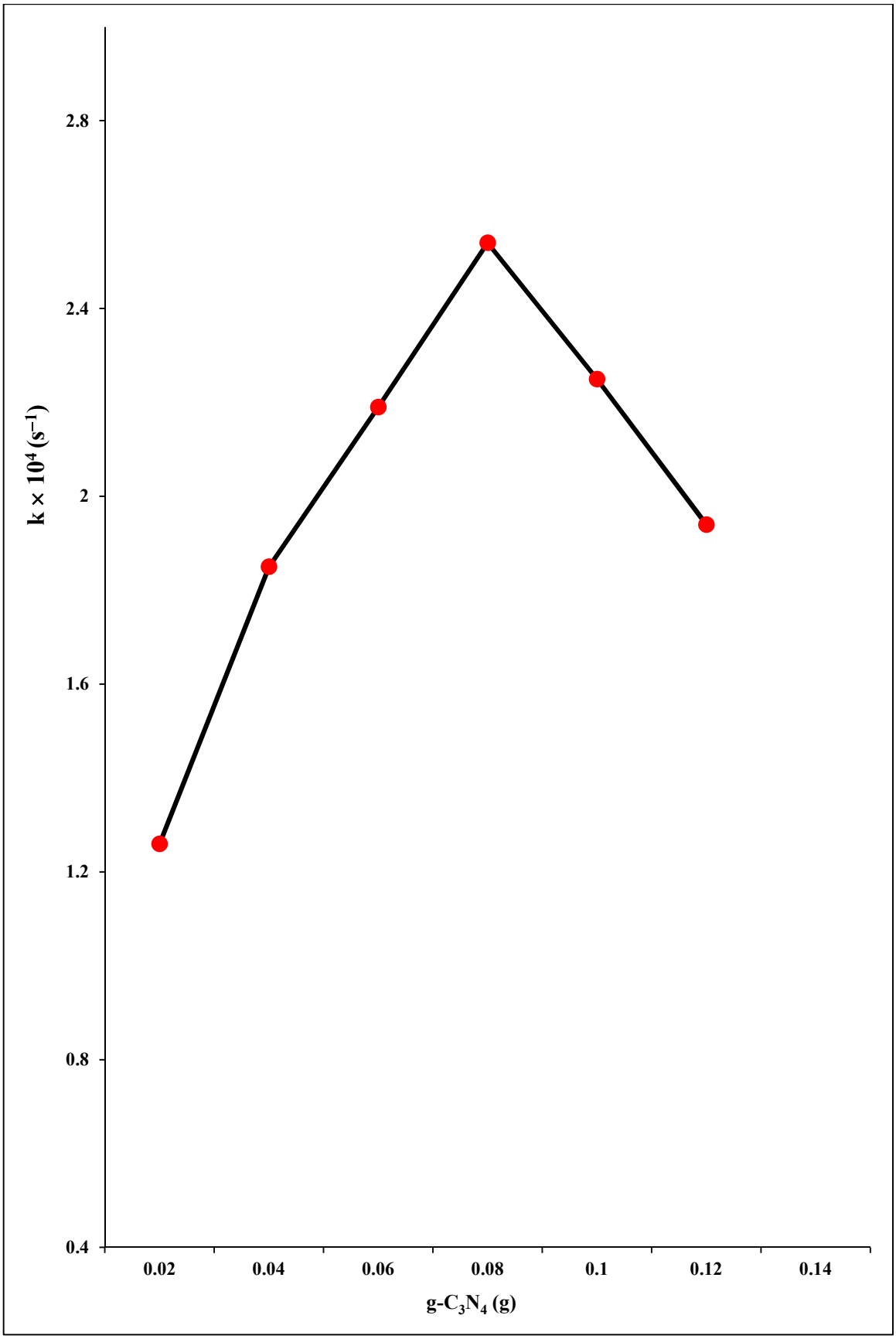

Fig. 3.1: Effect of amount of photocatalyst

3.2.4 Effect of Light Intensity

The effect of light intensity on the rate of degradation of azure-A was also observed from 20.0 to 70.0 $mWcm^{-2}$. The results are reported in Table 3.5: and Fig. 3.6:

Table 3.1: Effect of light intensity

[Azure-A] = 1.00×10^{-4} M pH = 7.0

g-C_3N_4 = 0.08 g

Light intensity (mW cm^{-2})	**Rate constant (k) × 10^4 (s^{-1})**
20.0	1.43
30.0	1.50
40.0	1.69
50.0	1.79
60.0	2.11
70.0	**2.54**

It was observed that rate of degradation of azure a increases as the light intensity was increased. There was an almost liner behaviour between rate and intensity of light.

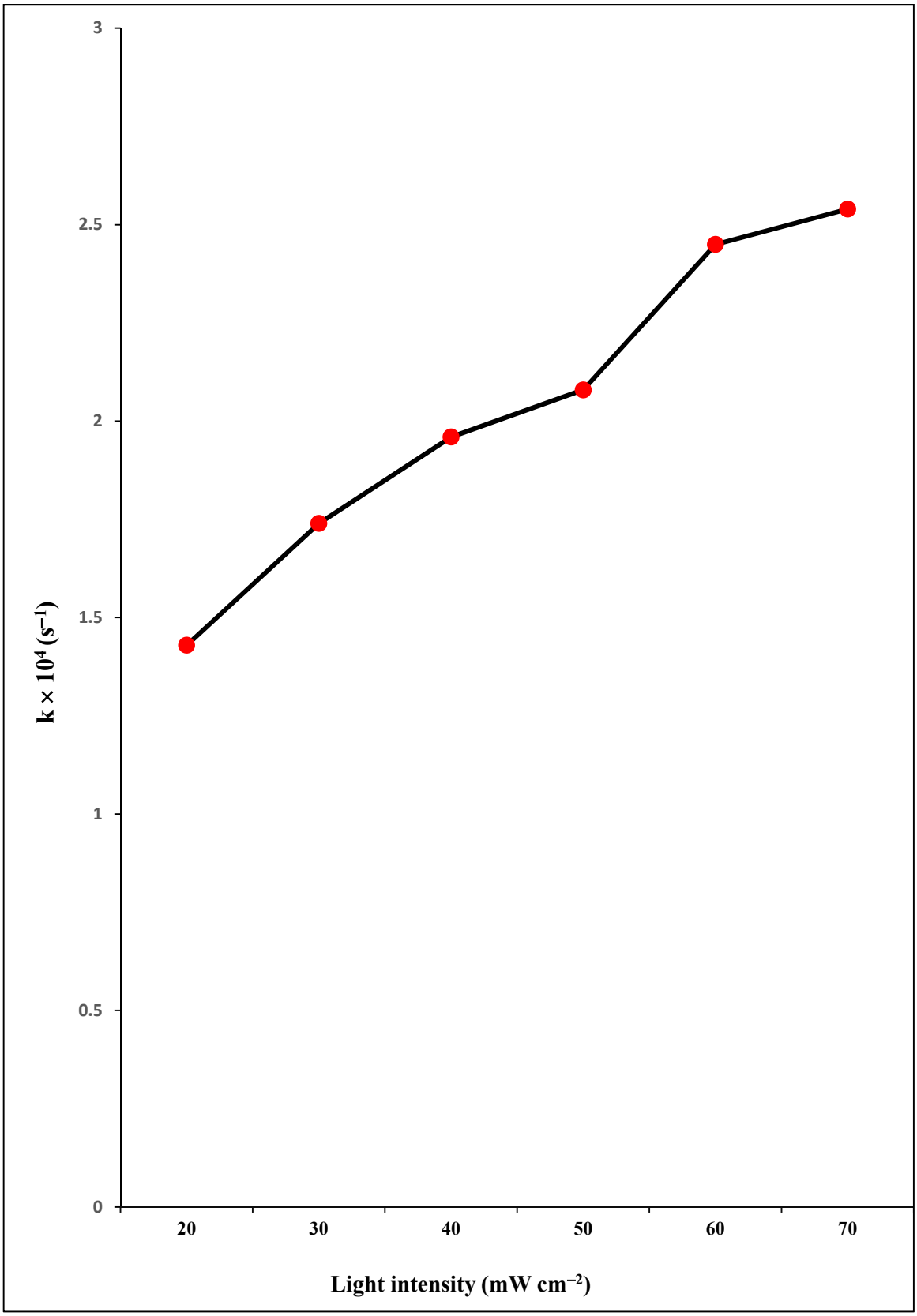

Fig. 3.6: Effect of light intensity

❐❐❐

CHAPTER – IIIB

EVANS BLUE- GRAPHITIC CARBON NITRIDE SYSTEM

CONTENTS

3.3 EVANS BLUE

Evans blue is a synthetic bis-azo dye, It is also named as T-1824 and Direct Blue 53. It is used for estimation of blood volume, detection of lymph nodes, and localization of tumours.

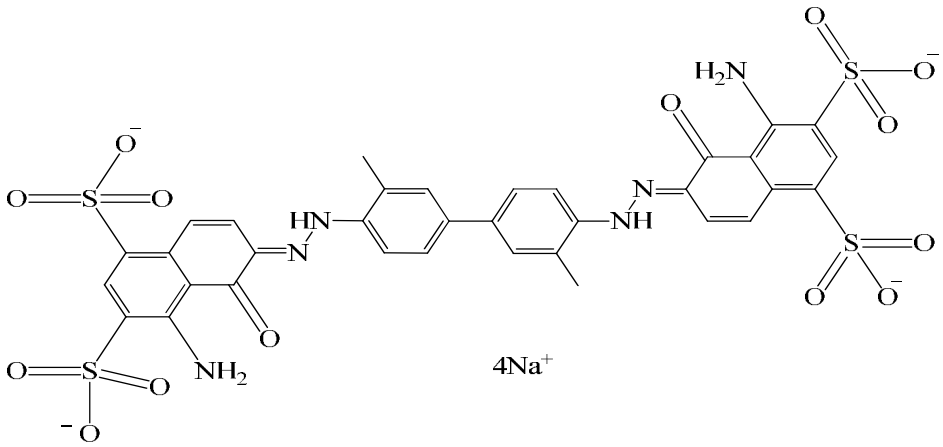

Fig. 3.7: Structure of Evans blue

IUPAC Name	:	Tetrasodium (6E,6'E)-6,6-[(3,3'-dimethylbiphenyl-4,4'-diyl) di(1E) hydrazin-2-yl-1-ylidene] bis (4-amino-5-oxo-5,6-dihydronaphthalene-1,3-disulfonate)
Molecular Formula	:	$C_{34}H_{24}N_6Na_4O_{14}S_4$
Molecular Mass	:	960.809 g mol^{-1}
λ max	:	608 nm
Solubility	:	Water

3.4 EXPERIMENTAL

A solution of Evans blue (HIMEDIA) 0.096 g was prepared by dissolving in 100.0 mL water to prepare 1.0×10^{-4} M and stored as a stock solution. The absorbance (A) of Evans blue dye solution was determined with the help of a spectrophotometer at λ max = 608 nm. The dye solution was placed in equal amounts in four beakers.

- The first beaker containing dye solution was kept in dark,

- The second beaker containing dye solution was exposed to 200 W tungsten lamp,
- The third beaker containing dye solution with 0.10 g photocatalyst graphitic carbon nitride was kept in dark, and
- The fourth beaker contain dye solution and 0.10 g photocatalyst graphitic carbon nitride was exposed to 200 W tungsten lamp.

The absorbance of dye solution was measured with the help of a spectrophotometer. It was observed that the absorbance of first beaker remained almost same after 3-4 h while the second beaker had a slight decrease in initial value of its absorbance. The initial absorbance value of the third beaker showed a slight difference. The initial absorbance value of the fourth beaker experienced a significant reduction. This observation confirmed that the reaction between Evans blue and photocatalyst is a photocatalytic reaction.

The photodegradation of Evans blue was monitored by taking absorbance of samples of dye solution 1.0×10^{-4}M containing 0.10 g photocatalyst (g-C_3N_4) and exposed to 200 W tungsten lamp (60.0 mW cm^{-2}) at pH = 9.5. The absorbance of Evans blue was found to decrease with increasing time of exposure. A plot of 1 + log A versus time was found to be linear. The rate constant of reaction was calculated with the following expression k = 2.303 × slope. The data of typical run are presented in Table 3.6: and graphically in Fig. 3.8:

Table 3.6: A typical run

pH = 9.5 g-C_3N_4 = 0.10 g

[Evans blue] = 1.00×10^{-4} M Light Intensity = 60.0 mW cm^{-2}

Time (min)	Absorbance (A)	1+ log A
0	0.407	0.6095
10	0.381	0.5809
20	0.359	0.5550
30	0.310	0.4913
40	0.295	0.4698
50	0.282	0.4502
60	0.270	0.4313
70	0.260	0.4149
80	0.240	0.3802
90	0.226	0.3541
100	0.216	0.3344

Rate constant (k) = 1.50×10^{-4} sec^{-1}

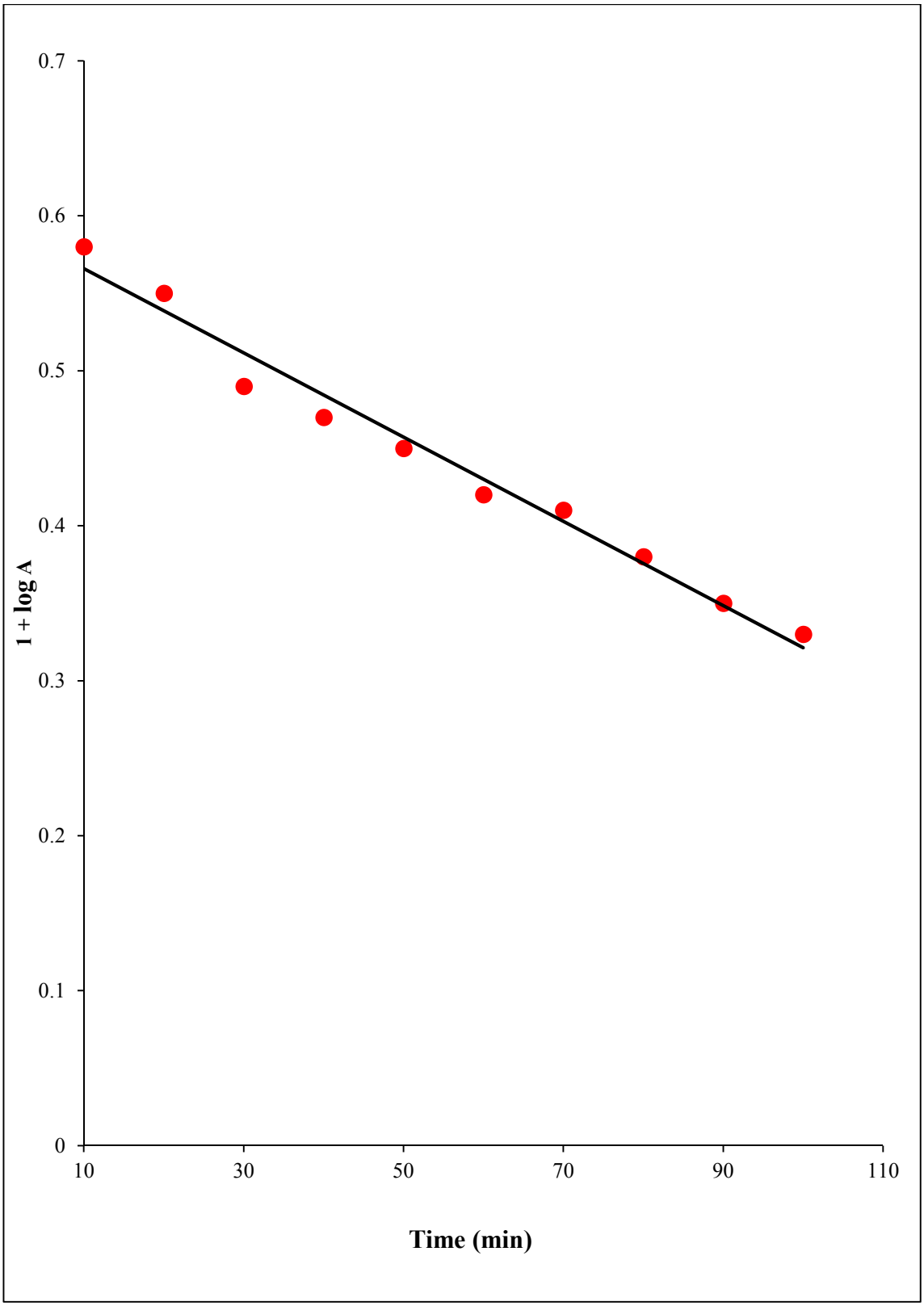

Fig. 3.8: A typical run

3.4.1 Effect of pH

The effect of pH on photocatalytic degradation was observed in the range of 6.0 to 10.5. The results are given in Table 3.7: and Fig. 3.9:

Table 3.7: Effect of pH

[Evans blue] = 1.00×10^{-4} M g-C_3N_4 = 0.10 g

Light Intensity = 60.0 mW cm^{-2}

pH	**Rate constant (k) × 10^4 (s^{-1})**
6.0	0.51
6.5	0.72
7.0	0.94
7.5	1.10
8.0	1.24
8.5	1.40
9.0	1.48
9.5	**1.50**
10.0	1.40
10.5	1.30

It was noticed that the degradation rate of Evans blue increases with increasing pH of solution up till 9.5, but above this value of pH, the rate of photodegradation of Evans blue started decreasing.

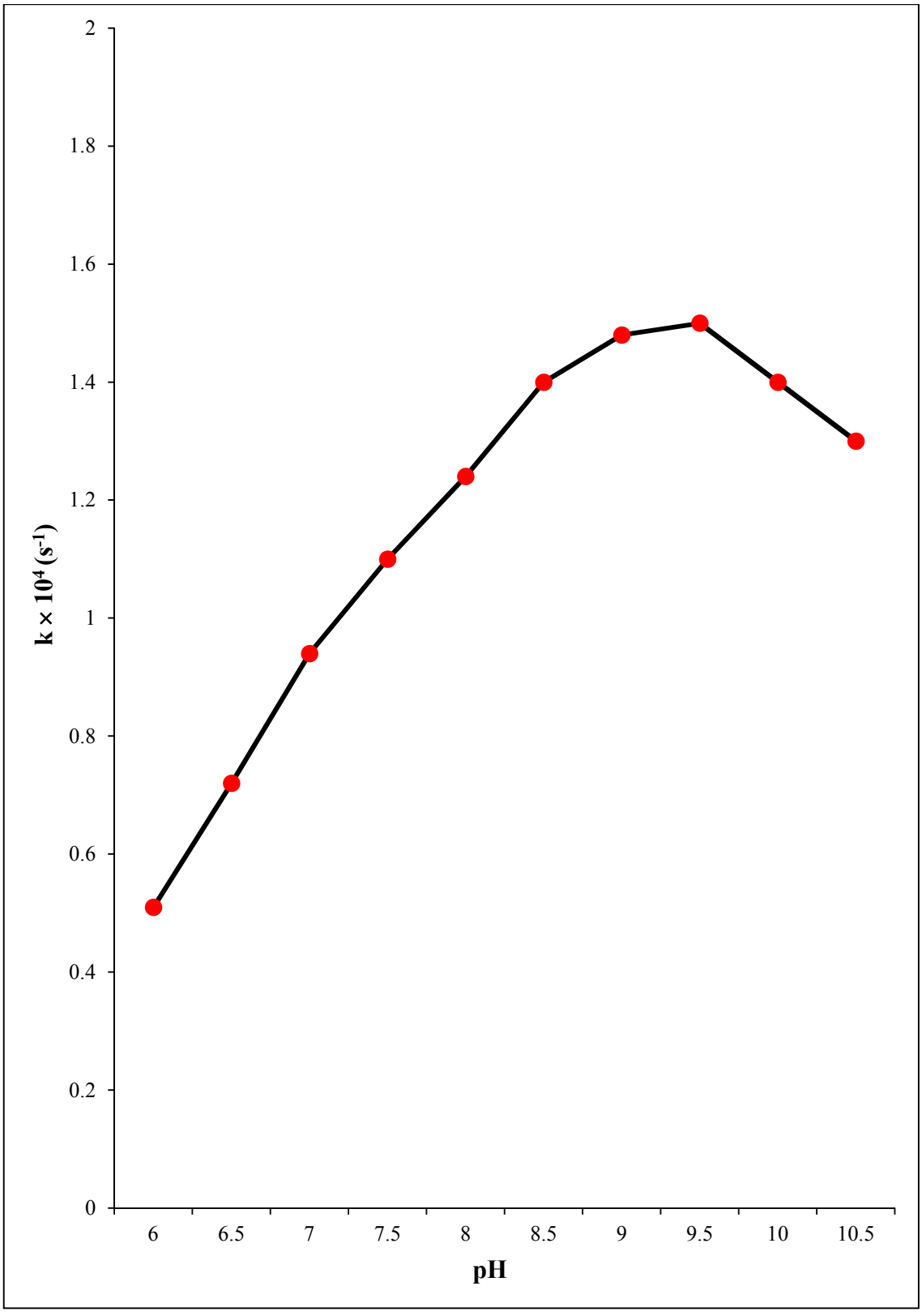

Fig. 3.9: Effect of pH

3.4.2 Effect of dye concentration

The effect of dye concentration on the rate of reaction was also observed using different concentrations of Evans blue solution (2.0×10^{-5}-1.8×10^{-4}M). The results are shown in Table 3.8: and Fig. 3.10:

Table 3.8: Effect of dye concentration

pH = 9.5 Light Intensity = 60.0 mW cm^{-2}

g-C_3N_4 = 0.10 g

[Evans blue] × 10^4 M	**Rate constant (k) × 10^4 (s^{-1})**
0.2	0.8
0.4	1.0
0.6	1.10
0.8	1.25
1.0	**1.50**
1.2	1.27
1.4	1.10
1.6	0.85
1.8	0.74

It was observed that the rate of photocatalytic degradation increases with increase in the concentration of the dye up to 1.0×10^{-4} M beyond which, it decreses.

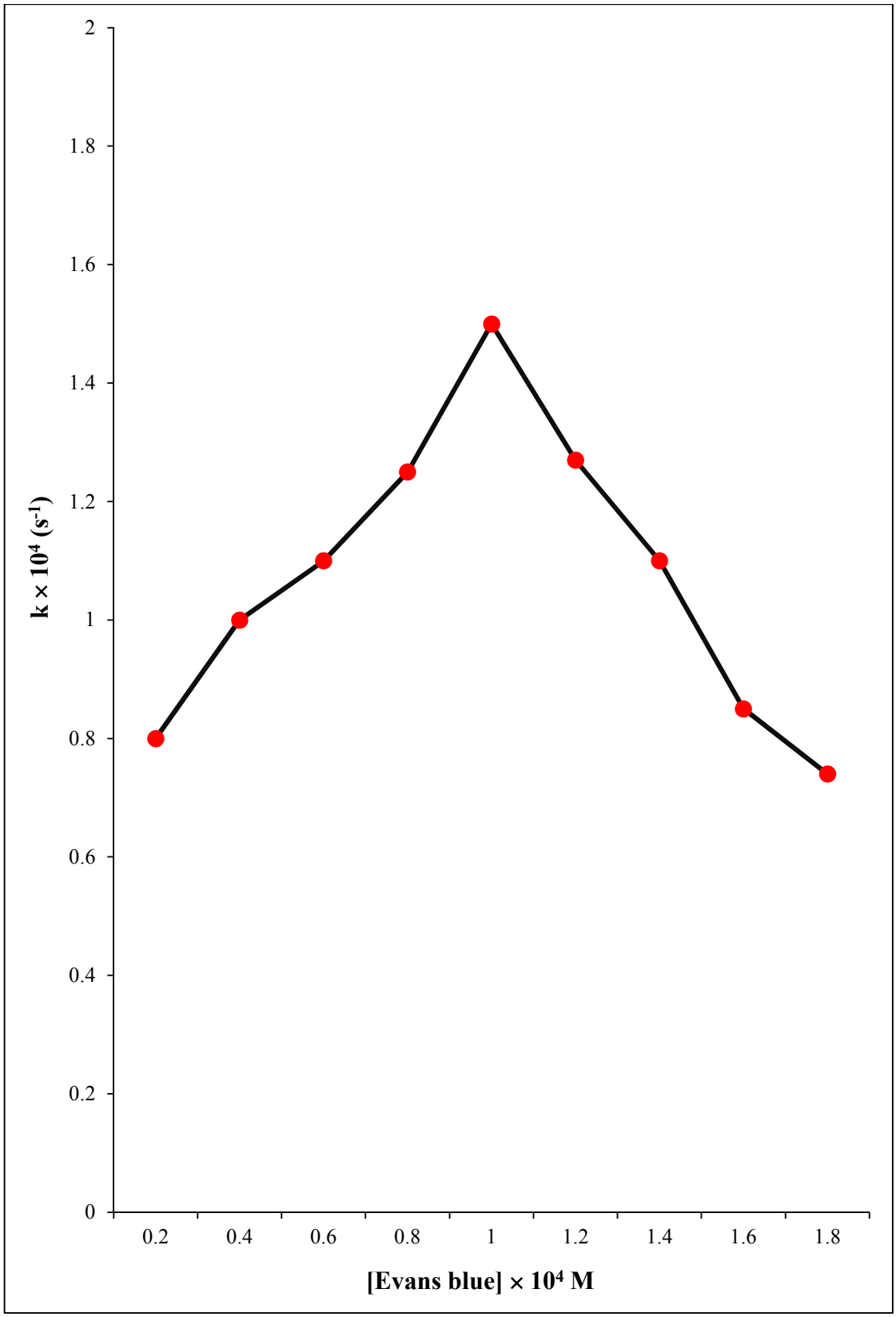

Fig. 3.10: Effect of dye concentration

3.4.3 Effect of amount of photocatalyst

The effect of amount of photocatalyst on the rate of photocatalytic degradation of Evans blue was also observed in the rang 0.02-0.16 g. The results are shown in Table 3.9: and Fig. 3.11:

Table 3.9: Effect of amount of photocatalyst

pH = 9.5 Light Intensity = 60.0 mW cm^{-2}

[Evans blue] = 1.00×10^{-4} M

g-C_3N_4 (g)	**Rate constant (k) × 10^4 (s^{-1})**
0.02	1.36
0.04	1.40
0.06	1.45
0.08	1.49
0.10	**1.50**
0.12	1.48
0.14	1.38
0.16	1.32

It was noticed that the rate of reaction increases with increase in the amount of photocatalyst up to 0.10 g, but above this value of photocatalyst, the rate of reaction decreased.

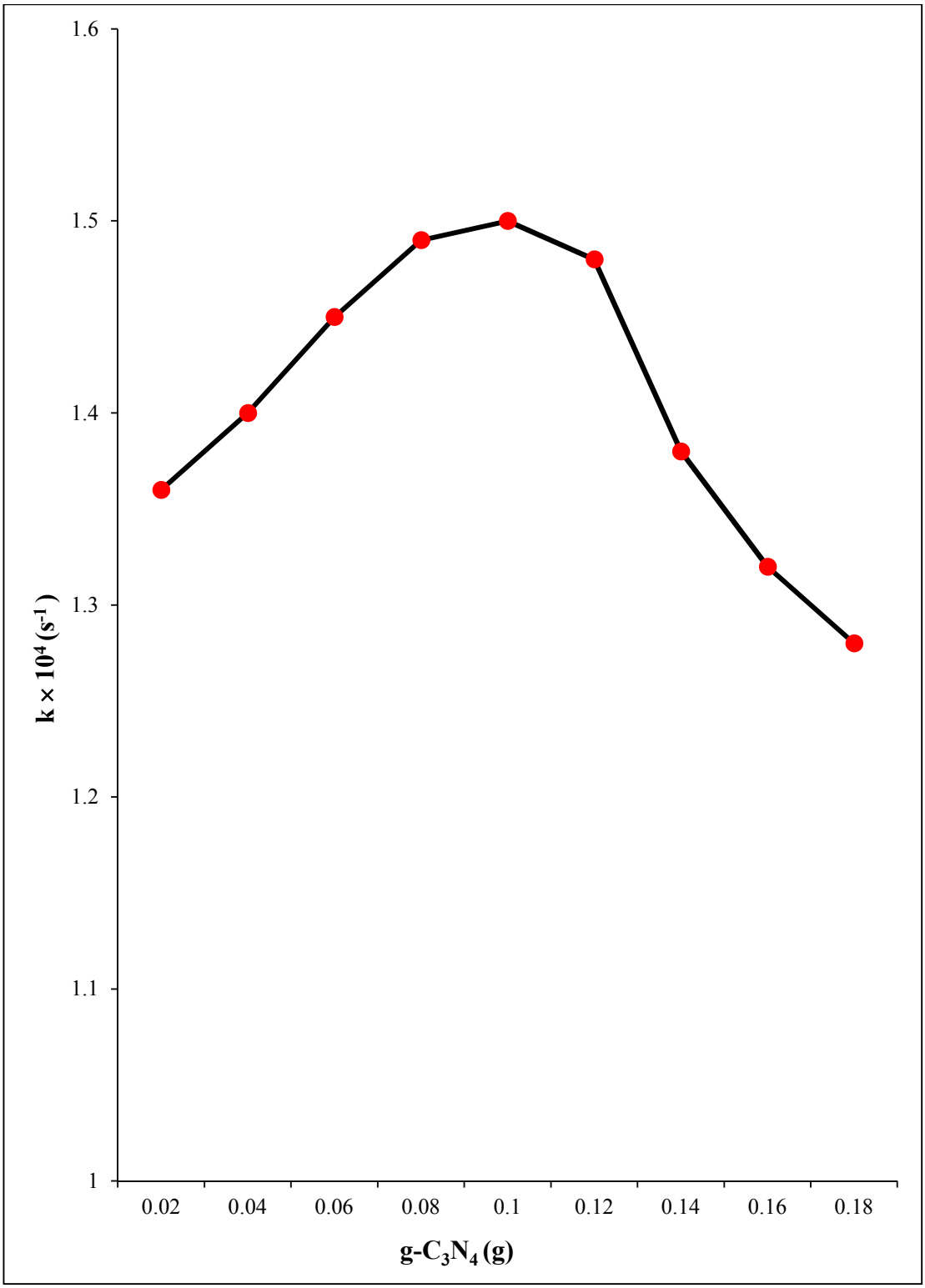

Fig. 3.11: Effect of amount of photocatalyst

3.4.4 Effect of light intensity

The effect of light intensity on the rate of Evans blue was also observed from 30.0 to 70.0 mW cm^{-2}. The results are reported in Table 3.10: and Fig. 3.12:

Table 3.10: Effect of light intensity

pH = 9.5 [Evans blue] = 1.0×10^{-4} M

g-C_3N_4 = 0.10 g

Light intensity (mW cm^{-2})	**Rate constant (k) × 10^4 (s^{-1})**
30.0	0.82
40.0	0.99
50.0	1.05
60.0	**1.50**
70.0	1.23

It was observed that the rate of degradation was increased on increasing light intensity, but there was a desrese above 60.0 mW cm^{-2}.

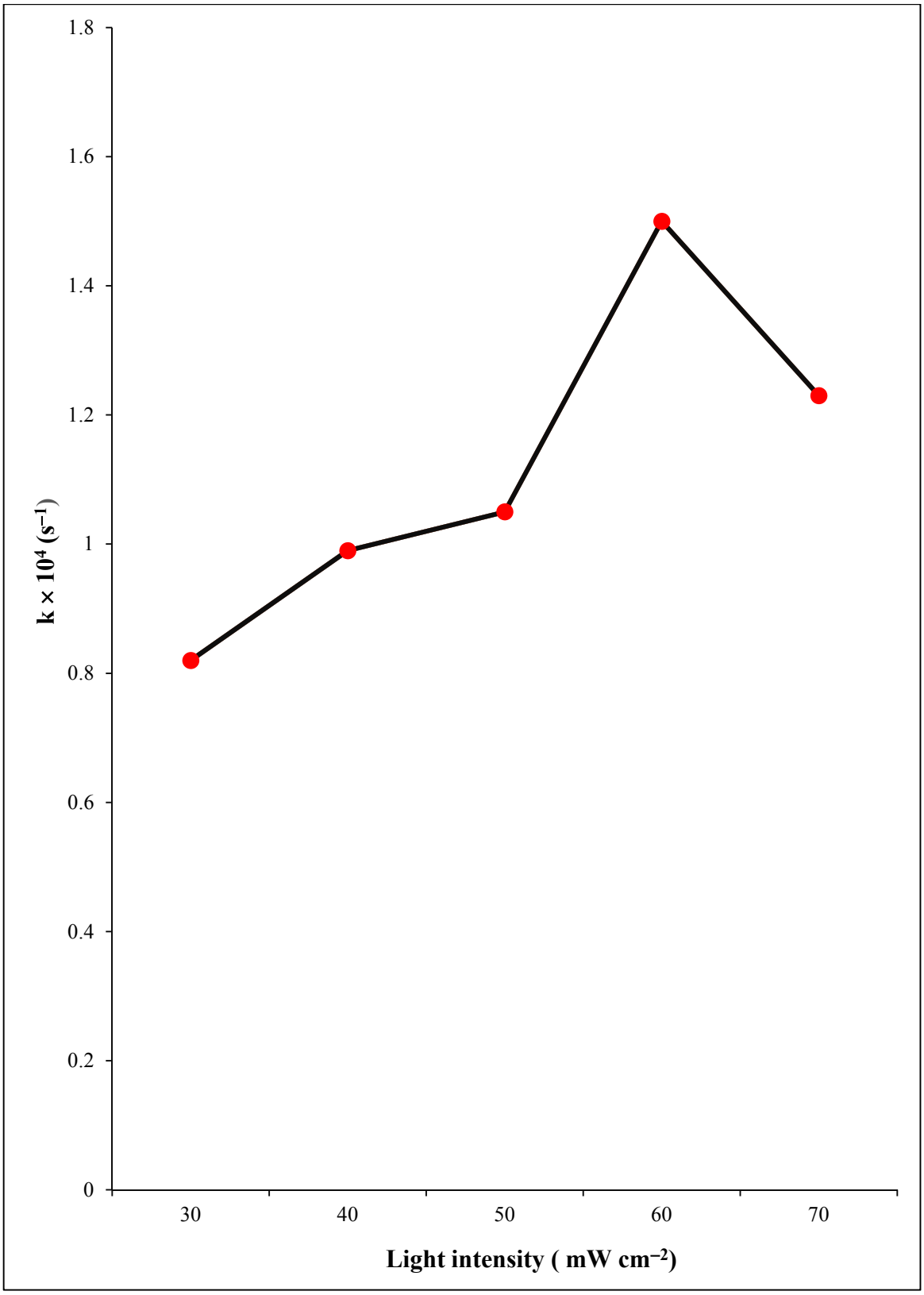

Fig. 3.12: Effect of light intensity

❐❐❐

CHAPTER – IIIC

ROSE BENGAL- GRAPHITIC CARBON NITRIDE SYSTEM

CONTENTS

3.5 ROSE BENGAL

Rose Bengal belongs to the class of organic compounds called xanthenes. Its sodium salt is commonly used in eye drops to stain damaged conjunctival and corneal cells and thereby, identify damage to the eye.

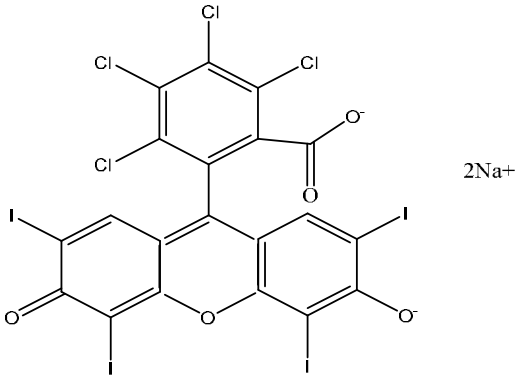

Fig. 3.13: Structure of Rose Bengal

IUPAC Name	:	4,5,6,7-Tetrachloro-3′,6′-dihydroxy-2′,4′,5′,7′-tetraiodo-3H- spiro [[2] benzofuran-1,9′-xanthen]-3-one
Molecular Formula	:	$C_{14}H_{14}ClN_3S$
Molecular Mass	:	973.67 g/ mol^{-1}
λ max	:	527 nm
Solubility	:	Water

3.6 EXPERIMENTAL

Solution of Rose Bengal (HIMEDIA) was prepared by dissolving 0.254 g in 250.0 mL water to get 1.0×10^{-4} M solution as a stock solution. The absorbance (A) of Rose Bengal dye solution was determined with the help of a spectrophotometer at λ max = 527 nm. The dye solution was placed in equal amounts in four beakers.

- The first beaker containing dye solution was kept in dark,
- The second beaker containing dye solution was exposed to 200 W tungsten lamp,
- The third beaker containing dye solution with 0.08 g photocatalyst graphitic carbon nitride was kept in dark, and

- The fourth beaker contain dye solution and 0.08 g photocatalyst graphitic carbon nitride was exposed to 200 W tungsten lamp.

The absorbance of dye solution was measured with the help of a spectrophotometer. It was observed that the absorbance of first beaker remained almost same after 3-4 h while the second beaker had a decrease in initial value of its absorbance. The initial absorbance value of the third beaker showed a slight difference. The initial absorbance value of the fourth beaker experienced a significant reduction. This observation confirmed that the reaction between Rose Bengal and photocatalyst is a photocatalytic reaction.

The photodegradation of Rose Bengal was monitored by taking absorbance of samples of dye solution (8.0×10^{-5}M) containing 0.08 g photocatalyst (g-C_3N_4) and exposed to 200 W tungsten lamp (70.0 mW cm^{-2}) at pH = 8.5. The absorbance of Rose Bengal was found to decrease with increasing time of exposure. A plot of 1 + log A versus time was found to be linear. The rate constant of reaction was calculated with the following expression k = 2.303 × slope. The data of typical run are presented in Table 3.11: and Fig. 3.14:

Table 3.11: A typical run

pH = 8.5 g-C_3N_4 = 0.08 g

[Rose Bengal] = 8.0×10^{-5} M Light Intensity = 70.0 mW cm^{-2}

Time (min)	Absorbance (A)	1 + log A
0.00	0.685	0.8356
10.0	0.684	0.8350
20.0	0.672	0.8273
30.0	0.654	0.8155
40.0	0.637	0.8041
50.0	0.621	0.7930
60.0	0.613	0.7874
70.0	0.588	0.7694
80.0	0.576	0.7604
90.0	0.574	0.7589
100	0.557	0.7458
110	0.543	0.7347

Rate constant (k) = 3.83×10^{-5} s^{-1}

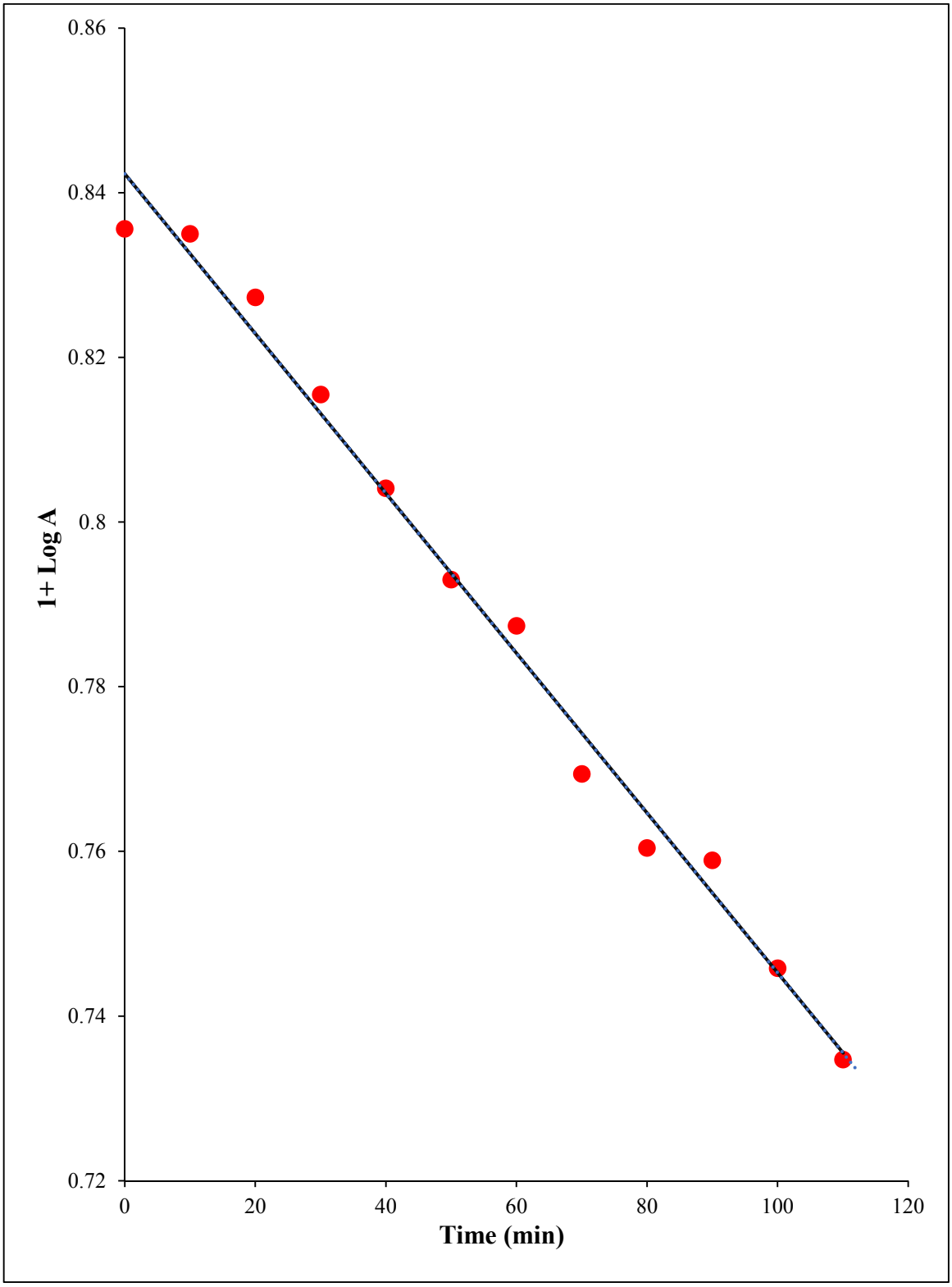

Fig. 3.14: A typical run

3.6.1 Effect of pH

The effect of pH on photocatalytic degradation was observed in the range of 6.5 to 10.0. The results are given in Table 3.12: and Fig. 3.15:

Table 3.12: Effect of pH

[Rose Bengal] = 8.0×10^{-5} M g-C_3N_4 = 0.08 g

Light Intensity = 70.0 mW cm^{-2}

pH	**Rate constant (k) × 10^5 (s^{-1})**
6.5	1.39
7.0	2.08
7.5	2.69
8.0	3.29
8.5	**3.83**
9.0	2.92
9.5	2.55
10	1.26

It was noticed that the degradation rate of Rose Bengal increases with increasing pH of solution up till 8.5, but above this value of pH, the rate of reaction of photodegradation of Rose Bengal started decreasing.

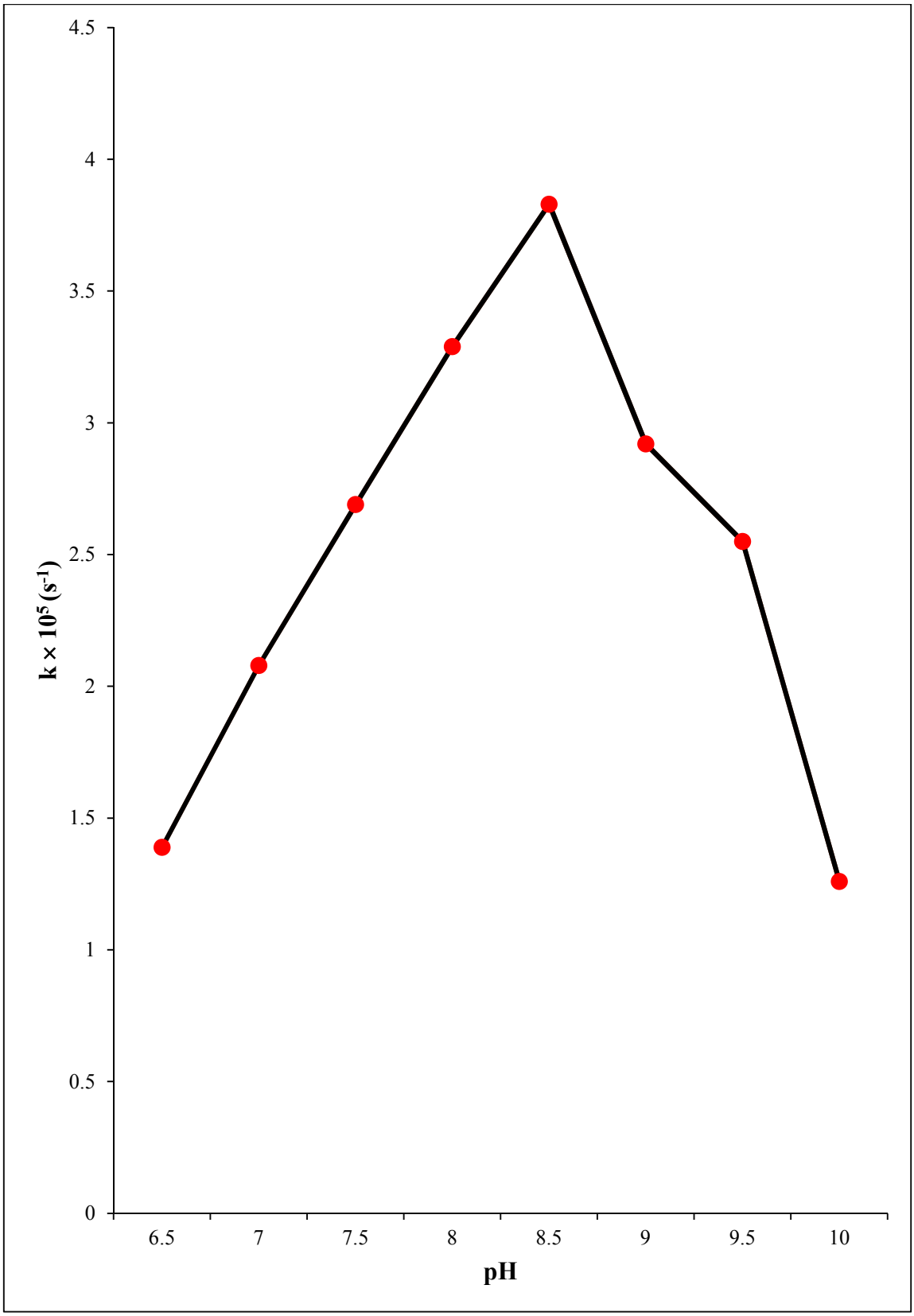

Fig. 3.15: Effect of pH

3.6.2 Effect of dye concentration

The effect of dye concentration on the rate of reaction was also observed using different concentrations of Rose Bengal solution (2.0×10^{-5}M-1.8×10^{-4}M) The results are shown in Table 3.13: and Fig. 3.16:

Table 3.13: Effect of dye concentration

pH = 8.5 Light Intensity = 70.0 mW cm^{-2}

g-C_3N_4 = 0.08 g

[Rose Bengal] × 10^4 M	**Rate constant (k) × 10^5 (s^{-1})**
0.2	1.58
0.4	2.02
0.6	2.54
0.8	**3.83**
1.2	3.01
1.4	2.63
1.6	2.18
1.8	1.69

It was observed that the rate of photocatalytic degradation increases with increase in the concentration of the dye up to 8.0×10^5 M, but therefore, it decreases.

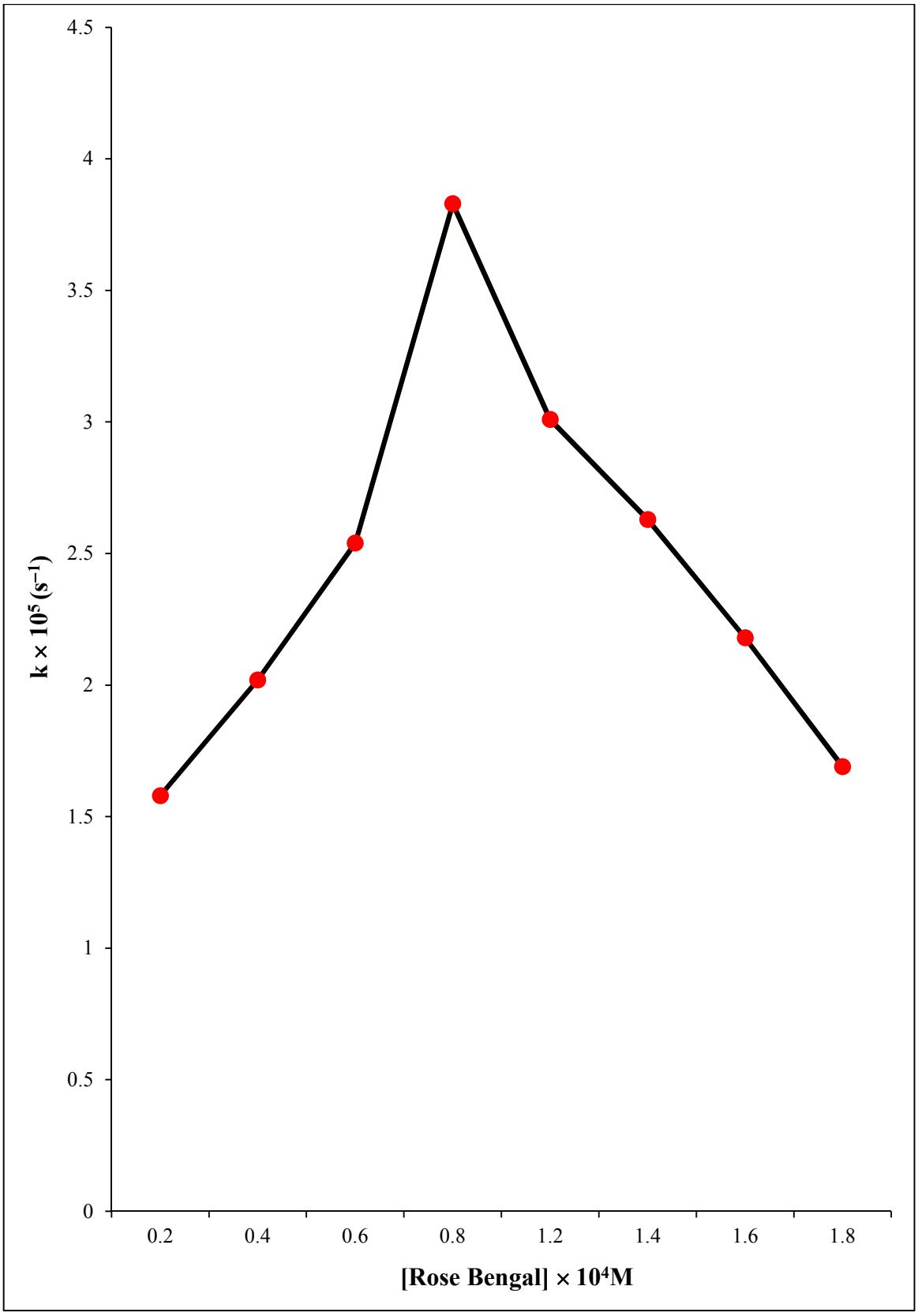

Fig. 3.16: Effect of dye concentration

3.6.3 Effect of amount of photocatalyst

The effect of amount of photocatalyst on the rate of photocatalytic degradation of Rose Bengal was also observed in the rang 0.02-0.18 g. The results are shown in Table 3.14: and Fig. 3.17:

Table 3.14: Effect of amount of photocatalyst

pH = 8.5 Light Intensity = 70.0 mW cm^{-2}

[Rose Bengal] = 8.0×10^{-5} M

g-C_3N_4 (g)	**Rate constant (k) × 10^4 (s^{-1})**
0.02	2.08
0.04	2.97
0.06	3.72
0.08	**3.83**
0.12	3.28
0.14	2.65
0.16	2.55
0.18	2.26

It was noticed that the rate of reaction increases with increase in the amount of photocatalyst up to 0.08 g, but above this value of photocatalyst, the rate of reaction decreased.

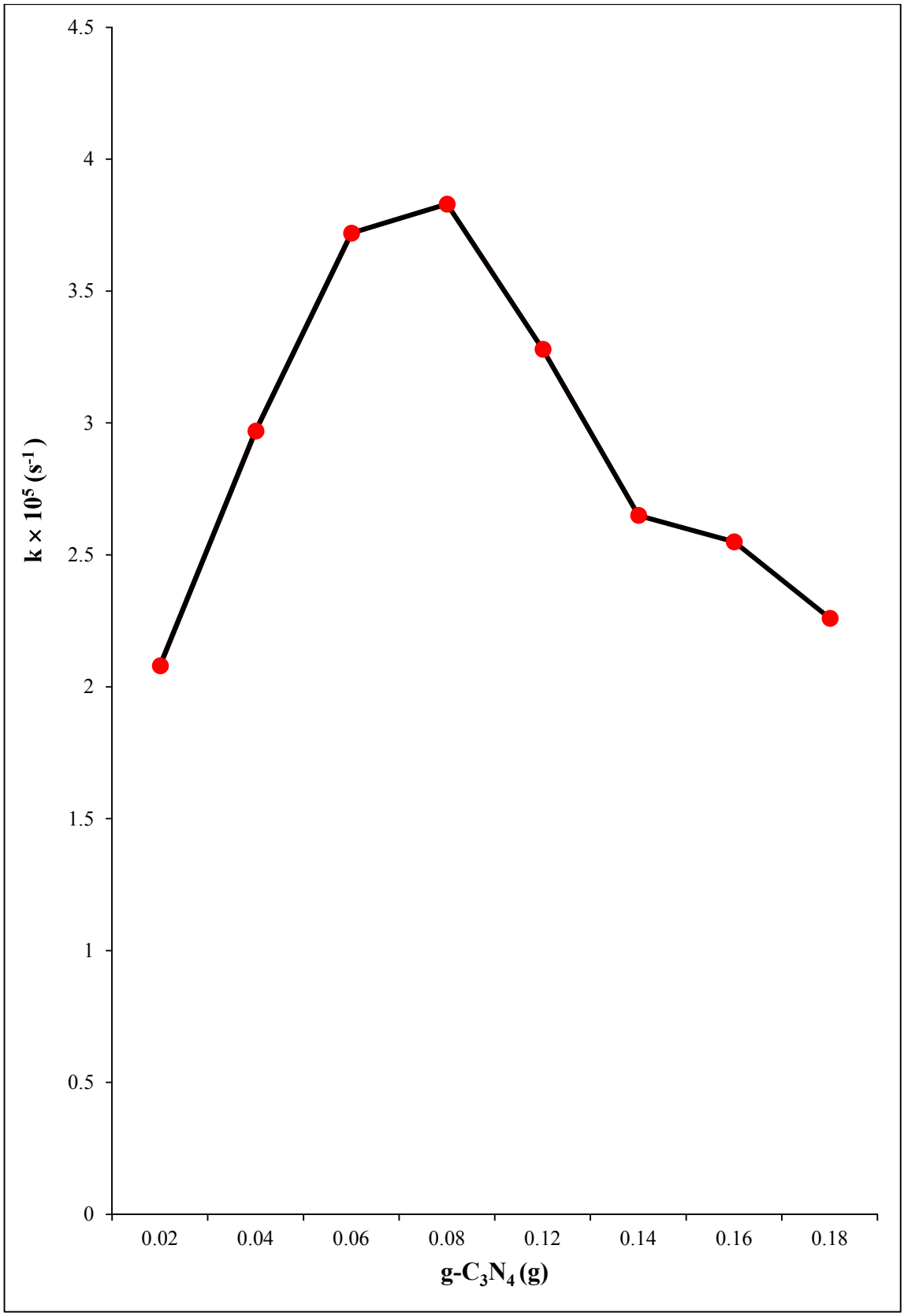

Fig. 3.17: Effect of amount of photocatalyst

3.6.4 Effect of light intensity

The effect of light intensity on the rate of Rose Bengal was also observed from 20.0 to 70.0 mW cm^{-2} The results are reported in Table 3.15: and Fig. 3.18:

Table 3.15: Effect of light intensity

pH = 8.5 [Rose Bengal] = 8.0×10^{-5} M

g-C_3N_4 = 0.08 g

Light intensity (mW cm^{-2})	**Rate constant (k) × 10^5 (s^{-1})**
30	0.35
40	1.78
50	3.10
60	3.59
70	**3.83**

It was observed that the rate of degradation increased on increasing light intensity.

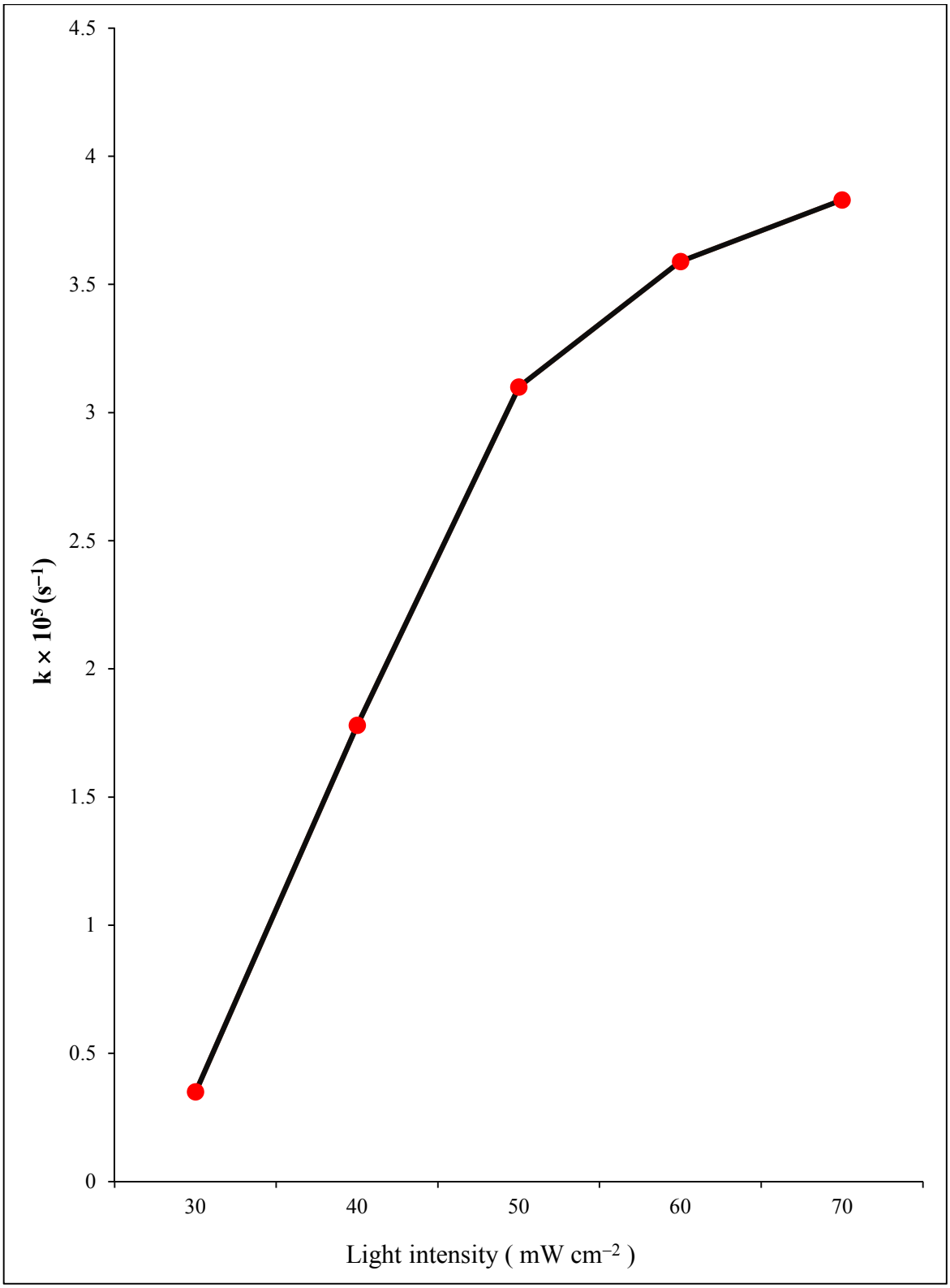

Fig. 3.18: Effect of light intensity

❐❐❐

CHAPTER – IIID

METHYLENE BLUE-GRAPHITIC CARBON NITRIDE SYSTEM

CONTENTS

3.7 METHYLENE BLUE

Methylthionine chloride is commonly called methylene blue. Its salt is used as a dye and for medication. It is mainly used to treat methemoglobinemia by chemically reducing the ferric iron in haemoglobin to ferrous iron

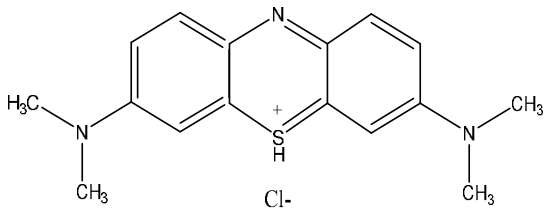

Fig. 3.19: Structure of Methylene Blue

IUPAC Name	:	3,7-Bis(Dimethylamine)-phenothiazin-5-ium chloride
Molecular Formula	:	$C_{16}H_{18}ClN_3S$
Molecular Mass	:	319.85 g mol^{-1}
λ max	:	664 nm
Solubility	:	Water

3.8 EXPERIMENTAL

A 1.0×10^{-4} M solution of methylene blue (HIMEDIA) was prepared by dissolving 0.0934 g of methylene blue in 250.0 mL of distilled water. This solution served as a stock solution. The absorbance of methylene blue dye solution was measured using a spectrophotometer at a wavelength of λ max = 664 nm. The dye solution was divided into four portions.

- The first beaker containing dye solution was kept in dark,
- The second beaker containing dye solution was exposed to 200 W tungsten lamp,
- The third beaker containing dye solution and 0.16 g of graphitic carbon nitride was kept in dark, and

- The fourth beaker containing dye solution and 0.16 g photocatalyst graphitic carbon nitride was exposed to 200 W tungsten lamp.

It was observed that the absorbance of the first beaker remained almost same even after 3 h. while the second beaker had a slight decrease in initial value of its absorbance. The initial absorbance of the third beaker also showed a slight decrease. The absorbance of the fourth beaker experienced a significant reduction. These observations indicate that the reaction between methylene blue and photocatalyst is a photocatalytic reaction only.

The 0.16 g of g-C_3N_4 was added to 1.50×10^{-4} M dye solution and then exposed to a 200 W tungsten lamp at pH = 8.5 and 60.0 mW cm^{-2}. The absorbance of methylene blue was found to decrease with increasing exposure time. A linear relationship was observed on plotting 1 + log A against time. The rate constant (k) of the reaction was calculated using the expression k = 2.303 × slope. The results are reported in Table 3.16 and Fig. 3.20.

Table 3.16: A typical run

pH= 8.5 [Methylene blue] = 1.50×10^{-4} M

g-C_3N_4 = 0.16 g Light intensity = 60.0 mW cm^{-2}

Time (min)	Absorbance (A)	1 + log A
0.00	1.138	1.0561
10.0	1.105	1.0433
20.0	1.014	1.006
30.0	0.755	0.8779
40.0	0.743	0.8709
50.0	0.661	0.8202
60.0	0.637	0.8041
70.0	0.599	0.7774
80.0	0.563	0.7505
90.0	0.530	0.7242
100	0.497	0.6963
110	0.413	0.6159

Rate constant = $1.65 \times 10^{-4} s^{-1}$

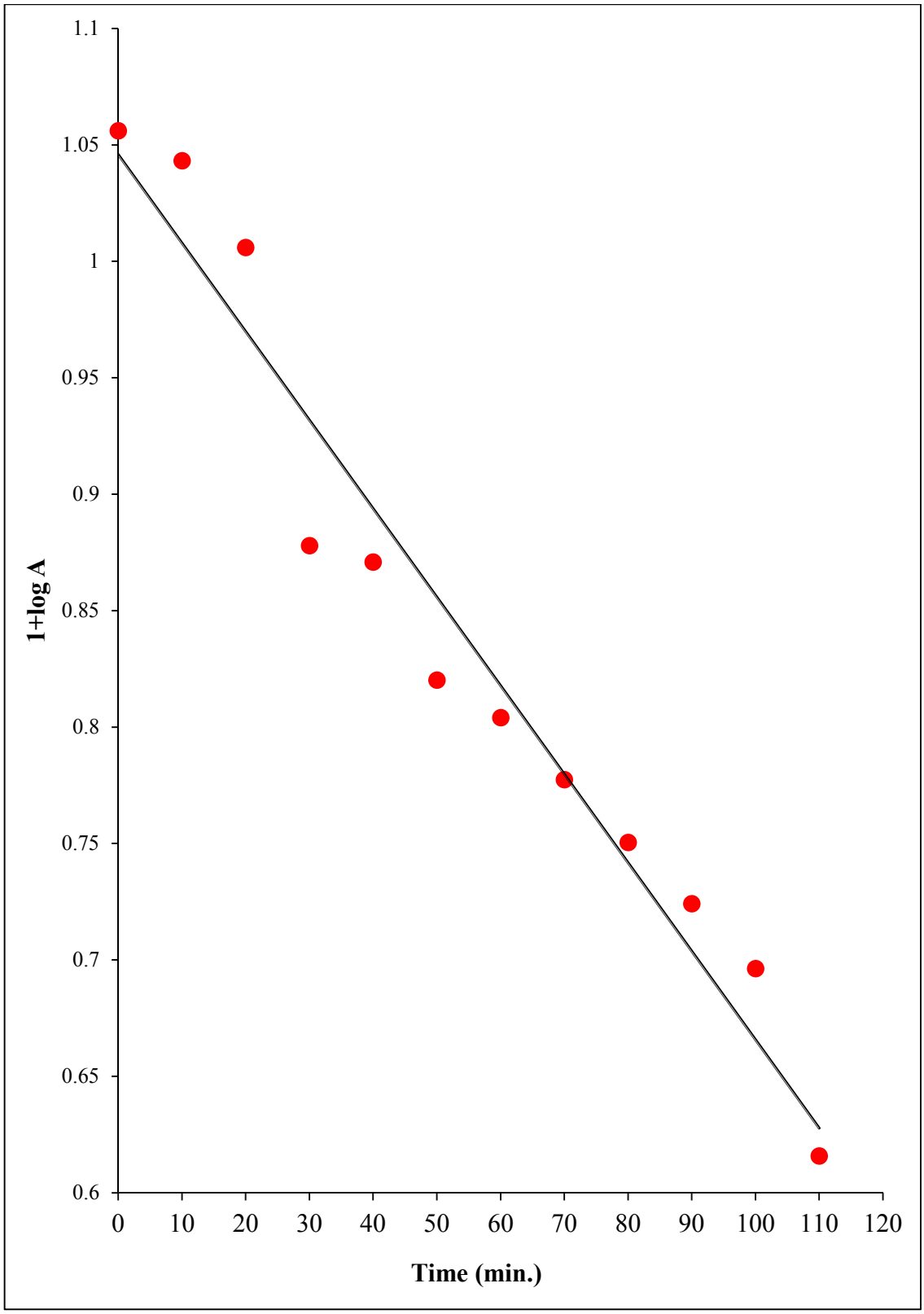

Fig. 3.20: A typical run

3.8.1 Effect of pH

The effect of pH on photocatalytic degradation was observed in the range of 5.5 to 9.5. The results are shown in Table 3.17: and Fig.3.21:

Table 3.17: Effect of pH

[Methylene blue] = 1.50×10^{-4} M g-C_3N_4 = 0.16 g

Light Intensity = 60.0 mW cm^{-2}

pH	**Rate constant (k)× 10^4 (s^{-1})**
5.5	0.47
6.0	0.88
6.5	1.19
7.0	1.32
7.5	1.59
8.0	1.76
8.5	**1.65**
9.0	1.29
9.5	1.02

The rate of degradation of methylene blue increases with increasing pH of solution up to 8.5, but above this value of pH, the rate of photodegradation of methylene blue started decreasing.

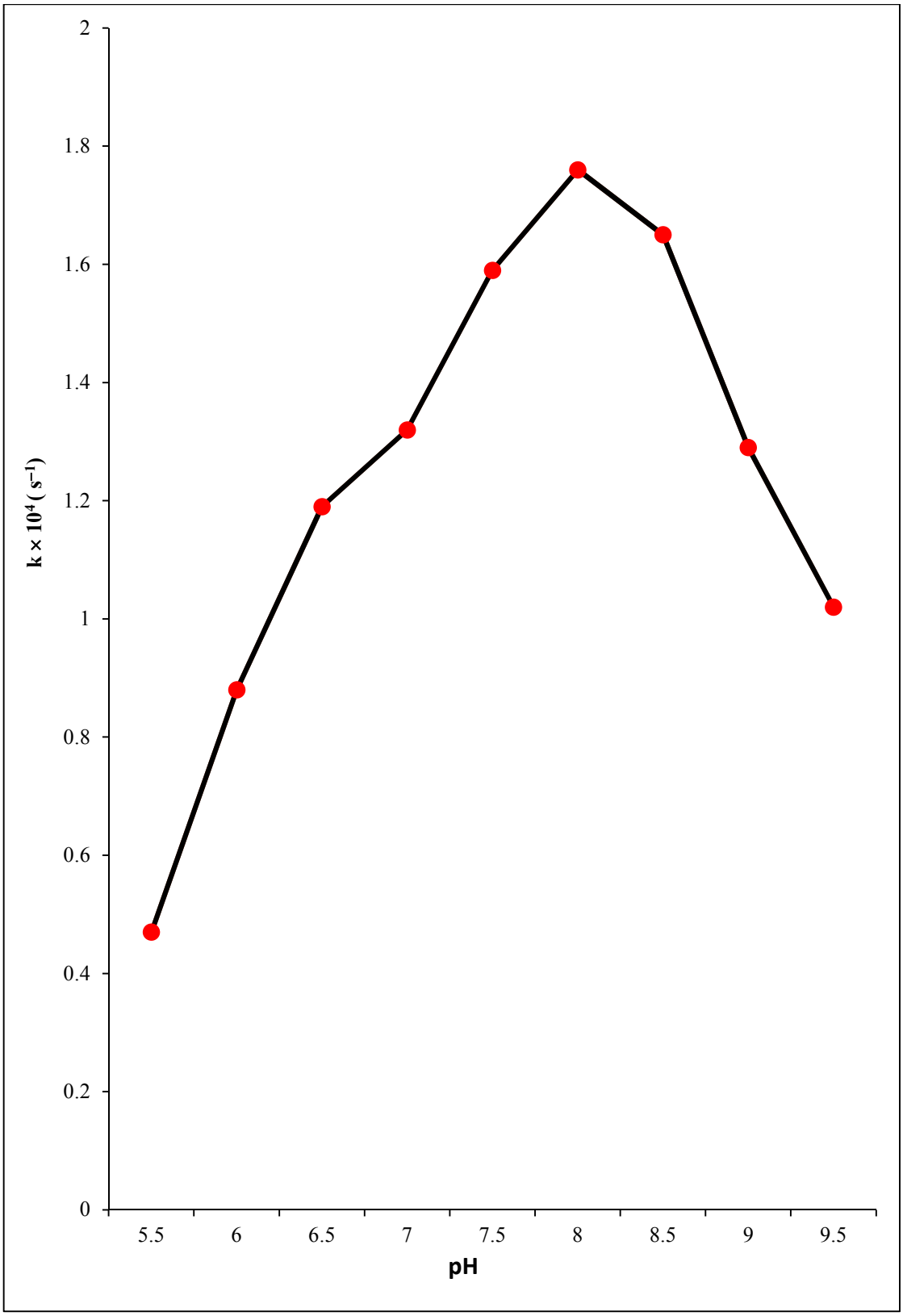

Fig. 3.21: Effect of pH

3.8.2 Effect of dye concentration

The effect of dye concentration of dye on the rate of reaction was also observed using different concentrations of methylene blue solution. The results are tabulated in Table 3.18: and presented in Fig. 3.22:

Table 3.18: Effect of dye concentration

pH = 8.5 Light intensity = 60.0 mW cm^{-2}

g-C_3N_4 = 0.16 g

[Methylene Blue] × 10^4 M	**Rate constant (k)× 10^4 (s^{-1})**
0.1	0.43
0.3	0.68
0.7	1.09
0.9	1.19
1.1	1.42
1.3	1.5
1.5	**1.65**
1.7	0.82
1.8	0.56

It was noticed that the rate of photocatalytic degradation increases with dye concentration up to 1.50 × 10^4 M, but it decreases on increasing the concentration of dye further.

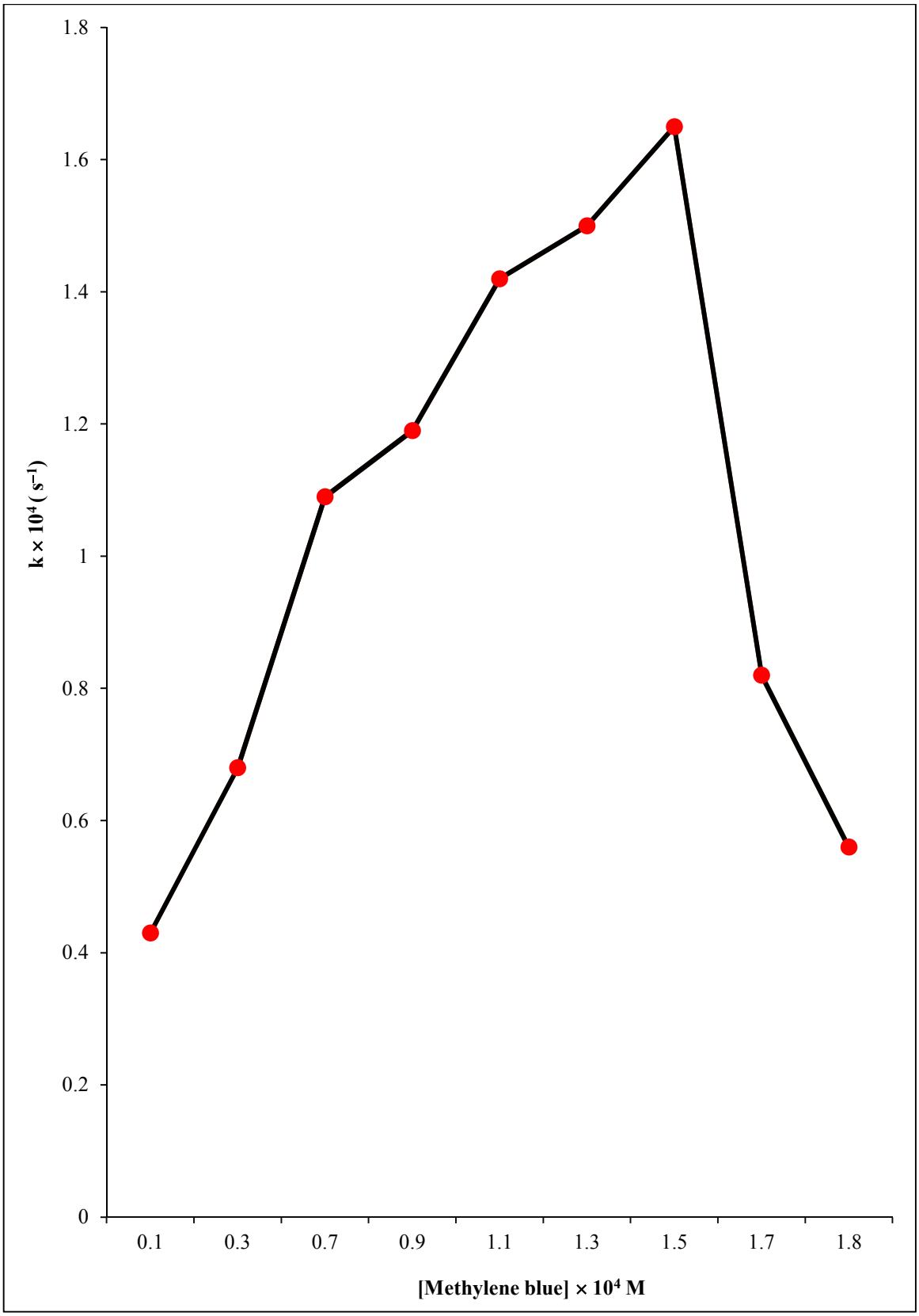

Fig. 3.22: Effect of dye concentration

3.8.3 Effect of amount of photocatalyst

The effect of amount of photocatalyst on the rate of photocatalytic degradation of methylene blue was also observed in the rang of 0.02-0.20 g. The results are shown in Table 3.19: and Fig. 3.23.

Table 3.19: Effect of amount of photocatalyst

[MB] = 1.50×10^{-4} M pH = 8.5

Light intensity = 60.0 mW cm^{-2}

g-C_3N_4 (g)	**Rate constant (k) × 10^4 (s^{-1})**
0.02	0.55
0.04	0.78
0.06	0.97
0.08	1.12
0.12	1.21
0.14	1.38
0.16	**1.65**
0.18	1.36
0.20	1.18

The reaction rate increased with increasing at larger quantity of photocatalyst till 0.16 g, beyond which, the rate started declining.

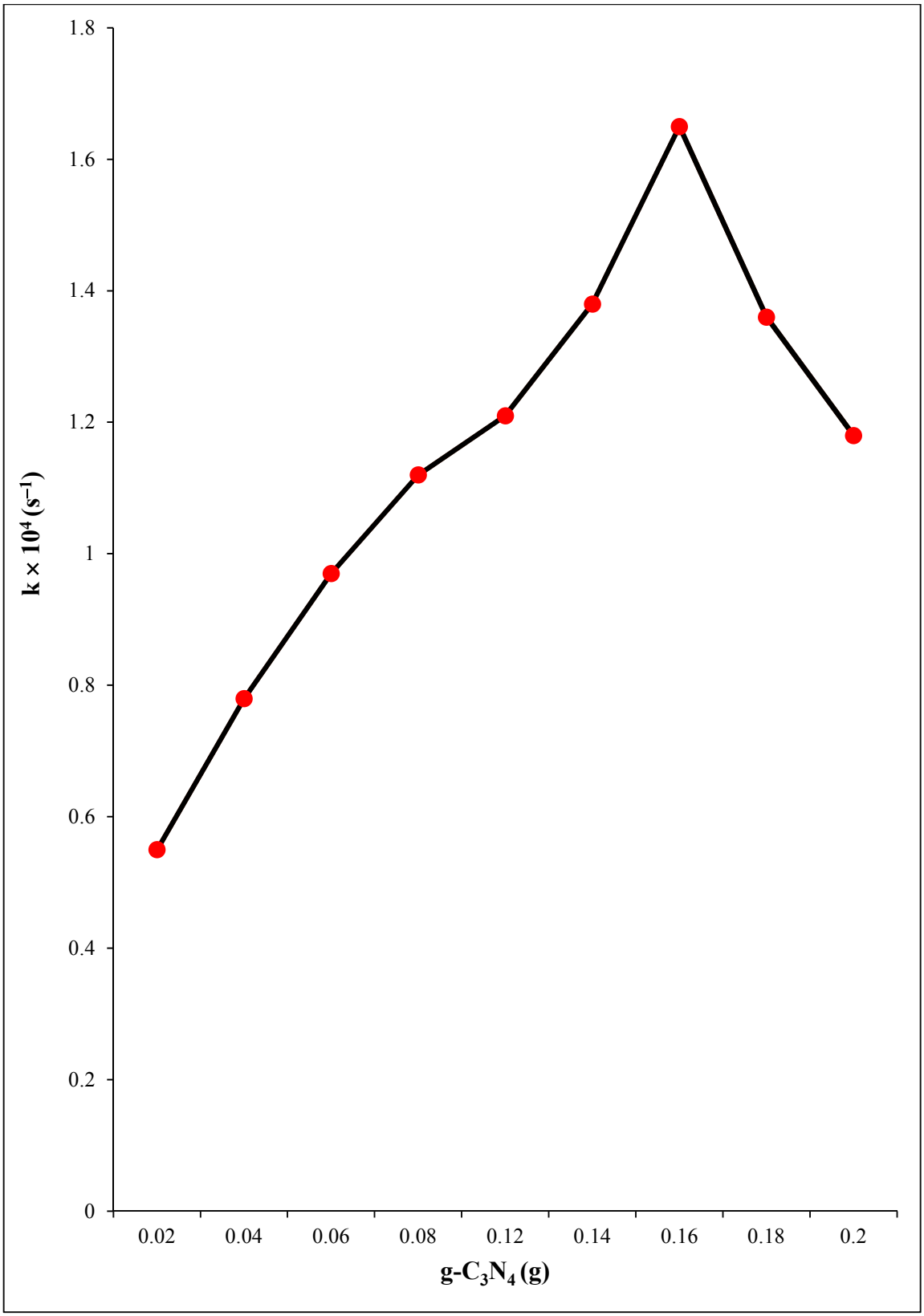

Fig. 3.23: Effect of amount of photocatalyst

3.8.4 Effect of light intensity

The effect of light intensity on the rate of degradation of methylene blue was also observed from 20.0-70.0 mW cm^{-2}. The results are reported in Table 3.20: and Fig. 3.24:

Table 3.20: Effect of light intensity

[MB] = 1.50×10^{-4} M pH = 8.5

g-C_3N_4 = 0.16 g

Light intensity (mW cm^{-2})	**Rate constant (k) × 10^4 (s^{-1})**
20.0	0.85
30.0	0.91
40.0	0.98
50.0	1.22
60.0	**1.65**
70.0	1.58

It was observed that the rate of degradation was increased on increasing light intensity up to 60.0 $mWcm^{-2}$ but above this value, the rate of degradation again decreased.

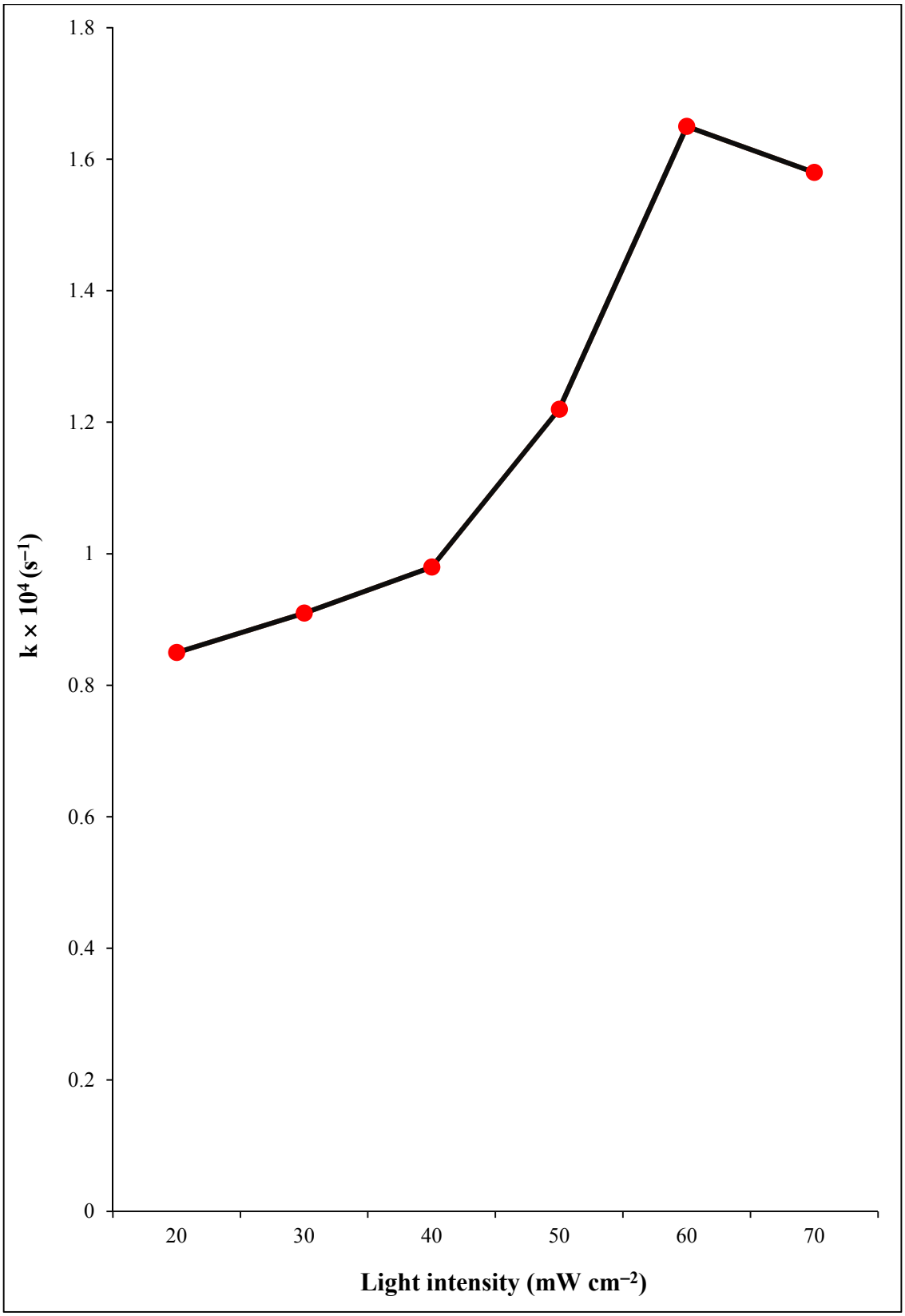

Fig. 3.24: Effect of light intensity

❐❐❐

CHAPTER – IIIE

RHODAMINE B- GRAPHITIC CARBON NITRIDE SYSTEM

CONTENTS

3.9 RHODAMINE B

Rhodamine B is a dye. It is often used as a tracer dye within water to determine the rate and direction of flow and transport. Rhodamine dye fluoresce and can be detected easily with fluorometer.

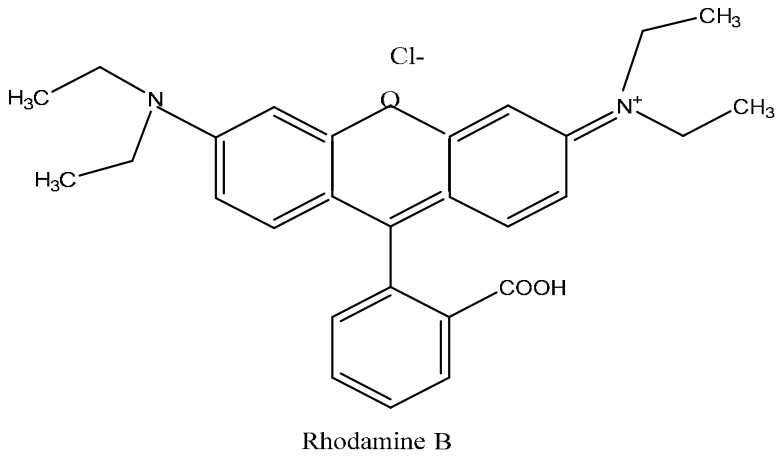

Rhodamine B

Fig. 3.25: Structure of Rhodamine B

IUPAC Name	:	9-(2-Carboxyphenyl)-6-(diethylamino)-N,N-diethyl-3H-xanthen-3-iminium chloride
Molecular Formula	:	$C_{28}H_{31}N_2O_3Cl$
Molecular Mass	:	479 g mol^{-1}
λ max	:	556 nm
Solubility	:	Water

3.10 EXPERIMENTAL

A 1.0×10^{-3} M solution of rhodamine B (HIMEDIA) was prepared by dissolving 0.120 g of rhodamine B in 250.0 mL of distilled water. This solution served as a stock solution. The absorbance of rhodamine B dye solution was measured using a spectrophotometer at a wavelength of λ max = 556 nm. The dye solution was divided into four portions.

- The first beaker containing dye solution was kept in dark,
- The second beaker containing dye solution was exposed to 200 W tungsten lamp,
- The third beaker containing dye solution and 0.12 g of graphitic carbon nitride was kept in dark, and
- The fourth beaker containing dye solution and 0.12 g photocatalyst graphitic carbon nitride was exposed to 200 W tungsten lamp.

It was observed that the absorbance of the first beaker remained almost same even after 3 h. while the second beaker had a slight decrease in initial value of its absorbance. The initial absorbance of the third beaker also showed a slight decrease. The absorbance of the fourth beaker experienced a significant reduction. These observations indicates that the reaction between rhodamine B and photocatalyst is a photocatalytic reaction only.

The 0.12 g of g-C_3N_4 was added to 1.00×10^{-3} M dye solution and then exposed to a 200 W tungsten lamp at pH = 7.5 and 60.0 m W cm^{-2}. The absorbance of rhodamine B was found to decrease with increasing exposure time. A linear relationship was observed on plotting 1 + log A against time. The rate constant (k) of the reaction was calculated using the expression k = 2.303 × slope. The results are reported in Table 3.21 and Fig. 3.26.

Table 3.21: A typical run

[Rhodamine B] = 8.00×10^{-4} M pH = 7.5

g-C_3N_4 = 0.12 g Light intensity = 40.0 mW cm^{-2}

Time (min)	Absorbance (A)	1 + log A
0.00	0.735	0.8662
10.0	0.676	0.8299
20.0	0.631	0.8000
30.0	0.603	0.7803
40.0	0.586	0.7678
50.0	0.466	0.7438
60.0	0.531	0.7250
70.0	0.555	0.7212
80.0	0.525	0.7201
90.0	0.522	0.7176
100	0.510	0.7075

Rate constant (k) = $9.51 \times 10^{-5} s^{-1}$

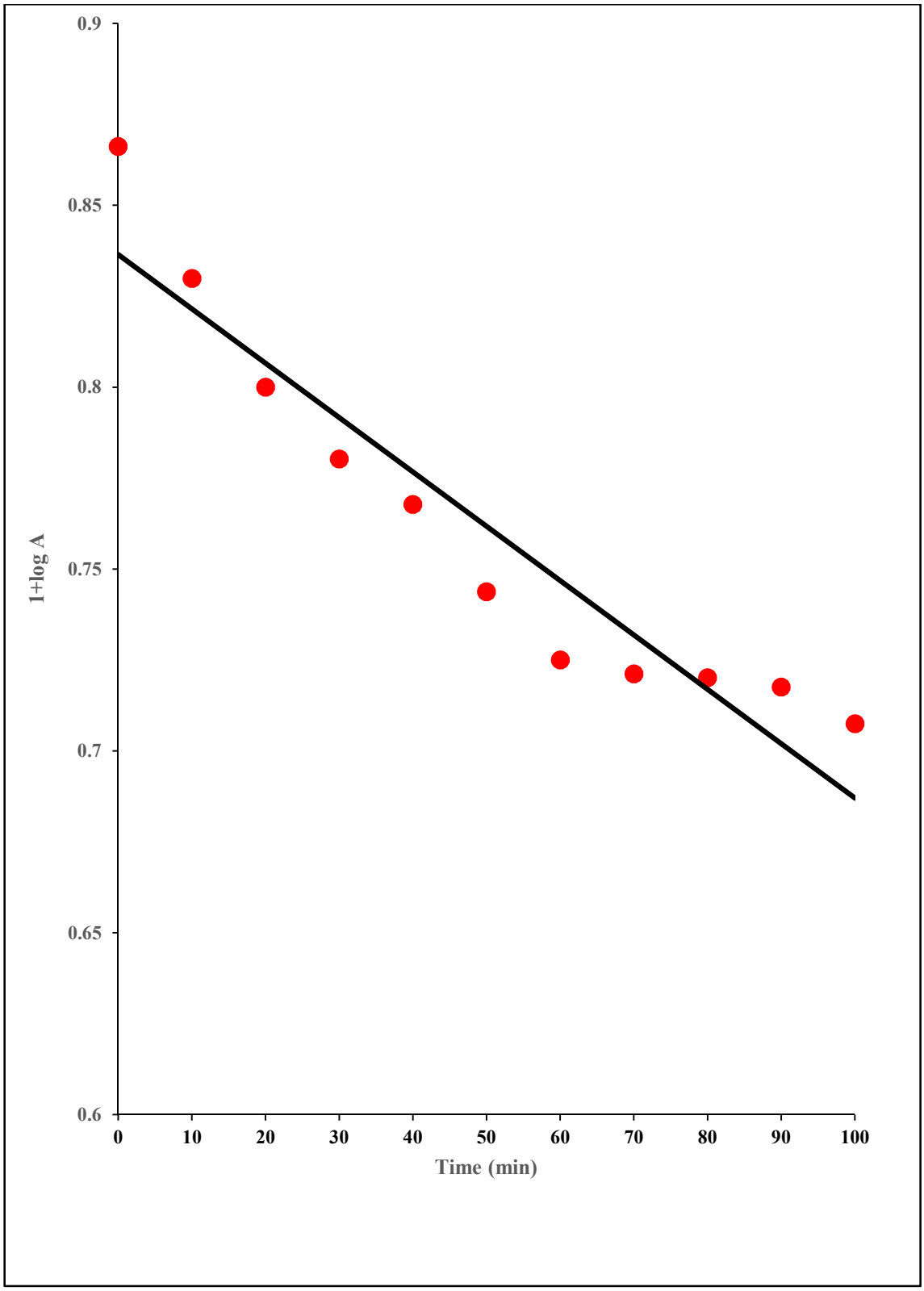

Fig. 3.26: A typical run

3.10.1 Effect of pH

The effect of pH on photocatalytic degradation was observed in the range of 5.5 to 9.0. The results are shown in Table 3.22: and Fig. 3.27:

Table 3.22: Effect of pH

[Rhodamine B] = 8.00×10^{-5} M g-C_3N_4 = 0.12 g

Light Intensity = 60.0 mW cm^{-2}

pH	**Rate constant (k) × 10^5 (s^{-1})**
5.5	3.00
6.0	3.34
6.5	4.01
7.0	5.72
7.5	**9.51**
8.0	7.11
8.5	4.74
9.0	3.36

The rate of degradation of Rhodamine B increases with increasing pH of solution up to 7.5, but above this value of pH, the rate of photodegradation of rhodamine B start decreasing.

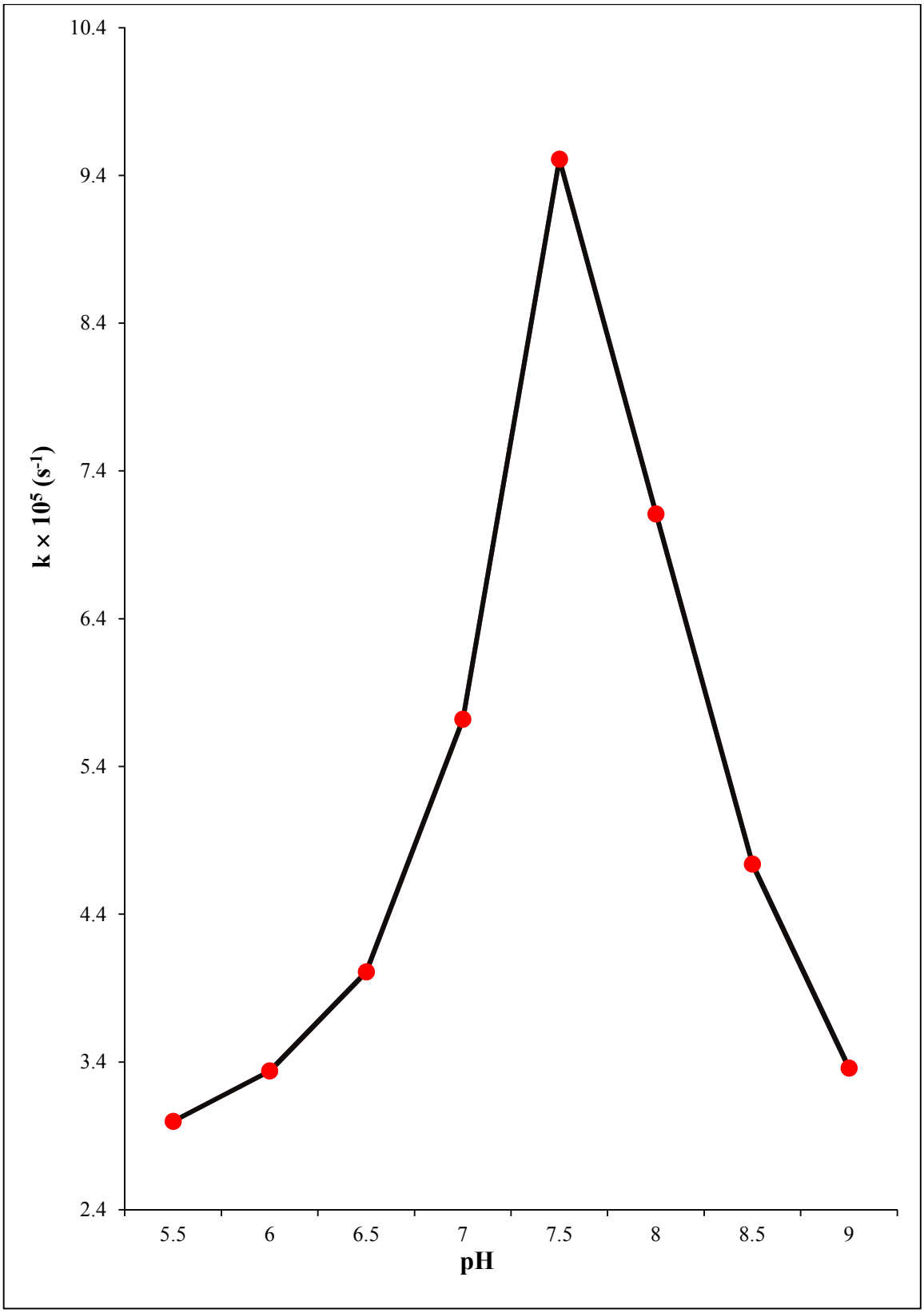

Fig. 3.27: Effect of pH

3.10.2 Effect of dye concentration

The effect of dye concentration on the rate of reaction was also observed using different concentrations of rhodamine B solution betweem 2.0×10^{-5} to 1.8×10^{-4}M. The results are tabulated in Table 3.23: and presented in Fig. 3.28:

Table 3.23: Effect of dye concentration

pH = 7.5 Light intensity = 60.0 mW cm^{-2}

g-C_3N_4 = 0.12 g

[Rhodamine B] × 10^4 M	**Rate constant (k)× 10^5 (s^{-1})**
0.2	3.24
0.4	3.94
0.6	6.75
0.8	**9.51**
1.0	8.43
1.2	6.64
1.4	5.71
1.6	3.99
1.8	2.12

It was noticed that the rate of photocatalytic degradation increases with dye concentration up to 8.0×10^{-5} M, but it started decreasing above this value.

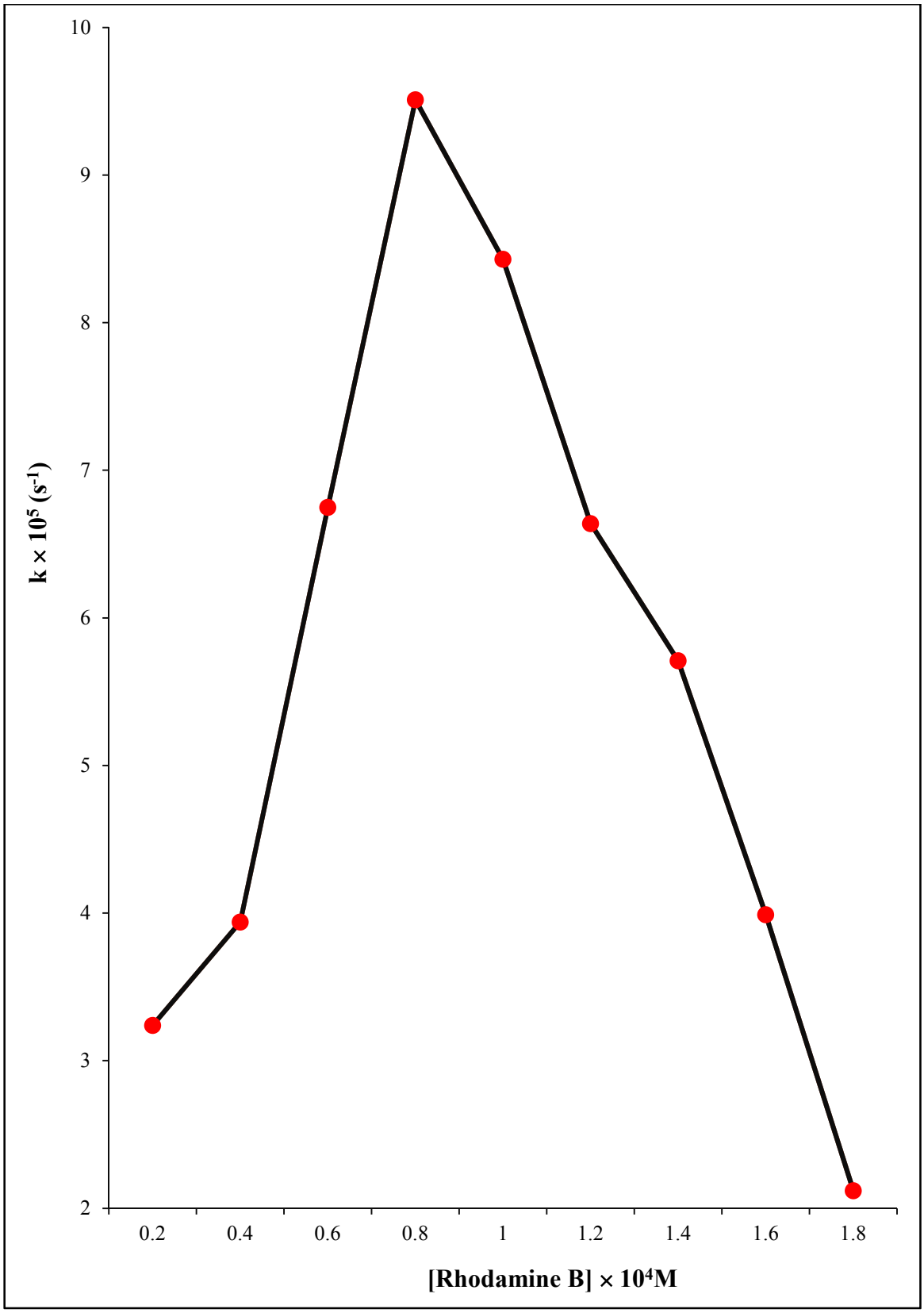

Fig. 3.28: Effect of dye concentration

3.10.3 Effect of amount of photocatalyst

The effect of amount of photocatalyst on the rate of photocatalytic degradation of Rhodamine B was also observed in the rang of 0.02-0.16 g. The results are shown in Table 3.24: and Fig. 3.29:

Table 3.24: Effect of amount of photocatalyst

[Rhodamine B] = 8.00×10^{-5} M pH = 7.5

Light intensity = 60.0 mW cm^{-2}

g-C_3N_4 (g)	**Rate constant (k) × 10^5 (s^{-1})**
0.02	4.24
0.04	4.67
0.06	5.21
0.08	6.86
0.10	8.18
0.12	**9.51**
0.14	8.03
0.16	6.99
0.18	5.83

The reaction rate was higher at larger quantity of photocatalyst till 0.12 g, beyond which, the rate started declining.

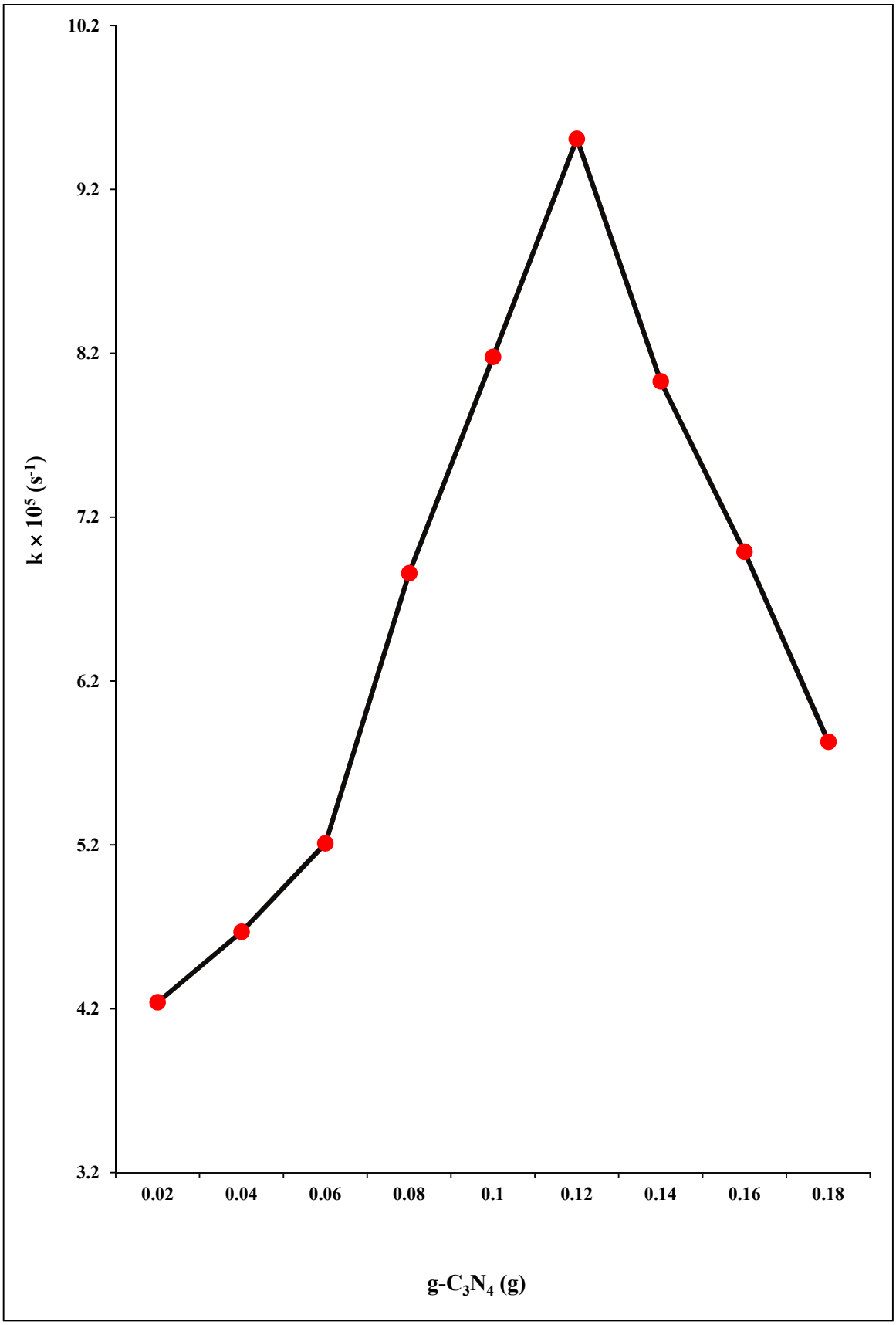

Fig. 3.29: Effect of amount of photocatalyst

3.10.4 Effect of light intensity

The effect of light intensity on the rate of degradation of Rhodamine B was also observed from 20.0 to 70.0 mW cm^{-2}. The results are reported in Table 3.25: and Fig. 3.30:

Table 3.25: Effect of light intensity

[Rh B] = 8.00×10^{-5} M pH = 7.5

g-C_3N_4 = 0.12 g

Light intensity (mW cm^{-2})	**Rate constant (k) × 10^5 (s^{-1})**
20.0	3.18
30.0	5.43
40.0	6.45
50.0	7.12
60.0	**9.51**
70.0	9.31

It was observed that the rate of degradation increased on increasing light intensity up to 60.0 mWcm^{-2}, but above this value, the rate of degradation again decreased.

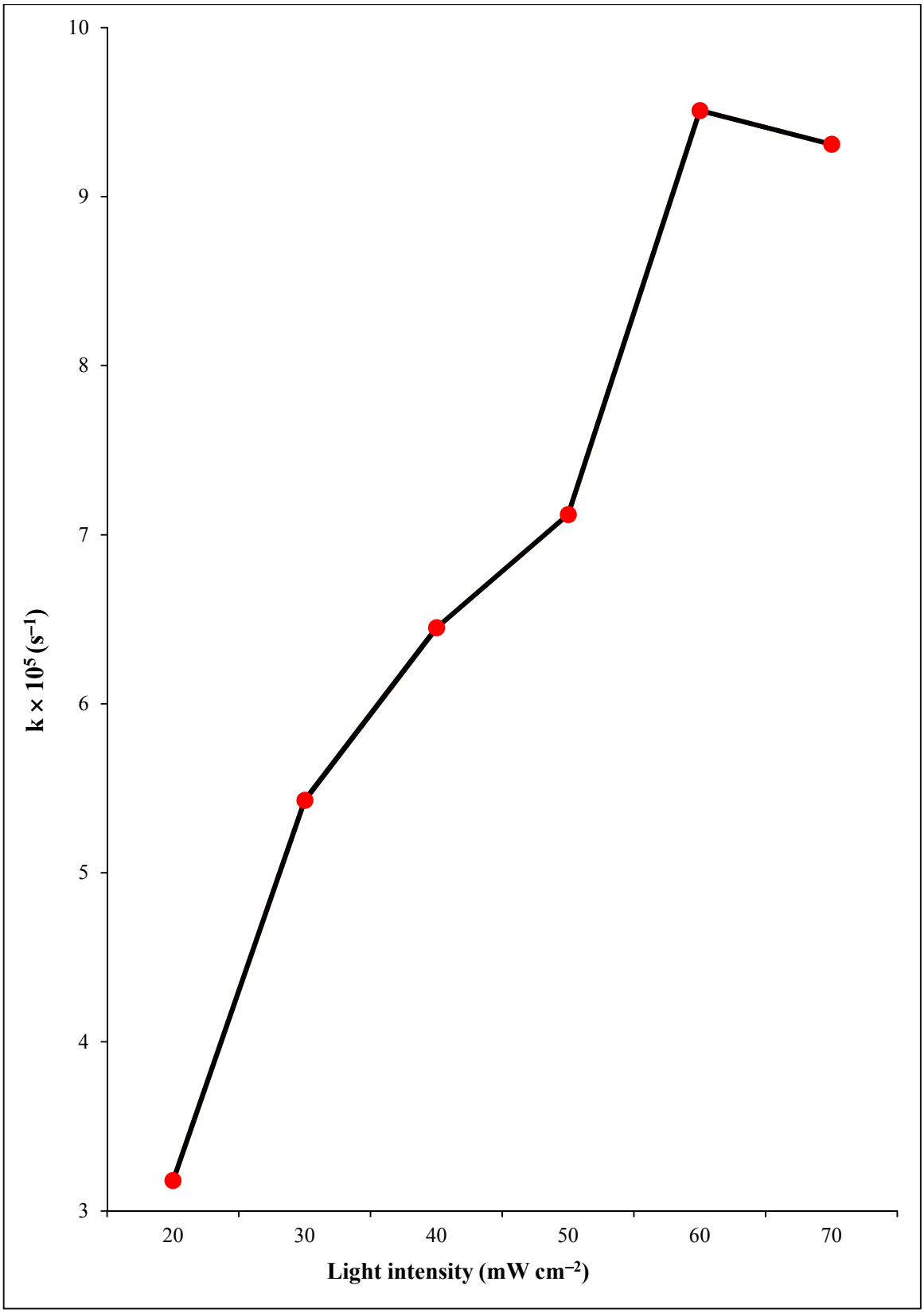

Fig. 3.30: Effect of light intensity

❐❐❐

CHAPTER – IIIF

ALIZARIN RED-S – GRAPHITIC CARBON NITRIDE SYSTEM

CONTENTS

3.11 ALIZARIN RED-S

Alizarin red-S is also known as mordant red 3, or alizarin carmine. Alizarin red-S is used to stain calcium deposits in tissues in histology.

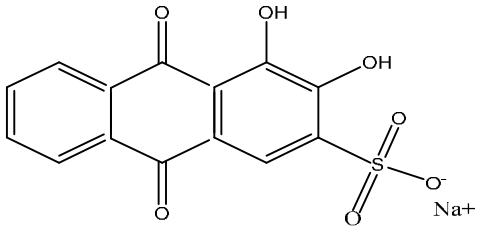

Fig. 3.31: Structure of Alizarin Red-S

IUPAC Name	:	3,4-Dihydroxy-9,10-dioxo-9,10-dihydroanthracene-2-sulfonic acid
Molecular Formula	:	C14H7NaO7S
Molecular Mass	:	342.2 g / mol−1
λ max	:	527 nm
Solubility	:	Water

3.12 EXPERIMENTAL

Solution of alizarin red-S (HIMEDIA) was prepared by dissolving 0.0342 g in 100.0 mL water to get 1.0×10^{-3} M stock solution. The absorbance (A) of alizarin red-S dye solution was determined with the help of a spectrophotometer at λ max = 527 nm. The dye solution was placed in equal amounts in four beakers.

- The first beaker containing dye solution was kept in dark,
- The second beaker containing dye solution was exposed to 200 W tungsten lamp,
- The third beaker containing dye solution with 0.12 g photocatalyst graphitic carbon nitride was kept in dark, and
- The fourth beaker contain dye solution and 0.12 g photocatalyst graphitic carbon nitride was exposed to 200 W tungsten lamp.

The absorbance of dye solution was measured with the help of a spectrophotometer. It was observed that the absorbance of first beaker remained almost same after 3-4 h while the second beaker had a slight decrease in initial value of its absorbance. The initial absorbance value of the third beaker showed a slight difference. The initial absorbance value of the fourth beaker experienced a significant reduction. This observation confirmed that the reaction between Alizarin red-S and photocatalyst is a photocatalytic reaction.

The photodegradation of alizarin red-S was monitored by taking absorbance of samples of dye solution containing 0.12 g photocatalyst (g-C_3N_4) and exposed to 200 W tungsten lamp (70.0 mW cm^{-2}) at pH = 8.0. The absorbance of alizarin red-S was found to decrease with increasing time of exposure. A plot of 1 + log A versus time was found to be linear. The rate constant of reaction was calculated with the following expression k = 2.303 × slope. The data of typical run are presented in Table 3.26: and graphically Fig.3.32:

Table 3.26: A typical run

pH = 8.0 g-C_3N_4 = 0.12 g

[Alizarin red-S] = 3.20×10^{-4} M Light Intensity = 70.0 mW cm^{-2}

Time (min)	Absorbance (A)	1+ log A
0	0.642	0.8075
10	0.627	0.7972
20	0.567	0.7535
30	0.528	0.7226
40	0.510	0.7075
50	0.478	0.6794
60	0.525	0.7201
70	0.466	0.6683
80	0.430	0.6334
90	0.401	0.6031
100	0.375	0.5740
110	0.355	0.5502

Rate constant (k) = 8.72×10^{-5} s^{-1}

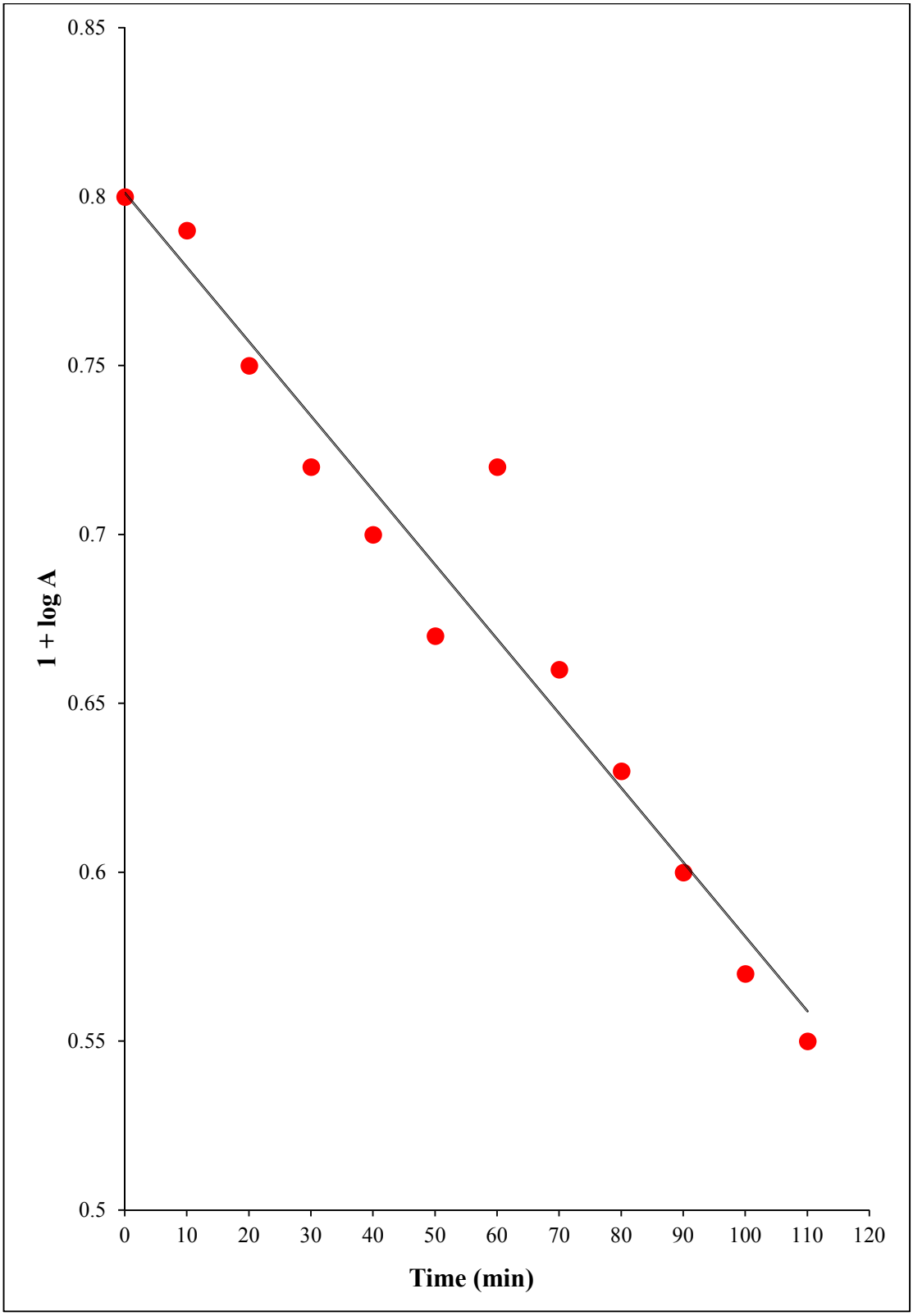

Fig. 3.32: A typical run

3.12.1 Effect of pH

The effect of pH on photocatalytic degradation was observed in the range of 6.5 to 10.0. The results are given in Table 3.27 and Fig. 3.33

Table 3.27: Effect of pH

[Alizarin red-s] = 3.20×10^{-4} M g-C_3N_4 = 0.12 g

Light Intensity = 70.0 mW cm^{-2}

pH	**Rate constant (k) × 10^5 (s^{-1})**
6.5	1.36
7.0	4.79
7.5	7.29
8.0	**8.72**
8.5	6.72
9.0	5.15
9.5	3.43
10.0	2.29

It was noticed that the degradation rate of Alizarin red-S increases with increasing pH of solution up till 8.0, but above this value of pH, the rate of photodegradation of Alizarin red-S started decreasing.

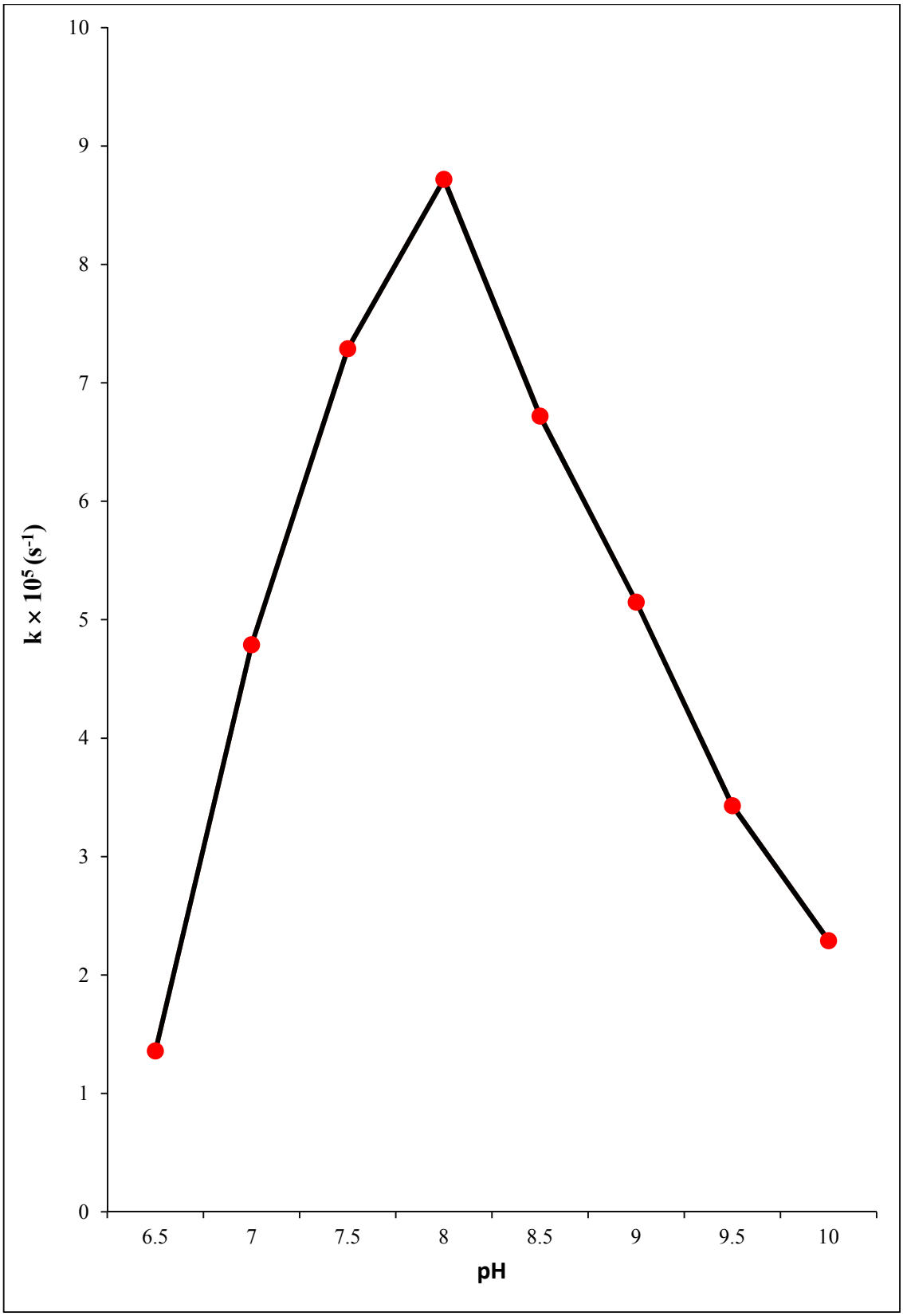

Fig. 3.33: Effect of pH

3.12.2 Effect of dye concentration

The effect of dye concentration on the rate of reaction was also observed using different concentrations of alizarin red-S solution. The results are shown in Table 3.28 and Fig. 3.34

Table 3.28: Effect of dye concentration

pH = 8.0, Light Intensity = 70.0 mW cm^{-2}

g-C_3N_4 = 0.12 g

[Alizarin red-S] × 10^4 M	**Rate constant (k) × 10^5 (s^{-1})**
2.6	4.33
2.8	4.67
3.0	5.30
3.2	**8.72**
3.4	5.72
3.6	5.41
3.8	4.79
4.0	4.50
4.2	3.53

It was observed that the rate of photocatalytic degradation increases with increase in the concentration of the dye up to 3.2 × 10^{-4} M, but it decreases on increasing concentration of dye further.

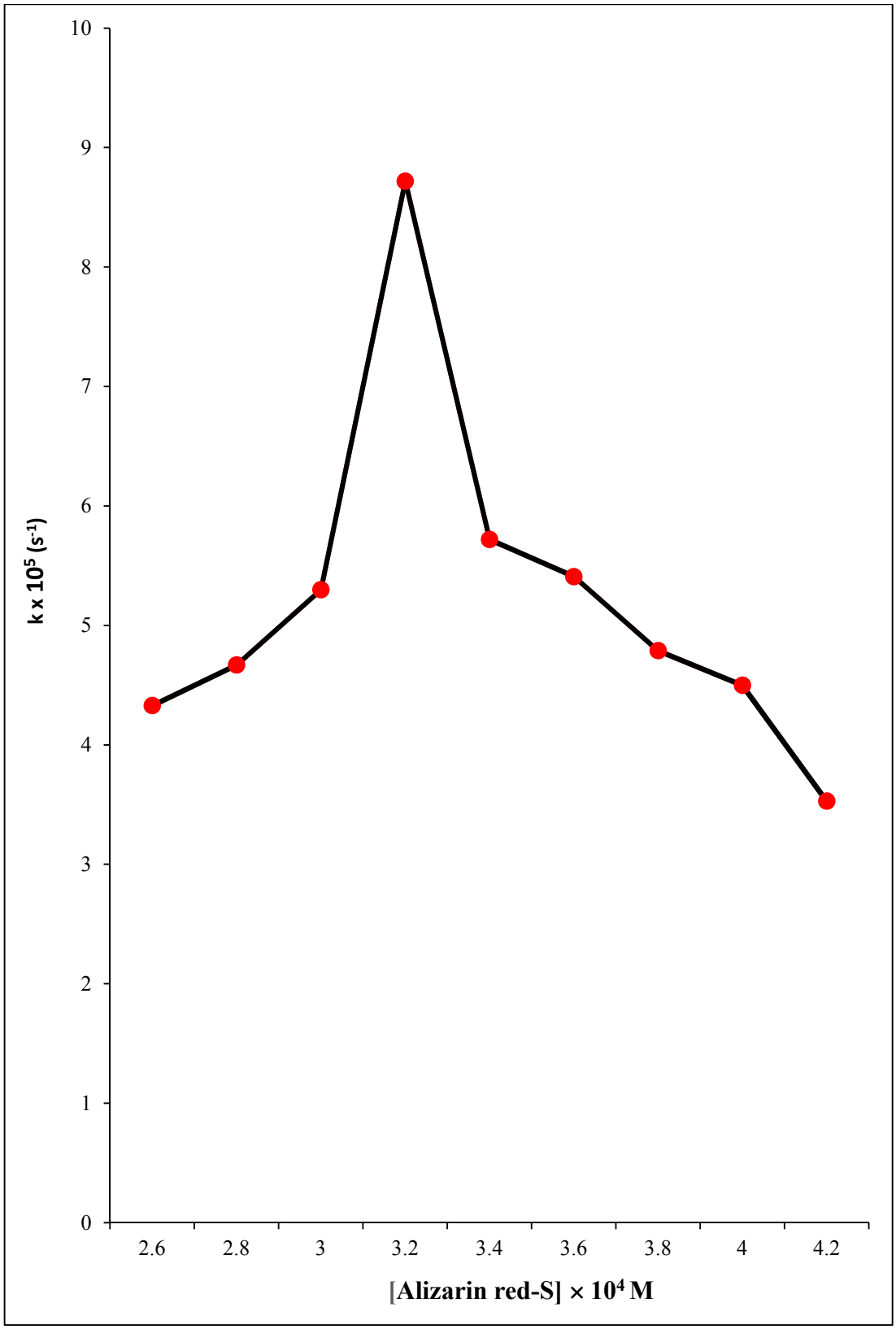

Fig. 3.34: Effect of dye concentration

3.12.3 Effect of amount of photocatalyst

The effect of amount of photocatalyst on the rate of photocatalytic degradation of alizarin red-s also observed in the rang of 0.02-0.18 g. The results are shown in Table 3.29 and Fig. 3.35

Table 3.29: Effect of amount of photocatalyst

pH = 8.0 Light Intensity = 70.0 mW cm^{-2}

[Alizarin red-S] = 3.2×10^{-3} M

g-C_3N_4 (g)	**Rate constant (k) × 10^5 (s^{-1})**
0.02	2.76
0.04	3.59
0.06	4.26
0.08	5.98
0.10	6.86
0.12	**8.72**
0.14	8.22
0.16	7.28
0.18	5.25

It was noticed that the rate of reaction increases with increase in the amount of photocatalyst up to 0.12 g, but above this value of photocatalyst, the rate of reaction decreased.

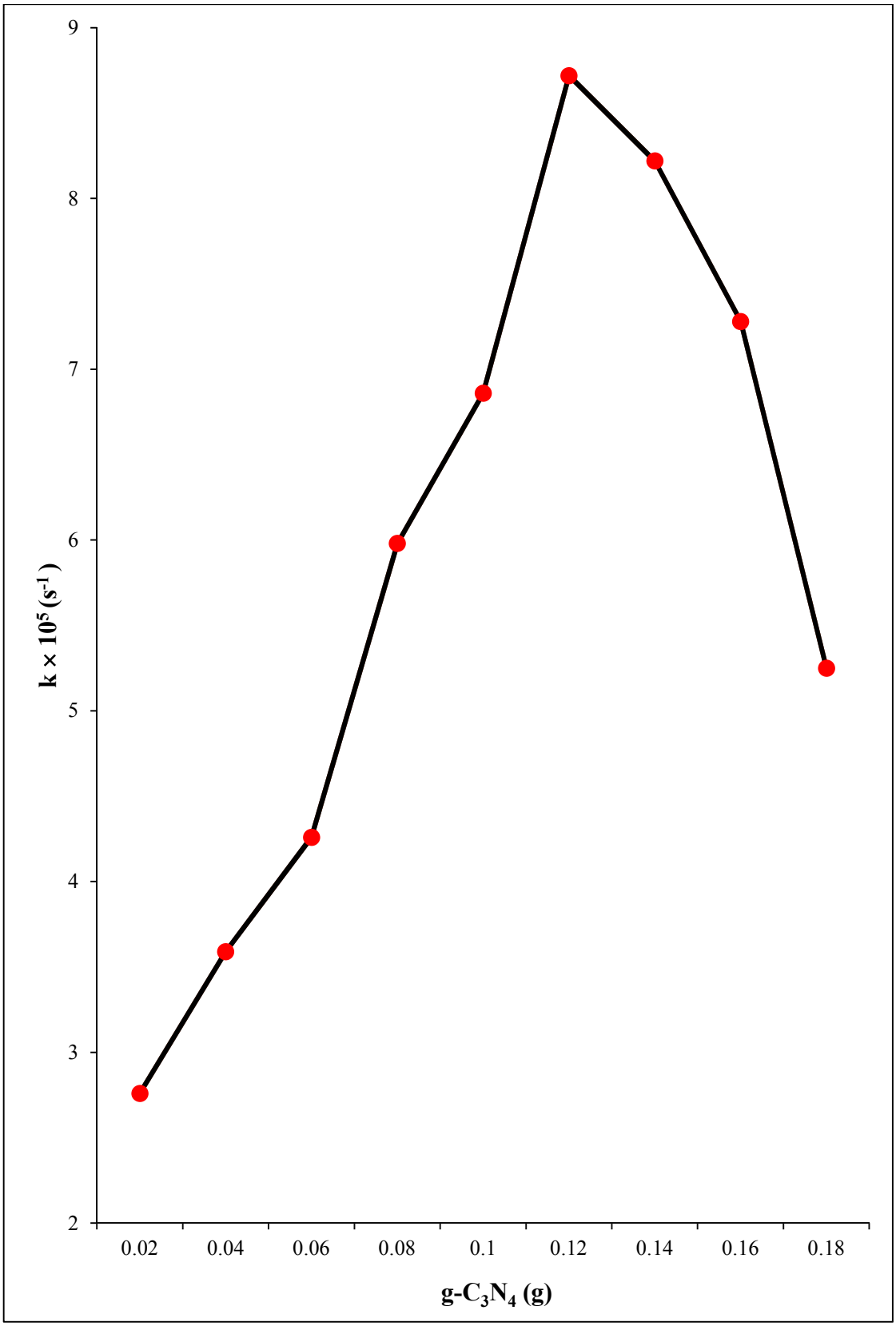

Fig. 3.35: Effect of amount of photocatalyst

3.12.4 Effect of light intensity

The effect of light intensity on the rate of Alizarin red-S was also observed from 20.0 to 70.0 m W cm^{-2}. The results are reported in Table 3.30: and Fig. 3.36:

Table 3.30: Effect of light intensity

pH = 8.0 [Alizarin red-S] = 3.2 $x10^{-4}$ M

g-C_3N_4 = 0.12 g

Light intensity (m W cm^{-2})	**Rate constant (k) × 10^5 (s^{-1})**
30.0	7.54
40.0	7.96
50.0	8.23
60.0	8.38
70.0	**8.72**

It was observed that the rate of degradation was increased on increasing light intensity.

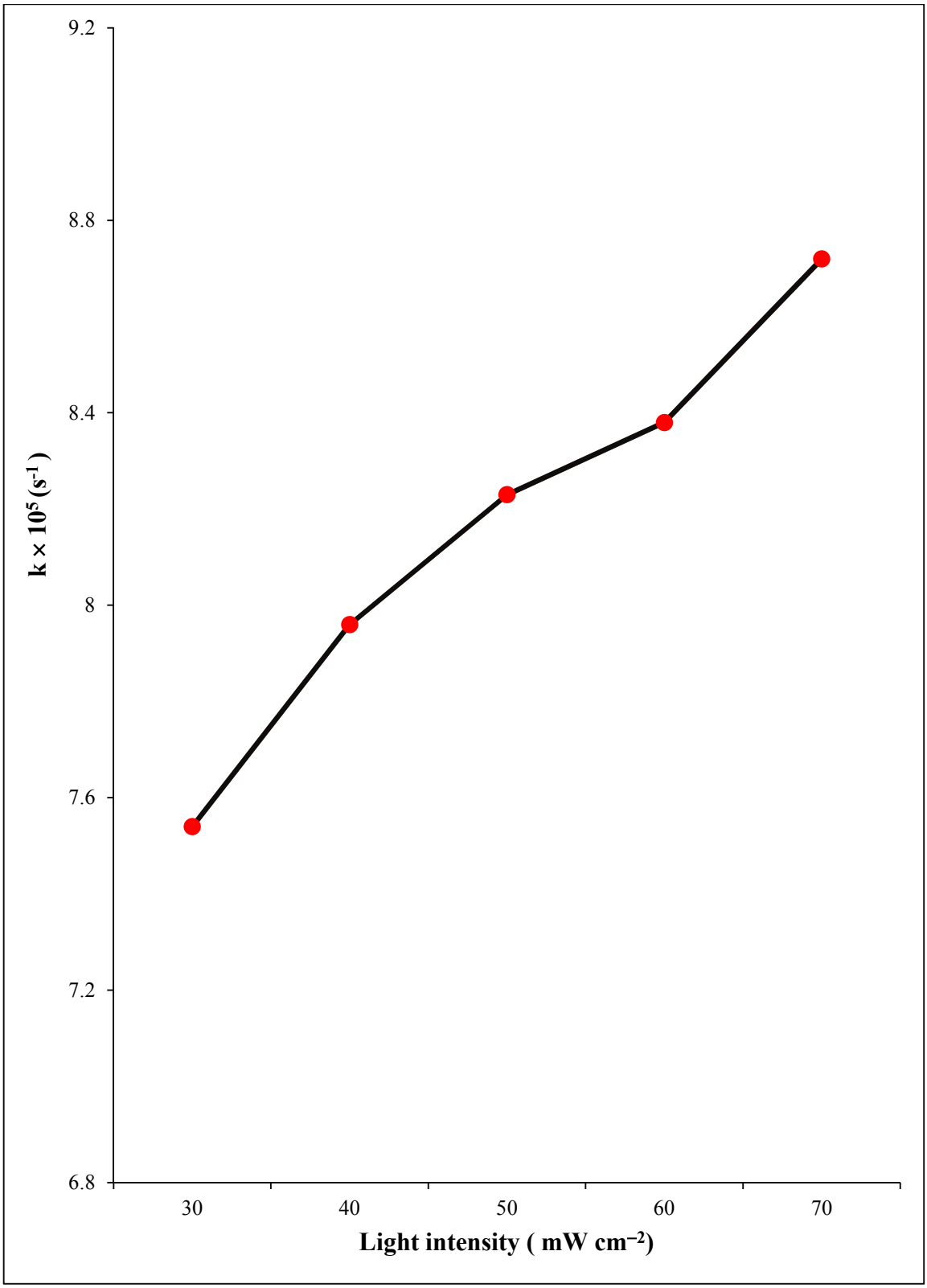

Fig. 3.36: Effect of light intensity

❐❐❐

CHAPTER – IV

DISCUSSION

CONTENTS

4.1 EFFECT OF pH

The effect of pH on photocatalytic degradation of dyes has been studied. The observations are reported in Tables 3.2, 3.7, 3.12, 3.17, 3.22 and 3.27. The optimum value of pH was observed as 7.0, 9.5, 8.5, 8.5, 7.5 and 8.0 for Azure A, Evans blue, Rose Bengal, Methylene blue, Rhodamine B and Alizarin red-S, respectively.

It has been observed that the rate of photocatalytic degradation of the dyes (Azure A, Evans blue, Rose Bengal, Methylene blue, Rhodamine B and Alizarin red-S) increases as pH was increased. On further increasing the pH above a particular value, rate of the reaction was decreased. This may be explained by increase in attraction between cationic dye molecules (Azure A, Methylene blue and Rhodamine B) and hydroxyl ions as pH was increased, and accordingly, the rate of photocatalytic degradation of the dye increases. Above an optimum pH, a decrease in the rate of photocatalytic degradation of the dye was observed, which may be due to the fact that cationic form of dye molecules is converted in its neutral form, which faces almost no attraction towards the negatively charged semiconductor surface. Hence, the rate was retarded. But in case of anionic dyes (Rose Bengal, Evans blue and Alizarin red-S) the dyes will start facing a force of repulsion between anionic dyes and negatively charged surface of the graphitic carbon nitride. As a result, the rate of degradation decreased.

4.2 EFFECT OF DYE CONCENTRATION

The effect of concentration on their photocatalytic degradation has been studied. The observation are reported in Tables 3.3, 3.8, 3.13, 3.18, 3.23 and 3.28. The optimum value of dye concentration was observed as 1.00×10^{-4}, 1.00×10^{-4}, 0.8×10^{-4}, 1.5×10^{-4} ,0.8×10^{-3} and 3.2×10^{-3} M for Azure A, Evans blue, Rose Bengal, Methylene blue, Rhodamine B and Alizarin red-S, respectively.

The rate of photocatalytic degradation of dye was found to increase on increasing the concentration of dye. It may be due to fact that as the dye concentration was increased, more dye molecules were available for excitation and energy transfer and hence, an increase in the rate of degradation of the dye was observed. The rate of photocatalytic degradation was found to decrease with increase in the concentration of the dye further, which may be due to the fact that dye itself will start acting as a filter for

the incident radiations. It may not permit the desird light intensity to reach the surface of photocatalyst and hence, the rate of degradation was decreased.

4.3 EFFECT OF AMOUNT OF PHOTOCATALYST

The amount of photocatalyst also affects photocatalytic degradation of dye and therefore, its effect has been studied by varying the amounts of photocatalyst. The observations are reported in Tables 3.4, 3.9, 3.14, 3.19, 3.24 and 3.29. The optimum value of amount of photocatalyst was found as 0.08, 0.10, 0.08, 0.16, 0.12 and 0.12 g for Azure A, Evans blue, Rose Bengal, Methylene blue, Rhodamine B and Alizarin red-S, respectively.

It was observed that the rate of reaction was increased with increase in amount of photocatalyst, graphitic carbon nitride. The rate of reaction shows a declining behaviour beyond a particular amount of photocatalyst. This may be due to fact that as the amount of photocatalyst was increased, its exposed surface area also increases resulting in enhanced rate of degradation. However, after a limiting value, any addition of photocatalyst will increase only thickness of its layer at bottom of the vessel and not the exposed surface area. In this case, multilayers are formed and as a result, the reaction rate decreases slightly, because multilayers permit the e^- h^+ recombination as particles of photocatalyst are in close contact. As a consequence, rate of degradation decreases.

4.4 EFFECT OF LIGHT INTENSITY

The light intensity affects photocatalytic degradation of dye and therefore. its effect has also been studied by variation of the intensity of light. The observations are reported in Tables 3.5, 3.10, 3.15, 3.20, 3.25, and 3.30. The optimum value of light intensity was observed as 70.0, 60.0, 70.0, 60.0, 60.0 and 70.0 m W cm^{-2} for Azure A, Evans blue, Rose Bengal, Methylene blue, Rhodamine B and Alizarin red-S, respectively.

It was observed that the rate of reaction was increased with increasing light intensity due to fact that the number of photons striking per unit area of the semiconductor per unit time also increases. However, at higher light intensities, some thermal side reaction may also start and hence, the rate of photocatalytic degradation was decreased on increasing the intensity of light further in some cases.

4.5 MECHANISM

The role of active oxidizing species was confirmed by using specific scavengers. It was observed that reaction rate was drastically reduced in presence of Isopropyl alcohol, which ascertained that hydroxyl radical played a major role in oxidative degradation of these dyes.

On the basis of these observation, a tentative mechanism for photocatalytic degradation of Azure A, Evans blue, Rose Bengal, Methylene blue, Rhodamine B and Alizarin red- S is proposed as-

$$^{1}Dye_0 \xrightarrow{h\nu} {}^{1}Dye_1 \quad ...(4.1)$$

$$^{1}Dye_1 \xrightarrow{ISC} {}^{3}Dye_1 \quad ...(4.2)$$

$$g\text{-}C_3N_4 \xrightarrow{h\nu} g\text{-}C_3N_4\,[h^+\,(VB) + e^-\,(CB)] \quad ...(4.3)$$

$$^{-}OH + g\text{-}C_3N_4\,(h^+) \longrightarrow {}^{\bullet}OH + g\text{-}C_3N_4 \quad ...(4.4)$$

$$^{\bullet}OH + {}^{3}Dye_1 \longrightarrow \text{Leuco Dye} \quad ...(4.5)$$

$$\text{Leuco Dye} \longrightarrow \text{Products} \quad ...(4.6)$$

The dye is excited to its first excited singlet state by absorbing a light of suitable wavelength. than, it is transferred to its triplet excited state by intersystem crossing (ISC). On the other hand the graphitic carbon nitride also absorbs light equivalent to its band gap.

As a consequence, an electron is excited from to its valence band to conduction band. The hole in the valence band of this photo catalyst abstracts and electron from hydroxyl ion by hole forming a hydroxyl radical.

This hydroxyl radical reacts with triplet state of dye to convert it to its leuco form, which is unstable. This leuco form is degraded to smaller fragments as products, which are almost harmless or less harmful such as Co_2, H_2O, inorganic ions, etc.

The order of rate of their photocatalytic degradation was found to be:

Azure A > Methylene blue > Evans blue > Rhodamine B > Alizarin red-S > Rose Bengal.

The use of a metal free semiconductor graphitic carbon nitride in the photocatalytic degradation of Azure A, Evans blue, Rose Bengal, Methylene blue, Rhodamine B and Alizarin red- S is welcome addition, as this process is ecofriendly in nature as it degrades organic pollutants into their less harmful or almost harmless counterparts such as CO_2, H_2O, and some inorganic ions, which can be easily removed by ion-exchange method. Time has come that such non-metallic photocatalyst may replace metal based photocatalyst in near future.

❐❐❐

PUBLICATIONS

PHOTOCATALYTIC DEGRADATION OF EVAN'S BLUE IN AQUEOUS SOLUTION USING GRAPHITIC CARBON NITRIDE

D. PATEL* and M. JANGID

Department of Chemistry, PAHER University, Udaipur- 313024 (Raj), INDIA
E-mail : bdeepikapatel@gmail.com

Abstract

The photocatalytic degradation of Evan's blue was carried out using graphitic carbon nitride (g-C_3N_4) as a photocatalyst. The effect of various parameters such as amount of catalyst, pH, light intensity and concentration of the dye has been studied on the rate of reaction. It was observed that this photocatalytic process followed pseudo-first order kinetics. The optimum conditions for degradation of Evans blue were achieved as:

pH = 9.5, [Evans blue] = 1.00 x 10^{-4} M, g-C_3N_4 = 0.10 g and light intensity = 60.0 mW cm^{-2}

Key Words: Photocatalytic degradation, Evan's blue, Graphitic carbon nitride, Advanced oxidation, visible light.

Published In: Ecology, Environment and Conservation, *30 (August Suppl. Issue): 2024; pp. (S26-S31) ISSN 0971–765X*

Photocatalytic Degradation of Azure-A in Aqueous Solutions using Graphitic Carbon Nitride

D. PATEL*and M. JANGID

Department of Chemistry, PAHER University, Udaipur-313024 (Raj). INDIA
E-mail: bdeepikapatel@gmail.com

Abstract

The photocatalytic degradation of Azure-A was studied using graphitic carbon nitride (g-C_3 N_4) as a photocatalyst. The effect of various parameters such as amount of catalyst, pH, light intensity and concentration of the dye has been studied on the rate of degradation. Kinetic studies revealed that this photocatalytic process followed pseudo-first order kinetics. A tentative mechanism for the photocatalytic degradation of Azure-A involving hydroxyl radical has been proposed.

Keywords: Photocatalytic degradation, Azure-A, Graphitic carbon nitride.

Published In: Research Journal of Chemistry and Environment; Vol. 28(7); 35-41; doi: doi.org/10.25303/287rjce035041; (2024)